Carderock Division
Naval Surface Warfare Center
Bethesda, MD 20084–5000

CDRKNSWC/SSD–93/54 September 1993
Ship Systems Directorate
Research and Development Report

Tipjet 80–Inch Model Rotor Hover Test Test No. 1198

by
Alan W. Schwartz

CDRKNSWC/SSD–93/54 Tipjet 80–Inch Model Rotor Hover Test: Test No. 1198

MAJOR DTRC TECHNICAL COMPONENTS

CODE 011 DIRECTOR OF TECHNOLOGY, PLANS AND ASSESSMENT

12 SHIP SYSTEMS INTEGRATION DEPARTMENT

14 SHIP ELECTROMAGNETIC SIGNATURES DEPARTMENT

15 SHIP HYDROMECHANICS DEPARTMENT

16 AVIATION DEPARTMENT

17 SHIP STRUCTURES AND PROTECTION DEPARTMENT

18 COMPUTATION, MATHEMATICS & LOGISTICS DEPARTMENT

19 SHIP ACOUSTICS DEPARTMENT

27 PROPULSION AND AUXILIARY SYSTEMS DEPARTMENT

28 SHIP MATERIALS ENGINEERING DEPARTMENT

DTRC ISSUES THREE TYPES OF REPORTS:

1. **DTRC reports, a formal series,** contain information of permanent technical value. They carry a consecutive numerical identification regardless of their classification or the originating department.

2. **Departmental reports, a semiformal series,** contain information of a preliminary, temporary, or proprietary nature or of limited interest or significance. They carry a departmental alphanumerical identification.

3. **Technical memoranda, an informal series,** contain technical documentation of limited use and interest. They are primarily working papers intended for internal use. They carry an identifying number which indicates their type and the numerical code of the originating department. Any distribution outside DTRC must be approved by the head of the originating department on a case-by-case basis.

REPORT DOCUMENTATION PAGE

1a. REPORT SECURITY CLASSIFICATION: UNCLASSIFIED	1b. RESTRICTIVE MARKINGS
2a. SECURITY CLASSIFICATION AUTHORITY	3. DISTRIBUTION/AVAILABILITY OF REPORT: Approved for public release; distribution is unlimited.
2b. DECLASSIFICATION/DOWNGRADING SCHEDULE	
4. PERFORMING ORGANIZATION REPORT NUMBER(S): CRDKNSWC/SSD-93/54	5. MONITORING ORGANIZATION REPORT NUMBER(S)
6a. NAME OF PERFORMING ORGANIZATION: Carderock Division, Naval Surface Warfare Center; 6b. OFFICE SYMBOL (If applicable): Code 22	7a. NAME OF MONITORING ORGANIZATION
6c. ADDRESS (City, State, and ZIP Code): Bethesda, Maryland 20084-5000	7b. ADDRESS (City, State, and ZIP Code)
8a. NAME OF FUNDING/SPONSORING ORGANIZATION: Office of Naval Research; 8b. OFFICE SYMBOL (If applicable): Code 442	9. PROCUREMENT INSTRUMENT IDENTIFICATION NUMBER
8c. ADDRESS (City, State, and ZIP Code): 800 N. Quincy Street, Arlington, VA 22217-5660	10. SOURCE OF FUNDING NUMBERS: PROGRAM ELEMENT NO. 62122N; PROJECT NO. RR22-M59; TASK NO. 8.1; WORK UNIT ACCESSION NO. DN500047

11. TITLE (Include Security Classification): Tipjet 80-Inch Model Rotor Hover Test: Test No. 1198

12. PERSONAL AUTHOR(S): Schwartz, Alan W.

13a. TYPE OF REPORT	13b. TIME COVERED	14. DATE OF REPORT (YEAR, MONTH, DAY)	15. PAGE COUNT
Final	FROM 1/91 TO 12/91	1993 September	100

16. SUPPLEMENTARY NOTATION

17. COSATI CODES			18. SUBJECT TERMS (Continue on reverse if necessary and identify by block number)
FIELD	GROUP	SUB-GROUP	Tipjet, Circulation Control, Reaction Drive, Hover Test

19. ABSTRACT (Continue on reverse if necessary and identify by block number)

An experimental investigation was conducted to examine the aerodynamic properties of a Tipjet integrated pneumatic lift/reaction-drive rotor system in hover. For this rotor system, a single source of compressed air directly powers the rotor as a radial outflow turbine while simultaneously supplying the high velocity jet sheet that produces lift by means of circulation control (CC) along the blades. A subscale model of such a fully pneumatic Tipjet rotor system was constructed and tested on the hover test facility at the David Taylor Model Basin. The model was tested to identify unique attributes of the integrated lift/drive system including mutual interference between tip nozzle flow and CC jet sheets and the impact of drawing CC supply air from a "flowing plenum." Test results are presented for the model in four configurations: (1) CC rotor with tip nozzles closed, (2) rotor locked with nozzles thrusting, (3) tip-drive CC rotor with controlled rpm, and (4) tip-jet self-drive equilibrium. The basic rotor lifting system, while exhibiting the highest augmentation ratio ever recorded for a CC rotor, suffers an induced power penalty due to the nonlifting region of the blade span where the tip nozzles are located. As expected, an internal pressure drop due to the flow rate in the blade duct was observed. There was no evidence of mutual interference effects between the lift and drive systems. Overall, the rotor exhibited a constant, linear response of lift versus pressure regardless of the slot height or the equilibrium tip speed.

20. DISTRIBUTION/AVAILABILITY OF ABSTRACT	21. ABSTRACT SECURITY CLASSIFICATION
☒ UNCLASSIFIED/UNLIMITED ☐ SAME AS RPT ☐ DTIC USERS	UNCLASSIFIED

22a. NAME OF RESPONSIBLE INDIVIDUAL	22b. TELEPHONE (Include Area Code)	22c. OFFICE SYMBOL
Alan W. Schwartz	(301) 227-4316	Code 512

(This page intentionally blank)

CONTENTS

CONTENTS (Continued)

FIGURES

FIGURES (Continued)

TABLES

ABBREVIATIONS AND SYMBOLS

A	Rotor disk area, ft^2
C_d	Airfoil drag coefficient
C_{d_o}	Airfoil profile drag coefficient
C_l	Airfoil lift coefficient
C_P	Rotor power coefficient ($Q/(\rho A V_t^2 R)$)
C_{P_i}	Rotor induced power coefficient
C_{P_o}	Rotor profile power coefficient
C_{P_s}	Rotor shaft power coefficient
C_T	Rotor thrust coefficient ($T/(\rho A V_t^2)$)
C_μ	Coefficient of slot jet momentum
k	Induced power factor
L	Rotor lift, lb
P_{Rroot}	Blade root pressure ratio
Q	Torque, ft-lb
Q_i	Rotor induced torque, ft-lb
Q_o	Rotor profile torque, ft-lb
R	Rotor blade radius, ft
T	Rotor thrust, lb
V_j	Tip-jet nozzle jet velocity, ft/sec
V_o	Jet velocity based on blade root pressure, ft/sec
V_t	Rotor blade tip speed, ft/sec
w	Weight flow of air, lb/sec
ρ	Air density, lb_m/sec
σ	Rotor solidity

(This page intentionally blank)

ABSTRACT

An experimental investigation was conducted to examine the aerodynamic properties of a Tipjet integrated pneumatic lift/reaction-drive rotor system in hover. For this rotor system, a single source of compressed air directly powers the rotor as a radial outflow turbine while simultaneously supplying the high velocity jet sheet that produces lift by means of circulation control (CC) along the blades. A subscale model of such a fully pneumatic Tipjet rotor system was constructed and tested on the hover test facility at the David Taylor Model Basin. The model was tested to identify unique attributes of the integrated lift/drive system including mutual interference between tip nozzle flow and CC jet sheets and the impact of drawing CC supply air from a "flowing plenum." Test results are presented for the model in four configurations: (1) CC rotor with tip nozzles closed, (2) rotor locked with nozzles thrusting, (3) tip-drive CC rotor with controlled rpm, and (4) tip-jet self-drive equilibrium. The basic rotor lifting system, while exhibiting the highest augmentation ratio ever recorded for a CC rotor, suffers an induced power penalty due to the nonlifting region of the blade span where the tip nozzles are located. As expected, an internal pressure drop due to the flow rate in the blade duct was observed. There was no evidence of mutual interference effects between the lift and drive systems. Overall, the rotor exhibited a constant, linear response of lift versus pressure regardless of the slot height or the equilibrium tip speed.

ADMINISTRATIVE INFORMATION

This work was conducted by the Ship Systems and Programs Directorate (Code 22) of the Carderock Division, Naval Surface Warfare Center. Funding was provided by the Office of Naval Technology, Air Vehicle Technology Block, Project No. RR22-M59, Task No. 8.1.

INTRODUCTION

BACKGROUND

A conceptual design was recently developed for a pneumatic rotor system application on a vertical takeoff and landing (VTOL), high-altitude, long-endurance unmanned air vehicle (UAV), Tipjet VTOL UAV (Ref.1). For a pneumatic rotor system, a single source of compressed air directly powers the rotor as a radial outflow turbine while simultaneously supplying the high velocity jet sheet that produces lift by means of circulation control (CC) along the blades.

Interest in the Tipjet concept led to the present research program including the investigation of the fundamental aerodynamic properties of the rotor system. A subscale model of such a fully pneumatic Tipjet rotor system was constructed and tested on the hover test facility at the David Taylor Model Basin (DTMB); see Fig. 1. The model incorporates the necessary configuration flexibility to parametrically evaluate the closely coupled lift and drive systems.

The Tipjet concept represents a new variation in the design of VTOL systems and displays unique characteristics with potential to benefit rotorcraft capabilities. As envisioned in a typical application, compressed air is supplied by a "cold-cycle" gas generator (e.g., the fan stage of a turbofan engine) through ducting to the rotor hub. Within the blades, the air flows radially toward nozzles at the tips for reaction drive. Along the way, a portion of the air is drawn off and passed through CC slots near the trailing edges of the rotor blades. The ejected air entrains the upper surface flow and produces lift via enhanced circulation. The height of the CC ejection slot and the blade internal pressure (thus the momentum of air ejected) determine the level of lift and, consequently, the induced torque required to drive the rotor. Similarly, the tip reaction jet area is adjusted to match drive power to the rotor requirements; see Fig. 2. Optimum system performance requires efficient use of the energy delivered to the blades by the gas producer.

The integration of CC with the cold-cycle (250°F) reaction-drive rotor results in a synergistic combination of lift and drive technologies. The mechanical simplicity of the reaction-drive system, without a heavy transmission and tail rotor, provides readily apparent advantages. Circulation control generates the high lift coefficients required to operate at the low tip speeds corresponding to efficient operation of the cold-cycle reaction-drive rotor. In addition, these high lift coefficients can be produced independent of incidence angle, thus rendering blade pitch control unnecessary. Without the complexities of blade articulation or flexbeam structural considerations, the structural design of the rotor is simplified. The blades can be integrated with the hub to comprise a single unit for optimum structural properties. Furthermore, with a cold-cycle system, lightweight composite construction can provide an efficient structural design with high stiffness. Finally, CC airfoil sections inherently have high internal volume which minimizes flow losses in the blade duct.

In general, the Tipjet rotor is an inherently variable rotation speed system where tip speed is determined by the relative levels of rotor lift and reaction-drive power. Both of these determining factors are directly linked to the supply pressure and can be controlled by adjusting the relative exit areas of the CC slots

and the tip-jet nozzles. A potential source of control interaction is that the internal flow effects in the blade ducts influence not only the drive power characteristics but also the CC lift response.

The Tipjet model rotor is a fixed area (slot and nozzle) system with pressure variation as the only mode of control. Although there may be direct applications for such a system, a more versatile arrangement is a constant supply pressure system with in-flight control of slot height and nozzle opening. For example, on an operational Tipjet VTOL UAV, additional features would be necessary to provide collective and cyclic control of blade lift (slot height) and to vary the drive power (tip-jet nozzle area). The impact of these requirements on rotor system weight will depend on the design details of the control systems.

TEST OBJECTIVES

The present model was designed for use in identifying several aspects regarding the integration of CC and reaction-drive rotor technologies. Specifically, the objectives of the test were to:

1. Evaluate the rotor system's aerodynamic and pneumodynamic properties including the mutual interference effects between the tip nozzle jets and the CC jet sheets and the impact of drawing CC supply air from a "flowing plenum;"
2. Identify characteristics unique to the integrated pneumatic lift/drive configuration including the response of tip speed to blade pressure and controllability of the rotation rate; and
3. Provide a data base for hover performance as a function of the design variables.

To efficiently address these test objectives, complexities involving direct remote actuation of the CC slots and tip nozzles were avoided. The model was designed, instead, with a ground-adjustable CC slot height capability and with modular, replaceable tip-drive nozzles. This afforded a high level of flexibility in configuring the controlling parameters and a wide range of operation about the design point. The parameters that define the test envelope, the design values of these parameters, and the ranges actually tested are listed in Table 1.

Note that while the model was designed with the capability to change the tip nozzle exit area, only a single nozzle area was tested. Also, due to a machining error that limited the capability of the blades to carry centrifugal loads, blade tip speed was limited to 500 ft/sec during the test.

The model was also designed as a "rigid" aerodynamic model with no attempt at dynamic scaling of the blade structure. In addition to simplifying the design, this also permitted clearer identification of the aerodynamic phenomena.

Preliminary tests were conducted with the electric motor drive to validate rotor performance by comparing the test data with analytical predictions and with data of previously tested CC rotors. Tests were also conducted to validate the tipjet nozzle performance by comparing results with tests of the duct/nozzle static model. Finally, the performance of the model rotor in the tip-jet self-drive mode was evaluated. Over 3000 data points were recorded during 25 shifts of testing.

TEST ARTICLE

DESCRIPTION

The Tipjet wing/rotor model is a 37-percent scale model of the 1200-lb Tipjet conceptual design. The model is constructed primarily of 7075-T5 Aluminum. The planform of the 80-in. two-bladed rotor model, the airfoil cross section, and details of the CC slot design are shown in Fig. 3. The model rotor geometric properties are summarized in Table 2. Circulation control slots are located on the leading and trailing edges of the blades beginning at 25-percent radius and extending to 93-percent radius. The leading edge slots, incorporated on the model to support future fixed-wing wind tunnel investigations, allowed hover testing in clockwise and counter-clockwise directions of rotation. Within the span range of the slots, the blade tapers in both thickness and chord. The outer contour is constant over the outboard 7 percent of the blade, which encloses the tip-jet nozzle. Inside the blade,the duct area is tapered as the flow negotiates the 0.5-in. radius turn and is ejected from the rectangular nozzle. The entire blade interior serves as the flow duct and is interrupted only by structural posts at 2-in. intervals located as close as possible to the leading and trailing edges. The slot height is adjustable by means of jacking screws located adjacent to each post; the tip-jet nozzles are replaceable modules allowing variations in nozzle exit area. As noted, only one nozzle exit area was used during the hover test.

The model consists of a single structural member from blade tip to blade tip which includes the airfoil lower surface Coanda trailing edges. Each "blade" has a separate upper member extending chordwise from slot to slot and spanwise for the length of the CC slot. There are upper covers over each of the tip-jet nozzle regions, end caps for each blade tip, and an upper cover over the rotor hub region; these covers are bolted to the main lower blade member. The tip-jet nozzle openings consist of Lexan modules with rectangular openings for the jet.

The wing/rotor assembly is a single unit with zero "blade" pitch. The Tipjet model has no cyclic control feature, and therefore pitch and roll moments cannot be introduced on the hover stand. The wing/rotor model attaches, via an adapter plate, to the top of the existing RBCCR rotor hub.

Air for tipjet operation and for CC blowing is supplied through the hub and through a scaled 3-in. diameter orifice at the wing/rotor centerline. A common central duct comprising most of the internal volume of the wing/rotor feeds pressurized air to both the tipjet nozzles and the CC slots. Airflow to the model is measured at a venturi tube upstream of the model and is controlled by the model operator via a Leslie valve. The wing/rotor is instrumented with Kulite pressure transducers mounted in the ducts. Each "blade" contains five transducers with three located at 50-percent chord at 25-, 65-, and 88-percent span. At 65-percent span, additional transducers are located in the leading and trailing edge ducts near the slot adjustment screws. Strain gauge bridges are installed on the wing outer surface near 20-percent span to measure normal bending.

DESIGN

The design criteria (Ref. 2) provided for a single model of the Tipjet wing/rotor to be tested on the existing DTMB hover stand and with an aircraft model in the DTMB wind tunnel. To isolate the aerodynamic performance, a structurally rigid model was desired (first flap bending natural frequency = 25 Hz). To allow for maximum flexibility, the CC slots and tip-jet nozzles are adjustable. Due to the subscale design, no cyclic control requirements were specified.

The two factors that predominately influenced the design were: (1) the centrifugal loads due to the upper blade sections and (2) the bending stresses in the CC slot flexure. The centrifugal loads became critical when a machining error severely compromised the load path designed to carry the upper blade centrifugal load; see Fabrication section. Centrifugal loads were also important in the design of the tip-jet nozzle assembly and led to the selection of Lexan for the nozzle modules.

Incorporating flexible, screw-adjustable CC slots on a rotor model previously had not been attempted. Duct flow requirements forced placement of the slot flexure as close as possible to the slot lip. Also, the desired range of CC slot adjustment was wide. These factors, combined with the material properties of 7075 aluminum made the slot flexure an area of critical stress in the model.

Extensive effort was taken to ensure the structural integrity of the model. Material properties of the actual aluminum stock used for the model were verified

by tension test of samples. Also, rough specimens of the flexures were fabricated, instrumented with surface strain gauges, and tested beyond the expected operational range of the model slots. The CC slot height settings were limited by the resulting stress in the flexure.

Based on risk reduction testing of flexure specimens, the acceptable deflections from the "relaxed" (no load on adjusting screws) position of the slots are:

STA	Maximum Deflection	Minimum Deflection
10	+0.008 in.	-0.016 in.
37	+0.008 in.	-0.008 in.

The design deflections for a fully operational capability were within these limits. Deflections to achieve the necessary slot height settings (i.e., fully closed and fully open) were dependent on the final "relaxed" position of the slot. The risk reduction test results indicate that the initial stress analysis was very conservative, and therefore a larger slot height envelope could be safely adopted.

The wing/rotor was originally designed to operate to extreme conditions of 2200 rpm with internal blade pressure of 30 psig. It is not expected that the model would be operated at more than 1860 rpm (V_t=650 ft/sec) or at greater than 22 psig (P_R=2.5). Due to a machining error, however, the rotation speed was limited to 1450 rpm for this investigation.

A complete description of the model design is provided in Ref. 3. Included are all the calculations related to the loads on the model structure and fasteners as well as predicted safety factors. The final drawings used for model fabrication are listed in Table 3.

FABRICATION

Most of the machining for the model was performed on numerically controlled (NC) equipment. The machining of the CC slot lips and the slot flexures was an expected challenge. Maintaining accuracy of the cuts was difficult, and resulted in the rejection of one upper blade section. Another of the delicate upper blade sections was damaged in handling. Eventually, improvements in the technique produced satisfactory results. Final contours at the slot lip were achieved with hand finishing. Cutting of the slot flexure went smoothly. Measurements of the slot lip positions before and after machining of the flexure indicated there was no deformation of the slot introduced due to internal stress within the material.

The machining error involving a key element of the load path between the upper and lower blade sections required substantial attention. Near completion of

the machining of the lower blade section, two small blocks of material were inadvertently removed. This material provided the studs that supported much of the centrifugal load of one of the upper blade sections. A design modification was incorporated that involved the installation of steel adapter blocks into the lower blade to replace the missing studs; see Fig. 4. This modification involved only one side of the wing, i.e., one blade. The resulting design had a significantly reduced safe load carrying capability but allowed the lower blade section to be salvaged. To compensate for this design compromise, the operational tip speed limit was reduced from 725 ft/sec to 500 ft/sec to maintain the original design safety factor. A cavity was machined into an interior face of the hub cover in order to install a lead plate to serve as a counterweight to offset the centrifugal imbalance due to the steel adapter blocks.

Contours for the airfoil surfaces and for the Coanda nozzle interior surfaces were verified by Validator measurements at three spanwise positi on each blade. The Coanda surfaces matched the prescribed coordinates with smooth transitions between the top and bottom surfaces. A few regions were hand-finished to correct minor ridges detectable by touch. The slot lip outer surfaces generally were rounded down to achieve the proper thickness at the lip. The lip thickness was measured at precisely 0.005 in. along the entire length of all slots. The lip edges were observed to be sharp and true.

MODEL ASSEMBLY AND INSTALLATION

The model required careful assembly and adjustment to ensure safe test operations. Shims were added to some of the attachment posts to raise the slot lip to the desired initial position. Viability of the tongue-and-groove design for the load path between upper and lower blade sections was dependent on simultaneous surface-to-surface contact along several faces. These areas were carefully hand worked and shimmed to ensure proper fit. In addition, at assembly, the faces were coated with aluminum impregnated Devcon epoxy to fill gaps and to help bond the surfaces.

Air leakage through seams between the various model parts was treated in a number of different ways. Foam rubber strips and/or silicone sealant was applied to interior contact surfaces of the hub cover and the tip nozzle covers. Rubber gaskets were installed inside the nozzle endplates and at the interface between the model adapter plate and the rotor hub. Additionally, aluminum tape was applied to the exterior of all seams during testing.

Rotor dynamic imbalance was checked using a vibration analyzer with an accelerometer mounted on the rotor mast in the fixed system. The model blade

endcaps are equipped with cavities which were used to install balancing weights as needed. The system was balanced over the operational rpm range to within a measured imbalance of 2 mils (Fig. 5). During the balancing procedure, it was necessary to remove the lead counterweight in the hub cover. This adjustment although fortuitous was not explainable. The final balanced configuration of the tip weights was satisfactory for all tip nozzles tested. The vibration meter was monitored continuously throughout the hover test.

MODEL PROPERTIES

The fully assembled wing model weighs 39.75 lb (not including the steel hub adapter plate). The moment of inertia about the axis of rotation was calculated to be 484 slug-in^4. With the model mounted to a rigid fixture on the bench, the first flapwise bending frequency was measured at 27 Hz, which was within the desired range.

While the model was mounted on the bench, measurements were also made of the blade twist. Using the interior duct floor of the nozzles as the indicating surface and the duct floor at the hub as a reference plane, the twist angle was determined for each blade tip relative to the hub. Blade 1 was found to have no measurable twist, while blade 2 has a nose-down (for counter-clockwise rotation) twist of about 0.25 deg.

TEST FACILITY

HOVER TEST STAND

Tests with the Tipjet model were conducted on the hover test facility developed for testing previous CC model rotors at DTMB; see Fig. 6. A four-component load cell balance measured lift as well as yaw, pitch, and roll moments. The balance is mounted on top of a stand so that the rotor plane of rotation is approximately 15 ft above the floor. The hover stand is equipped to supply drive power to the rotor via a drive belt from either electric or hydraulic power sources. The electric motor used for this test delivers 150 hp at 8000 rpm (gear ratio=3, rotor rpm=2666.7).

Airflow to the model is measured at a venturi flowmeter and controlled via a Leslie dome valve. The venturi has an upstream diameter of 2.90 in. and a throat diameter of 1.50 in. The air temperature in the venturi is measured by an iron/constantan thermocouple. Air total pressure and temperature are also measured in the rotor plenum at the base of the rotating shaft within the rotor mast.

Rotor rotation rate was measured by inductive signal generators triggered by 1/rev and 60/rev toothed gears on the rotating shaft. Pulses from the 60/rev gear are fed electrically to a counter and the number of pulses per second is of the same magnitude as rotor rpm. The measured frequency of the 60/rev gear was converted into a proportional voltage and supplied directly to the data acquisition system.

DATA ACQUISITION AND REDUCTION SYSTEM

The DTMB Portable Data Acquisition and Monitoring System (PDAMS) was used for both data acquisition and reduction. The PDP11-based system has the capability to handle up to 40 data channels with Vishay power supply/signal conditioning/amplifier units. Data can be stored on hard or floppy disks or on magnetic tape. The system has master controls for shunts and auto-zero balance.

The custom data acquisition and reduction software program, DIGITZ, was used to acquire and process the data. Modular routines for Tipjet data were written for the calculation of parameters and data output. Identifiers were built into the modules to ensure traceability of the equations and compatibility between the calculation and output modules. The identifier is included on all output to indicate the data reduction version used for the particular calculations. The software includes a routine used to calibrate the pressure transducers for this test. Another feature of PDAMS is the capability of real-time data monitoring. All data channels can be displayed on the screen (in volts or engineering units) and updated in near real-time during testing. An auxiliary CRT was located at the model operator's station to display this information continuously. PDAMS has built-in features to signal the onset of prescribed levels on the data channels. This feature also signals the onset of the maximum amplified voltage of 10 Vdc.

MODEL OPERATOR STATIONS

The model was operated remotely from a station within a control room adjacent to the test stand. The model operator controls the air supplied to the model and monitors rotor rpm, shaft vibration level, and rotor performance parameters in real time. The operator's station receives a continuous video image of the model.

In addition to the operator's station, an electric motor is operated by a variable frequency controller located in a separate building. The operator of this controller has real-time measurements of the controller frequency and the measured rotor shaft rpm. The motor operator is in constant voice contact with the model operator.

CALIBRATIONS

ROTOR BALANCE

The balance used for the Tipjet model hover test is a Lebow load cell balance (Model No. 6481, Serial No. 1) which measures lift as well as pitch, roll, and yaw moments. The balance was installed on top of the hover test stand and was calibrated using customized loading fixtures. The balance limits, as specified by the vendor, are:

Lift	1000 lb
Pitch	800 ft-lb
Roll	800 ft-lb
Yaw	200 ft-lb

The Tipjet model rotor thrusts up in opposition to the weight loads on the balance. The maximum load on the balance therefore occurs when no lift is on the rotor. In operation, the rotor lift should result in balance normal force loads at about one-third of the balance range. Pitch and roll calibration loads were applied with constant normal force at a level approximating the design rotor lift condition. First-order interaction coefficients were calculated for both positive and negative loadings. These coefficients are in good agreement with those obtained from previous calibrations of the same balance. A summary of the run and point numbers used to derive each loading component as well as the interaction coefficients for both positive and negative loads is provided in Table 4. The final interaction coefficient matrix was checked by applying a variety of combined loadings.

BLADE PRESSURE TRANSDUCERS

The Tipjet model was instrumented with 10 Kulite miniature pressure transducers mounted in various locations within the blade ducts. Two similar transducer models were used that varied primarily in size. Of the 10 transducers, 6 are model XCQ-080-50A transducers that are 0.080-in. diameter, 50-psia units; 4 are model XCQ-062-50A with 0.064-in. diameter and also 50-psia range. The XCQ-062 transducers have an external temperature compensation module. The XCQ-080 transducers are internally compensated. During calibration of the XCQ-080 units, 1000 ohm resistors were installed in series with the positive power lead at the computer patch panel. (This allows for operation at a higher excitation voltage with reduced temperature sensitivity.)

The Kulite transducers were bench calibrated using a precision Mensor pressure standard. Units of like model numbers were ganged and calibrated simultaneously. The calibration was performed with each transducer installed

in an aluminum mounting bracket which was later installed in the model. Pressure was applied to 22 psig (about 37 psia) in increments of 2 psi. The results show good linear responses for all ten transducers.

Final installation of the Kulite transducers included fitting the ends of the leads with miniature electrical connectors. These connectors were not installed at the time of calibration. Instead the leads were connected to the data acquisition system via screw-type connection blocks. Following calibration, span resistances were applied at the connection block across the negative power and negative signal leads. Span voltage readings (amplified) were recorded from the channel multiplexor display.

OTHER INSTRUMENTATION

Pressure transducers for the airflow venturi and for the rotor plenum were bench calibrated using a Mensor precision pressure standard. These transducers included: a transducer used to measure venturi upstream static pressure, a Druck PDCR 920-series 100-psig unit (S/N 238784), calibrated to 70 psig (about 85 psia) in 7-psi increments; a transducer used to measure venturi pressure differential, a Data Sensors 10-psig unit (S/N 132), calibrated to 5 psig (nominal) in 0.5-psi increments; and a transducer to measure pressure in the rotor mast plenum, a Druck PDCR 920-series 30-psig unit (S/N 227480), calibrated to 30 psig (about 45 psia) in 3.0-psi increments.

DATA REDUCTION

The test data initially were reduced and results were produced as hard copy and saved to floppy disks. The reduced data were transferred to a MacII desktop computer for analysis. This analysis revealed a few calculation errors and suggested additional useful parameters. The data base on the MacII was revised to reflect these corrections and additions. Appendix A lists the derived parameters and the corresponding equations.

RISK REDUCTION TESTS

FLEXURE SPECIMEN

As stated, the CC slot flexure was a critical component of the model design. Risk reduction activities focussed on proving the viability of the flexure design prior to fabrication of the rotor model.

The Tipjet model wing/rotor is designed with flexures running spanwise between the posts and the slot adjusting screws on the upper blade parts of the leading and trailing edges of the wing. These flexures allow the CC slot opening

to be adjusted by means of deflection. Due to limitations imposed by the model geometry, the location and size of the flexures resulted in a design with factors of safety well below the desired level of 4.0.

To verify the safety of the design, a more rigorous study of the expected flexure stress was conducted. Articles were fabricated to simulate sections of the slot lip and flexure region (Fig. 7). Separate sections simulate the geometry at blade station 10 and at blade station 37. Each specimen is approximately 4.5 in. long and includes three sets of blade attachment posts and adjustment screws. The screws, attachment bolts, posts, and flexure are identical in geometry to the wing design at STA 10 and STA 37. The remainder of the upper block (which simulates the Coanda nozzle top and slot lip) is an approximation of the actual contours. A flat horizontal lip replaces the slot lip to provide a flat surface for measurement of vertical deflection. Measurements were made of the vertical deflection of the lip using dial indicators positioned opposite the center of each of the three posts. Strain at the flexure (on the outer surface) was measured by resistance strain gauges bonded to the surface over the flexure and oriented in the chordwise and spanwise directions. Strain gauges were affixed at positions centered on an end post, centered on the center post, and midway between two posts. The primary gauges were part of bridges that included gauges mounted to the unstressed (but thermally equivalent) lower block. The adjustment screws were used to deflect the lip vertically in both directions over the anticipated range of the wing/rotor model. The positions were adjusted collectively with periodic checks on the sensitivity of stresses caused by deviations of a single position setting. Additionally, horizontal deflections of the upper block, as well as relative displacement of upper versus lower blocks, were also examined.

Data were recorded from the three strain gauge bridges (on each specimen) and the three dial indicators (input manually) on the Portable Data Acquisition and Monitoring System (PDAMS). Strain was computed based on the difference of the voltage ratio (V_{in}/V_{out}) between strained and unstrained conditions. Stress was then computed from the known modulus of elasticity for the material. The measured strain versus lip deflection slope for both flexure specimens was found to be about 45 percent of the predicted values, indicating that the analysis was highly conservative; see Figs. 8 and 9. Flexure strain was reduced at locations between posts by 60 and 20 percent for the STA 10 and STA 37 specimens, respectively. This is assumed to be due to the lack of structural stiffness at these locations where no post exists immediately behind the flexure. The lips appeared to be sufficiently stiff in the spanwise direction. Adjacent post screw settings could differ only by 0.001 in. at STA 10 and by 0.002 in. at STA 37 before extreme

force was required to advance the screws farther. This indicated that the risk of accidental damage of the Tipjet model flexure due to locally high deflections is minimal and that spanwise waviness of the lip would probably not be a problem.

Based on these test results, the flexure design was considered to be within acceptable safety criteria. The initial design analysis resulted in a Factor of Safety (FS) of 2.2 at the critical operating condition. This calculation was based on yield strength, not on ultimate strength. Furthermore, the tested yield strength of the actual model stock was used to compute FS.

ALUMINUM SPECIMEN TENSILE STRENGTH

To further support confidence in the model safety margins, tensile tests were conducted on samples of material taken from the aluminum stock used to fabricate the wing. Two specimens were cut for tensile testing in the direction of roll of the stock. Two other specimens were cut for testing perpendicular to the direction of roll. Results showed yield stresses of 64 ksi in the direction of roll and 61 ksi perpendicular to the direction of roll. (Published specifications for Al 7075-T5 indicate a yield strength of 66 ksi.) These test results were used for all safety factor calculations in the model stress analysis.

TEST DESCRIPTION

Tests were conducted with the Tipjet model rotor in four distinct modes of operation to investigate different attributes of the rotor system in the areas of: CC Rotor Performance, Reaction-Drive System Performance, Integrated Lift/Drive System Performance, and Special Tests. The modes of operation were:

1. Rotor locked. Allowed validation of tip-jet nozzle performance and measurement of system airflow rate under static conditions.
2. Electric motor drive.

   Tip-jet nozzles closed/slots open. Allowed validation of model lifting system by comparison with other CC rotors; also permitted isolation of lift system performance.

   Tip-jet nozzles open/slots closed. Allowed measurement of tip-jet nozzle performance under dynamic conditions.
3. Simultaneous electric motor and tip-jet drive. Allowed controlled (fixed V_t) exploration of integrated pneumatic lift/drive system performance.
4. Tip-jet self-drive. Allowed investigation of integrated lift/drive system performance in complete equilibrium.

With CC slot height and tip-jet nozzle area set by ground adjustment, the only controlling variables during testing were blade pressure and, if the electric motor was used, rotor tip speed. The test was therefore composed of (1) sweeps of blade pressure at either constant or variable V_t, and (2) sweeps of tip speed at nominally constant blade root pressure. Due to the bi-directional nature of the wing/rotor, hover tests were conducted with both clockwise (viewed from above) and counter-clockwise rotation with the majority of work in the counter-clockwise direction.

CC ROTOR PERFORMANCE

To investigate the performance of the CC lifting system, the tip-jet nozzle modules were replaced with solid plugs which continue the elliptical outer contour of the outboard blade section. Without CC slots, this tip region essentially is a section of nonlifting blade span. For this test, the rotor was shaft-driven by means of the electric motor. Testing began in this mode with a slot height setting of 0.013 in., which is consistent with the slot height-to-chord ratios tested on previous CC rotors. Once the basic model functionality was validated, the slot heights were reduced to 0.002 to 0.005 in., which are representative of values compatible with the Tipjet rotor design. Table 5 lists the runs in this mode with the nominal values of the control settings and operating conditions.

REACTION-DRIVE SYSTEM PERFORMANCE

The performance of the tip-jet drive system was evaluated with both leading edge and trailing edge slots taped over so that all airflow was ejected at the tip nozzles. In this configuration, very little lift was produced. With the rotor shaft locked, the rotor balance yaw moment measurement was used to derive the effective drive force at the tip nozzles and, thus, the nozzle performance coefficients. The nozzles were tested in this static mode separately and in pairs on both the leading edge and trailing edge of the blades.

The effects of rotation on nozzle performance were evaluated by using the electric motor to hold V_t constant at various levels while simultaneously operating the tip nozzles over a range of blade pressures. In this mode, the Lebow torque sensor measures the net torque required by the motor to maintain equilibrium at the desired V_t. The change in this net torque from the value corresponding to zero blade pressure represents the drive torque output of the tip nozzles. A summary of the runs made to evaluate the drive system in both static and dynamic modes is presented in Table 6.

INTEGRATED LIFT/DRIVE SYSTEM PERFORMANCE

The ultimate goal of the test was to determine the aerodynamic properties of the model rotor in the tip-jet self-drive mode. In this mode, the tip nozzle reaction force supplies all of the rotor drive power. Lift is produced simultaneously as a fraction of the air supply is used for CC. The rotor establishes an equilibrium tip speed at which the drive torque is balanced by the rotor torque (profile + induced) and bearing friction. On the DTMB hover stand, the motor was electrically disconnected, the drive belt remained connected, and the motor was allowed to free-wheel. No direct measurement of the drive system output was made during these tests since, for reaction drive, there is no net torque on the system.

The nature of rotor tip speed response to pressure input was uncertain at the outset of the test. The rotational response was especially critical due to structural limitations of the model, which set the maximum safe tip speed very near the desired operational condition. For these reasons, the test plan was adapted to map out the integrated system performance for a given slot height configuration prior to operating in the nozzle self-drive mode. The electric motor was used to hold tip speed constant at several levels while blade pressure, and thus nozzle drive force, was varied. Consequently, in this testing mode, the rotor torque reading was a measurement of the net torque shortfall that had to be supplied by the drive motor. Table 7 is a summary of the runs made to evaluate the performance of the integrated system in both equilibrium and constant V_t modes.

SPECIAL TESTS

Flowing Plenum Effect

Surveys of the CC slot exit pressure were conducted for a range of blade root pressures with the tip nozzle both open and closed. This test was conducted to quantify the static pressure drop within the blade duct due to the velocity of the airflow supplying the tip nozzles. The measurements were made using a probe fabricated from metal tubing. The probe end was flattened into an elliptical shape and filed to an outer width of about 0.011 in. This was sufficiently narrow to allow the probe tip to be inserted at the CC lip to get an accurate reading of total pressure. (Due to probe size, the slot exit pressure survey was conducted only at the 0.013-in. slot height setting.) The measurements were read from a Wallace and Tiernan dial gauge and recorded manually (not included in the digital data base).

CC Slot Taping

Analysis of early test results indicated that the region at the blade tip occupied by the tip nozzle may have a profound impact on the power requirements of the rotor. Previously tested CC rotors were designed with CC slots extending virtually to the blade tip. In addition, the position of the inboard end of the CC slots on the Tipjet model was substantially farther outboard than that of earlier rotors. To quantify the effect of the "nonlifting" blade tips and the increased root "cutout" of the Tipjet rotor, a series of tests was conducted wherein these regions were extended by incrementally taping over portions of the CC slots. For this testing, the tip nozzles were closed, and the electric motor was used for rotor drive.

A few test runs were devoted to taping over portions of the CC slots to study miscellaneous phenomena. Periodic interruption of the slot flow was investigated by applying 0.1-in. wide tape strips over the slots at 2-in. intervals along the span. The performance of very narrow spanwise CC slots near the blade tips was demonstrated. Also, taping of the slots was used as a quick method of temporarily reducing the total slot area (in lieu of tedious slot height adjustments) in attempts to produce high equilibrium tip speeds in the tip-jet self-drive mode. The runs which used CC slot taping and brief descriptions of the configu: ations are presented in Table 8.

Coanda Trips

Runs 85 and 86 were to investigate the effect of reducing CC augmentation by "tripping" the jet flow and inducing jet detachment. In Run 85, a length of nylon monofilament fishing line was taped to the Coanda surface near the trailing edge extending the full span of the slots. In Run 86, the monofilament line was replaced with lengths of plastic tape which provided a narrower ridge transverse to the flow direction.

Grit Strips

Runs 141 and 142 were to verify that performance characteristics were not due to low Reynolds number laminar flow over the airfoil surfaces. Garnet grit (#60) was applied in 1/4-in. strips along the upper surfaces of the blades at the 18-percent chord position.

Jet Flap Nozzles

In an attempt to produce a full-span lift distribution, a pair of closed nozzle modules was modified to a jet flap configuration. A line of holes (0.0625-in. diameter) was drilled through the underside of the modules so that, when

pressurized, the modules would eject a jet sheet which fixes the stagnation point. Testing was conducted with the slot height set at 0.003 in. and the model rotating clockwise (Runs 119 to 121 and 129 to 131). These modified modules also were tested with the CC slots taped (Run 137).

Static Mass Flow and Slot Height Checks

In most configurations of slot height and tip nozzle opening, a blade pressure sweep was conducted with the rotor shaft locked (rpm=0). Data from these test runs were used to validate airflow rate measurements and to monitor slot flexibility (i.e., change in slot height due to internal pressure). Table 9 lists the runs in this test category.

Tares

Prior to installation of the wing/rotor, the test stand was operated to determine the tares due to pneumatic pressure (Fig. 10) and bearing friction (Fig. 11). The pressure tare was subtracted from the measured balance forces during the initial data reduction. Due to its effects on rotor equilibrium, the friction tare was not generally subtracted from the measurements. In some analyses, however, data are presented with a correction for bearing friction.

RESULTS AND ANALYSIS

CC ROTOR PERFORMANCE

General plots of performance data are presented in Figs. 12, 13, and 14 representing the effects of slot height, tip speed, and direction of rotation, respectively. Each set of plots consists of 10 figures depicting:

Thrust Coefficient / Solidity versus Rotor Blowing Coefficient / Solidity
Rotor Thrust (lb) versus Blade Root Pressure Ratio
Rotor Thrust (lb) versus Blade Root Pressure (psig)
Air Flow Rate (lb/sec) versus Blade Root Pressure (psig)
Shaft Power Coefficient / Solidity versus Thrust Coefficient / Solidity
Total Power Coefficient / Solidity versus Thrust Coefficient / Solidity
Shaft Figure of Merit versus Thrust Coefficient / Solidity
Total Figure of Merit versus Thrust Coefficient/ Solidity
Shaft Figure of Merit versus Disk Loading (lb/ft^2)
Total Figure of Merit versus Disk Loading (lb/ft^2)

Data presented in Figs. 12 through 14 have not been corrected for the bearing friction tare. Consequently, parameters representing rotor power are biased somewhat high. This effect is evident in Fig. 13 at the low tip speeds.

For CC rotors, lift (thrust) is determined by the level of momentum in the jet sheet, expressed in nondimensional form as the jet momentum coefficient, $C_\mu = w / g * V_o / (\rho A V_t^2)$. Figure 15 shows the measured rotor thrust coefficient as a function of momentum coefficient for the model operating as a simple CC rotor (i.e., tip-jet nozzles closed) at various settings of the slot exit height. The lift gain, or augmentation ratio, is the slope of this curve and is the measure of efficiency of converting the slot flow momentum into lift. The augmentation rate of 29 in Fig. 15 is higher than that on any of the several previous CC rotors. The highest augmentation ratio measured during this test was 35 (Run 124, V_t = 500 ft/sec, h = 0.003 in., clockwise rotation). Of particular significance is that high augmentation was demonstrated at the very small slot height settings appropriate for the pneumatic rotor. The CC augmentation was observed to be sensitive to the rotation rate, as exhibited in Fig. 16 where higher tip speeds result in enhanced efficiency. The generally high lift-gain performance of this model as well as the sensitivity to tip speed are the direct results of tailoring the airfoil selection for optimum hover performance at a tip speed of 500 ft/sec.

Further fundamental properties of CC lift are evident from the characteristics of the dimensional lifting performance parameters. Fig. 17 shows, dimensionally, the relation of rotor thrust to blade root pressure. The slight deviations from a purely linear response will be shown to relate to operational characteristics in the tip-jet self-drive mode. The nature of the deviations from a purely linear response to pressure varies with slot height setting (Fig. 18). Due to the functional relationship between C_l and C_μ, the lift of CC airfoils produces a uniquely linear dependence of rotor lift on tip speed, at constant pressure (Fig. 19). Because induced torque tracks lift and tip speed, these characteristics of the CC lift system will strongly influence the establishment of tip-jet self-drive conditions.

The shaft power characteristic of the lift system directly determines the drive torque requirement of the tip-jet nozzles. The relationship between rotor shaft power coefficient and thrust coefficient was found to be independent of both tip speed and slot height. The characteristic shaft power trend revealed in Fig. 20 is substantially greater than that of the theoretically ideal (optimum spanwise lift distribution) rotor. The level of induced power evident in these data exceeds that experienced by any previous CC rotor. Accordingly, extensive effort was dedicated to identifying the physical phenomenon responsible for this behavior; see Special Tests, CC Slot Taping.

To quantify the induced power characteristic of the rotor, a relationship was derived that specifies the ratio of induced power to profile power at the condition of maximum power efficiency, $(C_T/C_{P_s})_{max}$. From basic helicopter theory, at $(C_T/C_{P_s})_{max}$ the expected ratio of induced power to profile power is two ($C_{P_i} = 2 * C_{P_o}$). This ratio arises directly from the function describing the induced power term, $C_{P_i} = C_T^{1.5}/1.414$. If C_{P_i} is proportional to C_T^x, then at $(C_T/C_{P_s})_{max}$ the ratio of induced power to profile power is 1/(x-1).

The C_{P_s} versus C_T relationship for the model exhibited a $C_T^{1.6}$ dependency; thus it follows that $C_{P_i} = 1.7 * C_{P_o}$ at $(C_T/C_{P_s})_{max}$. Examination of the data in Fig. 20, however, shows that the level of C_{P_s} is about two times the no-lift value (with bearing friction removed), implying that $C_{P_i} = C_{P_o}$. It is evident that a more precise identification of the true lift-induced component of power is required.

To correctly identify the power components from the test data, the profile power coefficient was adjusted to reflect the known effect of CC blowing to reduce the C_{d_o} for the airfoil sections used on the model. Representative CC airfoil data indicate that the slot flow momentum reduces drag with roughly 70 percent efficiency (i.e., $\Delta C_d = 0.7 * C_\mu$). For convenience, the C_μ is converted to the corresponding C_T using the C_T/C_μ ratio of 29; hence, the true C_{P_i} is defined as $C_{P_i} = C_{P_s} - (C_{P_o} - 0.024 * C_T)$. The ratio of power components, C_{P_i}/C_{P_o}, at optimum C_T is then approximately 1.7 (Fig. 21), which is consistent with the $C_T^{1.6}$ dependency.

With the true C_{P_i} now correctly identified, an induced power factor, k, can be used to describe the ratio of actual induced power to ideal induced power at a given thrust level. Figure 22 shows values of k for the model rotor that were derived from the test data. The variation of derived k with C_T is consistent with the C_{P_i} dependency on $C_T^{1.6}$ rather than on $C_T^{1.5}$. This variation also accounts for the ratio of power components being less than two at the optimum C_T.

The high value of shaft power (represented by a high k) and the variation of k with lift are both attributed to rotor geometry. The only fundamental differences between the Tipjet rotor model and other CC rotors are the substantial region of nonlifting span at the blade tips and an extended lift "cutout" at the blade root. It is hypothesized that due to the abrupt dropoff in lift, a strong "tip" vortex is trailed from a blade span position near the outboard end of the slot. With the strength of this vortex determined by the degree of discontinuity of lift, the aerodynamic effect of a drastically reduced blade span is simulated, especially at high C_T. The shortened effective blade span, brought about by the sharply truncated lift distribution, theoretically would result in a significant penalty in induced power efficiency. At very low blowing levels, blade camber contributes a substantial

portion of the total lift resulting in a lift distribution that is relatively continuous across the end of the slot. The effect of truncating the CC slot inboard of the blade tip would not be evident at this condition.

Interpretation of the shaft power characteristics as evidence of a reduced effective blade radius is supported by correlation of the test data with analytical models. The DTMB performance program for CC rotors, CRUISE4, was successfully employed to replicate the test results. Using a distributed momentum inflow model in conjunction with a tip loss model based on C_T, the CRUISE4 results shown in Figs. 23 and 24 were obtained. Good correlation was achieved for both the lift response to CC blowing and the rotor shaft power requirement. The excellent agreement of C_{P_s} versus C_T is critically dependent on modeling the reduced effective rotor disk area for the inflow momentum calculations. Fig. 25 describes the tip loss model used to describe the "effective" lifting disk of the rotor.

A final consideration with regard to power required is the pneumatic power used to supply the CC slot airflow. Although shaft power is independent of slot height, the pneumatic power component is not. Figure 26 depicts the magnitude of the pneumatic power term as well as its sensitivity to the slot setting. As shown, it is somewhat less efficient to produce lift at the small slot settings. This is due to the necessarily higher slot exit jet velocity, and hence higher pumping power, corresponding to a given C_μ level at a reduced exit area. Note from Fig. 26 that the relationship between shaft power and lift is independent of the slot height setting.

In summary, the high induced power exhibited by the rotor is believed to be directly due to the allocation of a portion of the span for the drive nozzle. While unusually high with respect to conventional rotors, the induced power requirement of the pneumatic rotor does not necessarily preclude its feasibility in practical applications. Additionally, with the sensitivity of induced power to nozzle cutout now clearly revealed, blade/nozzle design changes can be made to minimize nozzle span length. There is also the possibility that in future designs the jet nozzle can be positioned or directed in a manner to improve the lift distribution and/or directly mitigate the effects of the tip vortex.

REACTION-DRIVE SYSTEM PERFORMANCE

The efficiency of reaction-drive rotors is vitally dependent on the pneumatic losses and gains within the blade. Figure 27 depicts the spanwise changes in duct centerline pressure measured under a variety of operating conditions. The loss of pressure due to friction in the blade duct and turning losses in the tip-jet nozzles

are more than offset by the centrifugal pressure rise resulting from the rotor pumping action. The demonstrated centrifugal pumping rise, even with flow through the nozzles, is essentially the theoretical value. With tip-jet nozzles closed and the model not rotating, duct centerline pressure measurements show no spanwise loss of blade total pressure due to slot flow. The same measurements reveal less than 2 percent loss with the nozzles operating. A further pressure loss is imposed by turning the flow through the tip-jet nozzle.

Figure 28 shows the tip-jet nozzle performance coefficients as derived from static tests of the torque generated by the nozzles. The nozzle thrust coefficient shown is referenced to the blade duct centerline internal pressure at 88 percent radius. (The nozzle parameters inherently incorporate any duct losses that are not manifested in the duct centerline pressure.) Although the nozzle geometry is quite simple and no turning vanes or other special devices are employed, nozzle efficiency is considered to be reasonably high (5-percent thrust loss). Also shown in Fig. 28 is the nozzle contraction coefficient that represents the effective exit area reduction, as might arise from flow separation in the nozzle. The composite effect of the internal duct flow and the nozzle losses on the effective total pressure delivered to the tip-jet nozzle exit is shown in Fig. 27.

The performance of the rotor drive system as a radial outflow turbine is determined by the duct and nozzle losses, the extent of centrifugal pressure rise, and the Coriolis power to accelerate the tip nozzle flow to the rotor tip velocity. Reaction-drive efficiency was assessed by sealing (taping) the CC slots to prevent the generation of lift, effectively isolating the drive system. The electric motor was then used to hold a constant rotational speed while the duct pressure was varied. The resulting changes in torque measurements indicate the net output of the tip-jet drive system.

Full nozzle static thrust capability is not realized during rotation due to the effects of accelerating the duct flow to the blade tip speed. This Coriolis penalty reduces the net nozzle torque according to the ratio of blade tip speed to nozzle jet exit velocity (V_t/V_j). This effect is illustrated in Fig. 29 where drive torque measurements are shown for three blade tip speed conditions as well as for the static case. By applying the theoretical factor representing the Coriolis influence ($Q_{rotating}/Q_{static} = 1 - V_t/V_j$), the three sets of data collapse onto the static performance line. This collapse indicates that no other significant factors influence torque available under rotating conditions.

The overall efficiency of the radial outflow turbine can be expressed as the output power generated by the nozzle drive divided by the energy of the air supplied at the blade root. This drive system efficiency is dependent on the

relative, and offsetting, pneumatic effects within the blades. In Fig. 30, the turbine efficiency is plotted against the tip velocity ratio based on the blade root pressure for all of the tip speeds and pressure settings tested. Comparing the data in Fig. 30 with the generalized radial outflow turbine efficiency described by Nichols (Ref. 4), shows the relationship corresponds to pressure losses equivalent to 20 percent of blade root energy.

INTEGRATED LIFT/DRIVE SYSTEM PERFORMANCE

It has been assumed in Tipjet conceptual vehicle design that the rotor lift and drive systems have no mutual aerodynamic interference and that their performance can be modeled separately. Data from the present test can now be used to validate this assumption. Direct superposition of the properties of the independent lift and drive systems can be compared to the net performance of the integrated rotor. Any deviations in this comparison represent interference effects between the systems.

Fig. 31 (V_t = 400 ft/sec) and 32 (V_t = 500 ft/sec) are summaries of the test results for the lift production and torque requirements of the CC lifting system as well as for the torque production of the tip-jet drive system. Data are included for three nominal slot height settings. The figure shows the sensitivity of rotor lift to the slot momentum flow level and the consequent result in changing rotor torque requirements. With a fixed tip nozzle exit area and constant V_t, the slope of drive torque available versus pressure is fixed. Lift system output must be adjusted, via slot setting, to match the fixed drive system output. As an initial approximation (assuming separable systems), the slot heights required for equilibrium at a tip speed can be found by locating points of intersection between the torque required and torque available curves.

Rotor torque as a function of lift and speed is found to be independent of the slot height setting; therefore, the map of rotor torque requirements in Fig. 33 is valid for all values of slot height. Superimposed on this figure is the isolated nozzle drive capability (for the nozzle size tested) at the corresponding tip speeds for a variety of blade pressures. The pneumatic rotor system naturally seeks an equilibrium rotational rate which balances the torque available from the nozzles with torque required by the lifting system. If interference effects are negligible and superposition applies, Fig. 33 can be used to estimate the blade pressure required to produce a desired lift at a given tip speed, assuming that the slot height has been adjusted appropriately to correspond to that lift.

Combined Shaft/Reaction-Drive Mode

The ultimate goal of the test was to determine the aerodynamic properties of the model rotor in the tip-jet self-drive mode. Due to the design of the model, the slot and nozzle areas are set prior to testing; therefore, during a test run, the only rotor control available is the air pressure supplied to the blade. The nature of rotor tip speed response to pressure input was uncertain at the outset of the test. The rotational response was especially critical due to structural limitations of the model, which set the maximum safe tip speed very near the desired operational condition. For these reasons, the test plan was adapted to map out the integrated system performance for a given slot height configuration prior to operating in the nozzle self-drive mode. The electric motor was used to hold tip speed constant at several levels while blade pressure, and thus nozzle drive force, was varied. Consequently, in this test mode, the rotor torque reading was a measurement of the net torque shortfall that had to be supplied by the drive motor.

The resulting "net" torque measurements are compared with the performance of the isolated lift and drive systems in Fig. 34. In this figure, the isolated rotor torque requirements at a series of slot area ratios and the isolated nozzle drive torque are presented for V_t = 400 ft/sec. Surprisingly, the net torque from the simultaneous operation of the slot and nozzle matches the results of combining the individual torque curves for the lift and drive systems. This agreement is typical of the test results and verifies that superposition of the distinct lift and drive systems does apply. Thus there appears to be no adverse effects of operating the nozzles in close proximity to the CC boundary layer control airflow. At the same time, these results imply that the tip nozzle flow has no favorable influence on the span loading distribution; that is, the induced power efficiency, k, is not improved. At the "zero net" torque point (Fig. 34), the retarding torque caused by the lifting system (as determined by slot height) is balanced by the torque drive capability of the nozzles at a common pressure control input for a slot area ratio of 9 percent. This point represents a condition where equilibrium can be achieved with tip-jet drive alone.

Also apparent in Fig. 34 is the nonlinear response (inflections) of the torque required to the pressure input. These inflections are the direct result of minor deviation from true linearity in the pressure-to-lift transfer function, as can be seen in Fig. 17. It will be shown subsequently that this characteristic has notable implications with regard to the tip speed response of the rotor when self-driven.

Tip-jet Self-drive Mode

Once the fundamental behavior of the rotor system was examined, the model was freed to operate in the tip-jet self-drive mode. With the motor drive disconnected and the configuration fixed, the blade pressure input is the only determining factor of the equilibrium operating condition. As shown in Fig. 35, at a given slot height setting, the response of the rotor is to increase the rotational rate until a limiting tip speed is reached. The limiting tip speed is a function of the slot height. Because CC-based lift is not solely dependent on local velocity, the lift response is not limited and continues to increase with pressure ratio regardless of the V_t behavior (Fig. 36). In fact, as shown in Fig. 37, the lift response is independent of tip speed and slot height for all of the tip-drive equilibrium conditions. Furthermore, the lift as well as the nozzle static thrust are both linear functions of the input pressure. These observations imply that the thrust gain factor (rotor lift divided by nozzle static thrust) is relatively constant at all conditions tested. Thus the pneumatic rotor system has the overall feature of converting the in-plane tip-nozzle static thrust into a vertical lift with a gain of five regardless of the equilibrium tip speed that results from the combination of flow exit areas.

The limiting tip speed characteristic of the rotor response is of particular interest. The condition that coincides with the onset of the tip speed limit is the ratio of the induced and profile (including bearing friction) torque components corresponding to optimum rotor performance. In Fig. 38, the rotor torque components are broken down for a typical set of performance data. It is hypothesized that the rotational rate increases to compensate for the difference between the nozzle drive power supply and the rate of absorption of induced power. As the effect of the induced component increases, due to higher pressure and higher V_t, the rate of V_t change declines. Eventually, a condition is reached where the increment in supply power due to an increase in pressure is completely consumed by the induced drag associated with lift production. Beyond this threshold, minor variability in the equilibrium tip speed can be attributed to the nonlinear rotor torque response exhibited in Fig. 34 that results in the torque required and torque available curves being nearly parallel over a large pressure range.

In more specific terms, the limiting velocity occurs when the rate of induced torque growth equals the rate of drive torque growth with respect to pressure. If the approximation is made that lift is linearly proportional to pressure, then the thrust scale in Fig. 33 can be viewed as a pressure scale, at least for a specific V_t. Furthermore, drive torque available can be approximated

as a linear response to blade pressure (Fig. 29). Limiting V_t occurs when the rotor torque required curve and the drive torque available curve produce a tangency point. The locus of tangency points also constitutes the conditions for optimum rotor aerodynamic efficiency (maximum L/Q). Thus there is an association between peak velocity with peak aerodynamic efficiency.

In the ideal case of a linear pressure-to-lift response at constant tip speed, increasing pressure from the condition of limiting velocity will cause a shortfall in drive torque, and the rotor will slow to re-establish $Q_{noz} = Q_i + Q_o$. Lift, however, will continue to increase directly from the increasing pressure. In Fig. 35, the suggestion of more than one limiting speed is really a wavering of maximum V_t due to the inflections in the torque required curves, as noted in regard to Fig. 34.

With these concepts and the unique properties of CC aerodynamics, the remarkable finding that lift is independent of tip speed and slot height can now be explained (Fig. 37). Initially, at low pressure, the rotor accelerates rapidly, because Q_i (lift) is low and therefore the power is consumed by Q_o. This increase in V_t effects an increase in lift through a $\sqrt{Q_0}$ relationship:

$$L \sim P_R A_S V_t \sim P_R A_S \sqrt{Q_0 / C_{P_0}} .$$

At higher lift associated with increased speed and pressure, Q_i begins to absorb the drive torque at a rate approaching the rate of delivery. The lift increases in accordance with

$$L \sim \sqrt{Q_i V_t / k} .$$

In this context, Q_i represents all power directly related to producing lift including that for slot flow pumping. The net result is that both components of power have the same functional relationship between lift and torque. Therefore, no matter how the drive torque is distributed between Q_o and Q_i, the gain in lift is essentially the same.

SPECIAL TESTS

Flowing Plenum

It was expected that the high duct flow rate supplying the tip jets would reduce the pressure available at the CC slot to produce jet momentum. Reduction arises directly from static pressure changes and from increases in viscous losses. To quantify this "flowing plenum" effect, CC slot exit (h=0.013 in.) total pressure

was measured along the span for several values of blade root pressure (Fig. 39). Slot exit pressure at the outboard end of the blade is reduced by 18 percent relative to the root end pressure. (There is no discernible reduction in slot pressure when the nozzles are closed.) About half of this loss can be attributed directly to the static pressure changes with the remainder due to viscous (total pressure) losses. Note that at the location of maximum pressure within the tip-jet nozzle exit flow, the pressure is only 4 percent lower than that measured at the blade root.

The result of the spanwise drop in effective slot exit pressure can be seen in Fig. 40 where rotor lift is plotted versus blade root pressure for configurations with and without tip nozzle flow. The reduced lift corresponding to the run with nozzle flow is consistent with the measured spanwise pressure drop measured statically. This is verified in Fig. 41 where the reference blade pressure ratio for the case with the nozzles open is corrected for an 8-percent (average) static pressure drop.

CC Slot Taping

The cause of the excessive induced power was suspected to be the nonlifting regions of tip and root blade span. To verify this speculation, a series of tests was conducted wherein these regions were extended by taping over portions of the CC slot. Figure 42 shows the increase in shaft power requirement corresponding to incrementally increasing the extent of taping at the tip and the root. The composite effect of taping the slot to effectively double the nonlifting span at the tip and of incrementing the position of the inboard lift "cutout" is seen in Fig. 43. When the sensitivities of power to the extent of unblown root and tip sections are applied to the baseline (no tape) data set, the C_{P_s} versus C_T relationship is very close to that of other full-span slot CC rotors (Fig. 44).

Coanda Trips

Results from the test runs where boundary layer trips had been installed on the Coanda surfaces are shown in Figs. 45. While the trips effectively reduced the augmentation rate, there was no discernable effect on the power requirement characteristics of the rotor. These results are consistent with the finding that the induced power effects are dominated by the spanwise lift distribution on the blade.

Grit Strips

As expected, the grit strips had no effect on rotor performance (Fig. 46). Most likely, the leading edge slot lip (0.005-in. step) acts as a trip to transition the flow.

Jet Flap Nozzles

The testing of the jet-flap nozzle modules produced results which were inconclusive. Fig. 47 shows that the addition of the jet-flap modules failed to produce an expected increase in rotor lift. The jet-flap ejection holes were enlarged but still produced no measurable increase in lift. Even when tested in isolation (Run 137, with the CC slots completely taped over), the jet-flap modules did not produce a positive lift increment. Resources were not available to pursue this investigation further, and the results remain an anomaly.

Static Mass Flow and Slot Height Checks

The results of the static (no rotation) blowing tests are shown in Figs. 48 and 49. Using mass flow and pressure measurements, the effective slot exit area was deduced for nominal zero-pressure slot settings of 0.002, 0.003, and 0.005 in. (Fig. 48). The consistent slope of slot height versus pressure is substantial, especially at the smallest setting where expansion results in a 75-percent increase in slot area at high pressure. This characteristic influences rotor behavior by enhancing the lift (and torque) increment resulting from an increase in supply pressure. Fig. 49 shows the typical distribution of the air supply between the CC slots (12 percent) and the tip nozzles (88 percent).

Tares

Prior to installation of the rotor model on the hover stand, tare data were collected. With the hub sealed and not rotating, balance measurements were recorded as plenum pressure was varied. The sensitivities measured for the four rotor balance channels are:

d /d(Plenum)	
Lift	-0.0095 lb/psig
Yaw	-0.2477 ft-lb/psig
Pitch	+0.0111 ft-lb/psig
Roll	-0.0105 ft-lb/psig

The sensitivity of yaw moment to plenum pressure (Fig. 10) was accounted for in the data reduction program; other sensitivities are insignificant.

The shaft bearing friction tare was assessed by varying the rotational rate with the plenum both pressurized and unpressurized. Fig. 11 shows the measured torque at the Lebow sensor at a constant level of -1 ft-lb regardless of

the rotation rate. Runs during the course of the test led to a more refined calculation of rotor torque due to friction of 2.5 ft-lb. Furthermore, friction was found to be a function of both lift (bearing load) and direction of rotation (bearing/belt wear patterns). The following formulas can be used to correct rotor torque measurement for the effect of bearing friction:

Clockwise rotation

ΔQ (ft-lb) = 2.5 + 0.019 * Lift (lb)

Counter-clockwise rotation

ΔQ (ft-lb) = 2.5 + 0.031 * Lift (lb)

Due to difficulties in interpreting the meaning of the friction measurement during tip-drive (equilibrium) runs, the torque tare was not directly applied in the data reduction. To accurately identify the rotor aerodynamic characteristics, some of the data presented are with a correction to the measured torque.

SUMMARY AND CONCLUSIONS

A comprehensive hover test of the Tipjet model rotor was conducted to provide the data base needed to evaluate the Tipjet VTOL Aerial Vehicle concept in hover. Basic model performance was compared to that of a previous CC rotor model to validate the model functionality. Tip-jet nozzle performance was compared to the data base produced as a result of static tests of a duct/nozzle model. Lift and drive system performance was evaluated both separately and collectively to identify mutual interference effects and the behavior of the integrated system.

Fundamental parameters were identified that determine the performance of a fully pneumatic rotor system. Due to the combined characteristics of pneumatic lift augmentation by circulation control and pneumatic reaction-drive, the rotor lift is the same constant, essentially linear, function of blade pressure regardless of rotational speed. This relationship results in lift equaling five times the tip nozzle static thrust and is valid over the full range of operating conditions.

Internal flow losses are low and, combined with the centrifugal pressure rise, result in an effective nozzle drive pressure higher than the root pressure. Lift gain from the slot flow (augmentation ratio of 29) was the highest yet experienced on a CC rotor. In contrast, test results reveal significantly higher induced power due to the nonlifting tip nozzle region and to the larger region of nonblowing span at the root of the blade. This span loading effect was quantified and is sufficiently understood to allow for performance improvements by design

optimization. The rotor rotational speed displays a self-limiting behavior. The onset of the limiting speed condition is related to the optimum aerodynamic efficiency condition of the rotor.

ACKNOWLEDGMENTS

The author expresses appreciation to the following CDNSWC individuals for their valuable contributions and support:

Mr. Ernest Rogers provided valuable advice and assistance during the test activity and contributed substantially to the data analysis presented, as excerpted from Ref. 5.

Mr. Fred Behnaz designed the Tipjet wing/rotor model and provided technical assistance during fabrication.

Mr. Eugene Schwartbart, the principal NC programmer and machinist, produced a quality model essential to the success of the test program.

(This page intentionally blank)

REFERENCES

1. Reader, K.R., J.S. Abramson, A.W. Schwartz, and J.C. Biggers, "Tipjet VTOL UAV Summary: Volume I - 1200-Pound Tipjet VTOL Unmanned Aerial Vehicle," Report DTRC/AD-8901 (Jan 1989).
2. Schwartz, A.W., "Tipjet VTOL UAV 80-Inch Powered Wing/Rotor Conceptual Description and Design Specifications," CDNSWC, Code 169, (Feb 1989).
3. Behnaz, F.F., "Tipjet VTOL UAV Blade Stress Analysis," CDNSWC, Code 1431 (Jul 1989).
4. Nichols, J.B., "The Pressure-Jet Helicopter Propulsion System," Aeronautical Journal (Sep 1972), pp.552-565.
5. Schwartz, A. and E. Rogers, "Hover Evaluation of an Integrated Pneumatic Lift/Reaction-Drive Rotor System," AIAA 92-0630, Presented at the 30th Aerospace Sciences Meeting and Exhibit, Reno, Nev. (Jan 1992).

(This page intentionally blank)

APPENDIX A

DERIVED PARAMETERS AND CONSTANTS

Parameters are listed as they appear in the final data reduction listings. Included for each parameter is the function defining its value and a brief description of the quantity (including units). Parameter definitions also are provided for the constants used in calculations of the derived parameters.

Derived Parameters:

Mnemonic	Function	Description / Comments
AREA	Pi * RADIUS**2	ROTOR DISK AREA
PATM	FLOAT(IPATM) / 1000	ATMOS. PRESSURE (PSI)
TATM	TAMB + 125	ATMOS. TEMPERATURE (DEG F)
RHO	PATM*144 / (G * R * (TATM+459.6))	ATMOS. DENSITY
RPM	RPMdat	ROTOR RPM
OMEGA	RPM * 2 * Pi / 60	ROTOR ROTATIONAL SPEED (RAD/SEC)
VTIP	OMEGA * RADIUS	ROTOR TIP SPEED (RADIUS=3.33 FT)
QTIP	0.5 * RHO * VTIP**2	ROTOR TIP DYNAMIC PRESSURE (PSF)
ZMTIP	SQRT(5.0*((PATM + QTIP/144) / PATM)**EXP1 - 5.0)	ROTOR TIP MACH NUMBER
DENOM1	RHO * VTIP**2 * AREA	GEN. PURPOSE DENOMINATOR
DENOM2	DENOM1 * RADIUS	GEN. PURPOSE DENOM.
DENOM3	DENOM1 * VTIP	GEN. PURPOSE DENOM.
DPVENT	XDPVENT	VENTURI DELTA PRESS. (PSI)
PVENT	XPVENT	VENTURI STATIC PRESS. (PSI)
TVENT	XTVENT + 125	VENTURI TEMPERATURE (DEG F)
SMDOT	FROM SUBROUTINE WTFLOW	VENTURI MASS FLOW RATE (LB/SEC)
PRROOT	(PATM + PMID25(1)) / PATM	BLADE ROOT PRESSURE RATIO (PSF)
PRTIP	(PATM + PMID88(1)) / PATM	BLADE OUTBOARD PRESS. RATIO
TPLEN	XTPLEN + 125	ROTOR PLENUM TEMP. (DEG F)
CCMACH	SQRT(5.0 * (PRROOT**EXP1 - 1.0))	BLADE ROOT JET MACH NUMBER
TJMACH	SQRT(5.0 * (PRTIP**EXP1 - 1.0))	TIPJET NOZZLE JET MACH NUMBER
CCVJET	SQRT(GAM * G * R * (TPLEN+459.6)) * CCMACH /SQRT(1.0*CCMACH**2)	BLADE ROOT JET VELOCITY (FT/SEC)
TJVJET	SQRT(GAM * G * R * (TPLEN + 459.6)) * TJMACH /SQRT(1.0 + 0.2 * TJMACH**2)	TIPJET NOZZLE JET VELOCITY (FT/SEC)
HPPNEU	SMDOT * (TPLEN+459.6) * (PRROOT**EXP1 - 1.0) * J * CP / 550	PNEUMATIC HP FOR CC/TJ
TORQUE	TORQ	ROTOR SHAFT TORQUE (FT-LB)
HPSHFT	TORQUE * OMEGA / 550	ROTOR SHAFT HORSEPOWER (TORQUE FROM LEBOW SENSOR)
HPTOT	HPPNEU + HPSHFT	TOTAL ROTOR HORSEPOWER
CT	ZLIFT / DENOM1	ROTOR THRUST COEFFICIENT (ZLIFT FROM ROTOR BALANCE)
CMY	YAW / DENOM2	ROTOR YAW COEFFICIENT (YAW FROM ROTOR BALANCE)

Mnemonic	Function	Description / Comments
CMP	PITCH / DENOM2	ROTOR PITCH MOMENT COEFF. (PITCH FROM ROTOR BALANCE)
CMR	ROLL / DENOM2	ROTOR ROLL MOMENT COEFF. (ROLL FROM ROTOR BALANCE)
CPSHFT	HPSHFT * 550 / DENOM3	SHAFT POWER COEFFICIENT
CPPNEU	HPPNEU * 550 / DENOM3	PNEUMATIC POWER COEFFICIENT
CPTOT	HPTOT * 550 / DENOM3	TOTAL POWER COEFFICIENT
CTSIG	CT / SIGMA	CT OVER SOLIDITY
CMYSIG	CMY / SIGMA	CMY OVER SOLIDITY
CMPSIG	CMP / SIGMA	CMP OVER SOLIDITY
CMRSIG	CMR / SIGMA	CMR OVER SOLIDITY
CPSSIG	CPSHFT / SIGMA	CPSHFT OVER SOLIDITY
CPPSIG	PPNEU / SIGMA	
CPTSIG	CPTOT / SIGMA	CPTOT OVER SOLIDITY
FMSHFT	0.707 * CT**1.5 / CPSHFT	ROTOR FIGURE OF MERIT (SHAFT)
FMTOT	0.707 * CT**1.5 / CPTOT	ROTOR FIGURE OF MERIT (TOTAL)
CMUR	SMDOT / G * CCVJET / DENOM1	CC MOMENTUM COEFF. (SMDOT=LB/SEC)
CMURS	CMUR / SIGMA	ROTOR C_μ OVER SOLIDITY
DISCLD	ZLIFT / AREA	ROTOR DISK LOADING (PSF)
WINGLD	DISCLD / SIGMA	WING LOADING (PSF)
ZLOVM	ZLIFT / SMDOT	ROTOR LIFT/UNIT AIRFLOW (LB/LB/SEC)
SMCORR	SMDOT * SQRT(TVENT + 459.6)/ (PVENT + PATM)	VENTURI WEIGHT FLOW (CORRECTED)
VPRAT	PPVENT / (PVENT + PATM)	VENTURI PRESSURE RATIO
ADUCT	HDUCT * WDUCT	NOZZLE ENTRANCE AREA (IN^2)
WDOVWN	WDUCT / WNOZ	NOZZLE WIDTH CONTRACTION RATIO
ANOZ	ANOZ/1000.	NOZZLE EXIT AREA (IN^2)
ADOVAN	ADUCT / ANOZ	NOZZLE CONTRACTION RATIO
THRNOZ	YAW / RPRIM	TIPJET NOZZLE THRUST (LB)
VJNOZ	THRNOZ / SMDOT * G	TIPJET NOZZLE JET VELOCITY (FT/SEC)
PTJ	PATM/(1.0-(VJNOZ**2/((2*GAM*R*G)/ (GAM-1))/(TPLEN+459.6)))**3.5-PATM	DERIVED NOZZLE EXIT PRESS. (PSI)
PJOVPD	PTJ / PMID88(1)	RATIO OF NOZZL EXIT/ ENTRANCE PRESSURE
PR	PATM / (PMID88(1) + PATM)	NOZZLE EXIT PRESS. RATIO

Mnemonic	Function	Description / Comments
AJIDL	SMDOT / G / (PMID88(1)*COEFF1* SQRT(GAM/(R*G)/(TPLEN+459.6)))	NOZZLE ENTRANCE AREA (IDEAL) (FOR PR <= 0.528)
AJIDL	SMDOT / G / (PMID88(1)*SQRT((2* GAM/ ((GAM-1.)*R*G)/(TPLEN+459.6))* (PR**(2/GAM)- PR**((GAM+1)/GAM))))	NOZZLE ENTRANCE AREA (FOR PR > 0.528) (IDEAL)
CD	AJIDL / ANOZ	NOZZLE DISCHARGE COEFFICIENT
VJIDL	SQRT((2*GAM*R*G/(GAM-1)) * (TPLEN+459.6)*(1.0 - PR**EXP1))	NOZZLE IDEAL JET VELOCITY (FT/SEC)
CV	VJNOZ / VJIDL	NOZZLE VELOCITY COEFFICIENT
CC	CD / CV	NOZZLE CONTRACTION COEFF.
HNOZ	ANOZ / WNOZ	NOZZLE EXIT HEIGHT
RNOVWN	RNOZ / WNOZ	NOZZLE RADIUS-TO-WIDTH RATIO
ZLNOVW	ZLNDZ / WNOZ	
ANGLE	ATAN(ROLL / PITCH) * 180 /Pi	NOZZLE JET EJECTION ANGLE (DEG)

Constants:

Mnemonic	Value	Desciption / Comments
EXP1	0.2857	(GAM -1) / GAM
Pi	3.141592654	
G	32.174	ACCELERATION DUE TO GRAVITY
R	53.35	GAS CONSTANT
RADIUS	3.333	ROTOR RADIUS: 40 INCHES, 3 1/3 FEET
GAM	1.4	RATIO OF SPECIFIC HEATS
J	778.26	
CP	0.240	SPECIFIC HEAT, CONSTANT PRESS.
SIGMA	0.11003	ROTOR SOLIDITY
COEFF1	0.578703	(2/(GAM+1))**((GAM+1)/ (2*(GAM -1)))
RPRIM	3.2223	RADIUS TO NOZ EXIT CENTERLINE
WDUCT	2.872	NOZZLE ENTRANCE WIDTH (IN)
HDUCT	0.530	NOZZLE ENTRANCE HEIGHT (IN)
WNOZ	1.91	NOZZLE EXIT WIDTH (IN)
ZLNOZ	1.33	NOZZLE LENGTH (IN)

The final data, designated Version No. 1010, were processed using the EXCEL spreadsheet program to update selected parameters and to create new parameters. Equations used for these computations are:

Data Corrections:

HPPNEU* = HPPNEU / (PR ^ 0.2857)

(to correct for "compressor" inlet temperature; assumes 100-percent efficiency)

HPTOT* = (HPPNEU*) + HPSHFT

CPPNEU* = (HPPNEU*) * 550 / DENOM

CPTOT* = (HPTOT*) * 550 / DENOM

CPPNEU/S* = (CPPNEU*) / 0.11003

CPTOTAL/S* = (CPTOT*) / 0.11003

FMTOT* = 0.707 * (CT ^ 1.5) / (CPTOT*)

TJVJET* = TJVJET * SQRT ({TPLENUM + 459.6 + [(0.88 * VTIP) ^ 2/ 12019.07]} / {TPLENUM + 459.6})

(12019.07 = 2 * 32.174 * 778.26 * .24)

Data Additions:

VT/V0 = VTIP / CCVJET

VT/VJ = VTIP / (TJVJET*)

CT/CPS = CT / CPSHAFT

CT/CPTOT = CT / (CPTOT*)

TORQUEF = TORQUE - 2.5 - LIFT * {[0.019 * (RUN < 103)] + [0.031 * (RUN > 102)]}

(0.019 for CCW rotation; 0.031 for CW rotation)

HPSHFTF = TORQUEF * VTIP / 3.333 / 550

CPSHFTF = HPSHFTF * 550 / DENOM

FMSHFTF = 0.707 * (CT ^ 1.5) / CPSHFTF

where:

DENOM = RHO * (VTIP ^ 3) * 34.8996 (area = 34.8996)

(This page intentionally blank)

APPENDIX B

RUN LOG

The run log summary for the Tipjet 80-in model wing/rotor hover test is presented in this appendix. The configuration and details of the operating conditions are described for each test run.

RUN NO.	POINT NOS. FIRST/LAST	NOZZLE POS. #1 LE	#1 TE	#2 LE	#2 TE	SLOT POS. #1 LE	#1 TE	#2 LE	#2 TE	MODE	RPM	BLADE PRESSURE RANGE (PSI)	COMMENTS	DATE
1	1/2												Dummy data for code debug	
2	3/3									OTH			Rotor bal. internal shunts	7/2/90
2	4/4									OTH			Sample venturi data	7/10/90
3	5/12									OTH			Venturi flow sweep	7/12/90
5	18/32									OTH			Pressure Tares	7/19/90
6	33/50												Friction Tares, No pressure	7/23/90
7	51/60												Friction Tares, 1000 rpm, press.	7/25/90
8	61/69	C	C	C	C					OTH			Debug runs, low press, rpm = 0	2/1/91
9	70/79	C	C	C	C	C	Open	C	Open	OTH	0-550		Dyn. Balance, braces off	2/6/91
10	80/100	C	C	C	C	C	Open	C	Open	OTH	550-1500		Dyn. Balance, braces off	2/6/91
11	101/115	C	C	C	C	C	Open	C	Open	OTH	300-1500		Dyn. Balance, braces off	2/6/91
12	116/129	C	100%	C	100%	C	Taped	C	Taped	NOZ	0		Crude nozzle perf, 100% open	2/6/91
13	130/137	C	100%	C	100%	C	Taped	C	Taped	CCTJ	0-260		Drive belt connected	2/6/91
14	----												Tape drive malfunction	
15	138/155	C	C	C	C	C	.013	C	.013	CCSH	1000	0-7	CC performance, V_T = 350	2/7/91
16	156/171	C	C	C	C	C	.013	C	.013	CCSH	1150	0-5.8	CC performance, V_T = 400 fps	2/7/91
17	172/185	C	C	C	C	C	.013	C	.013	CCSH	1290	0-4.8	CC performance, V_T = 450 fps	2/7/91
18	186/200	C	C	C	C	C	.013	C	.013	OTH	0	0-8	Airflow rate, press. gradients	2/7/91
19	201/218	C	C	C	C	C	.013	C	.013	OTH			Repeat Run 18	2/8/91
20	219/233	C	C	C	C	C	.013	C	.013	CCSH	1290	0-6	CC perf., V_T = 450, 500	2/8/91
	234/246										1433	0-5		
21	247/263	C	C	C	C	C	.013	C	.013	CCSH	1000	0-7	CC perf., V_T = 350, 400	2/8/91
	264/280										1150	0-6.5		
22	281/301	C	C	C	C	C	.013	C	.013	CCSH	716	0-11.7	CC perf., V_T = 250 fps	2/8/91
	302/305										1000-1433	No Blowing	Constant pressure	
	306/313										1433-1000	2 psi	RPM sweeps	
	314/320										1000-1433	4 psi		
	321/323												Misc. pts.	
23	224/342	C	C	C	C	C	Taped	C	Taped	OTH	0	0-10 psi	Transducer check	2/15/91
24	343/347	C	C	C	C	C	Taped	C	Taped	OTH	0	0	Check Loads	2/20/91
25	348/359	C	C	C	C	C	Taped	C	Taped	CCSH	0-1433	0	Cent. press. dist.	2/20/91

* CCSH-CC/SHAPT DRIVE; CTJ-CC/TIPJET; NOZ-TIPJET NOZZLE PERF; OTH-OTHER

RUN NO.	POINT NOS. FIRST/LAST	NOZZLE POS. #1 LE	#1 TE	#2 LE	#2 TE	SLOT POS. #1 LE	#1 TE	#2 LE	#2 TE	MODE	RPM	BLADE PRESSURE RANGE (PSI)	COMMENTS	DATE
26	360/376	C	C	C	C	0	Taped	0	Taped	CCSH	800,1433	0-5	Cent. press. dist.	2/20/91
27	377/388	C	C	C	C	0	.013	0	.013	CCSH	0-1433	0	CC Perf., No blowing	2/20/91
	389/410										573	0-8	V_T = 200 fps	
28	411/432	C	C	C	C	0	.013	0	.013	CCSH	716	0-10	CC Perf., V_T = 250 fps	2/20/91
	433/453										859	0-9	V_T = 300 fps	
29	454/476	C	C	C	C	0	.013	0	.013	CCSH	1002	0-10	CC Perf., V_T = 350 fps	2/20/91
	477/494										1146	0-7	V_T = 400 fps	
30	495/509	C	C	C	C	0	.013	0	.013	CCSH	1289	0-7	CC Perf., V_T = 450 fps	2/20/91
	510/522										1433	0-6	V_T = 500 fps	
31	523/528	C	C	C	C	0	.013	0	.013	OTH	0	0	Check Loads	2/21/91
32	529/535	C	C	C	C	0	.013	0	.013	CCSH	600-1400	No Blowing	CC Perf.	2/21/91
	536/540											1	RPM Sweeps at	
	541/545											2	constant blade	
	546/550											3	root pressure	
	551/555											4		
	556/561											5		
33	562/569	0	100%	0	100%	0	.013	0	.013	CCSH CCTJ	600-1400	No Blowing	Perf. with TJ nozzles	2/21/91
	570/581										716	0-7.7	(Elect. motor drive)	
34	582/599	0	100%	0	100%	0	.013	0	.013	CCSH CCTJ	1146	0-7	Perf. with TJ nozzles	2/21/91
	600/612										1433	0-6	(Elect. motor drive)	
35	613/628	0	100%	0	100%	0	.013	0	.013	CCSH CCTJ	1433	0-7	Perf. with inbd. 15-1/2" slot taped	2/21/91
36	629/645	0	0	0	100%	0	0	0	0	NOZ	0	0-10	Prelim. check on noz. perf.	2/28/91
37	646/663	0	100%	0	100%	0	0	0	0	NOZ	0	0-11	Prelim. check on noz. perf.	2/28/91
38	664/670	0	100%	0	100%	0	0	0	0	OTH	0	0	Check Loads	3/4/91
39	671/694	0	100%	0	100%	0	0	0	0	NOZ	0	0-15	TJ Noz. Perf.	3/4/91
40	695/720	0	0	0	100%	0	0	0	0	NOZ	0	0-15	TJ Noz. Perf.	3/4/91
41	721/735	0	0	0	0	0	0	0	0	OTH	0	0-14	Press. Tare Check (N-S)	3/4/91
42	736/752	0	0	0	0	0	0	0	0	OTH	0	0-14	Press. Tare Check (NE-SW)	3/4/91
43	753/767	0	100%	0	0	0	0	0	0	NOZ	0	0-14	TJ Noz. Perf.	3/4/91
44	768/772	0	100%	0	0	0	0	0	0	OTH	0	0	Check Loads	3/5/91
45	773/790	0	100%	0	0	0	0	0	0	NOZ	0	0-15	TJ Noz. Perf.	3/5/91
46	791/808	100%	0	0	0	0	0	0	0	NOZ	0	0-15	TJ Noz. Perf.	3/5/91

* CCSH-CC/SHAPT DRIVE; CCTJ-CC/TIPJET; NOZ-TIPJET NOZZLE PERF; OTH-OTHER

RUN NO.	POINT NOS. FIRST/LAST	NOZZLE POS. #1 LE	#1 TE	#2 LE	#2 TE	I #1 LE	SLOT POS. #1 TE	#2 LE	#2 TE	MODE	RPM	BLADE PRESSURE RANGE (PSI)	COMMENTS	DATE
47	809/831	100%	0	100%	0	0	0	0	0	NOZ	0	0-15	TJ Noz. Perf.	3/5/91
48	832/839	100%	0	100%	0	0	0	0	0	NOZ	0	0-15	TJ Noz. Perf.	3/5/91
49	840/857	0	0	100%	0	0	0	0	0	NOZ	0	0-15	TJ Noz. Perf.	3/5/91
50	858/862	0	0	100%	0	0	0	0	0	OTH	0	0	Check Loads	3/6/91
51	863/880	0	0	100%	0	0	0	0	0	NOZ	0	0-15	TJ Noz. Perf.	3/6/91
52	881/898	0	0	0	No Nozzle	0	0	0	0	NOZ	0	0-15	TJ Noz. Perf. (No nozzle)	3/6/91
53	899/904	0	0	0	0	0	.005	0	.005	OTH	0	0	Check Loads	3/11/91
54	905/914	0	0	0	0	0	.005	0	.005	CCSH	0-1433	0	CC Rotor Perf. (No blowing)	3/11/91
	915/938										716	0-15	CC Rotor Perf., V_T = 250 fps	
55	939/962	0	0	0	0	0	.005	0	.005	CCSH	1146	0-15	CC Rotor Perf., V_T = 400	3/11/91
	963/982										1433	0-14	CC Rotor Perf., V_T = 500	
56	983/1000	0	0	0	0	0	.005	0	.005	CCSH	1289	0-15	CC Rotor Perf., V_T = 450	3/11/91
	1001/1017										1002	0-15	CC Rotor Perf., V_T = 350	
57	1018/1043	0	0	0	0	0	.005	0	.005	CCSH	600-1400	6,10,14	CC Rotor Perf., RPM sweeps	3/11/91
58	1044/1062	0	0	0	0	0	.005*	0	.005*	CCSH	1433	0-14	CC Rotor Perf., V_T = 500, outboard 1" of slot taped	3/11/91
59	1063/1067	0	0	0	0	0	.005	0	.005	OTH	0	0	Check Loads	3/12/91
60	1068/1102	0	0	0	0	0	.005	0	.005	OTH	0	0-15	Mass flow check	3/12/91
61	1103/1122	0	100	0	100	0	0	0	0	CCTJ	716	0-15	TJ Drive/No CC Blowing	3/12/91
62	1123/1140	0	100	0	100	0	0	0	0	CCTJ	1146	0-14.4	TJ Drive/No CC Blowing	3/12/91
	1141/1156										1433	0-13.5		
63	1157/1171	0	100	0	100	0	.005	0	.005	CCTJ	1146	0-10.5	TJ Rotor Perf., V_T = 400 fps	3/12/91
	1172/1185										1433	0-10	TJ Rotor Perf., V_T = 500	
64	1186/1201	0	100	0	100	0	.005	0	.005	CCTJ	716	0-11.4	TJ Rotor Perf., V_T = 250	3/12/91
	1202/1216										573	0-11.5	TJ Rotor Perf., V_T = 200	
65	1217/1234	0	100	0	100	0	.005/ .003	0	.005/ .003	CCTJ	716	0-15	TJ Rotor Perf., V_T = 250	3/13/91
	1235/1251										1146	0-15	TJ Rotor Perf., V_T = 400	
66	1252/1268	0	100	0	100	0	.005/ .003	0	.005/ .003	CCTJ	VAR.	0-15	TJ Rotor Perf., TJ Drive	3/13/91
67	1269/1285	0	100	0	100	0	0	0	0	OTH	0	0-15	Nozzle Thrust Check	3/13/91
68	1286/1291	0	100	0	100	0	.003	0	.003	CCTJ	0	0	Check Loads	3/14/91
69	1292/1311												Bad Run	3/14/91
70	1312/1329	0	100	0	100	0	.003	0	.003	CCTJ	1146	0-15	TJ Rotor Perf., V_T = 400	3/14/91

*CCSH-CC/SHAPT DRIVE; CCTJ-CC/TIPJET; NOZ-TIPJET NOZZLE PERF; OTH-OTHER

RUN NO.	POINT NOS. FIRST/LAST	NOZZLE POS. #1 LE	#1 TE	#2 LE	#2 TE	SLOT POS. #1 LE	#1 TE	#2 LE	#2 TE	MODE	RPM	BLADE PRESSURE RANGE (PSI)	COMMENTS	DATE
71	1347/1364	0	100	0	100	0	.003	0	.003	CCTJ	1433	0-15	TJ Rotor Perf., V_T = 500	3/14/91
	1365/1377										VAR.	0-15	TJ Rotgor Perf., TJ Drive	
72	1378/1392	0	100	0	100	0	.003	0	.003	OTH	0	0-15	Mass Flow Check (w/nozzle)	3/14/91
73	1393/1410	0	0	0	0	0	.003	0	.003	CCSH	1146	0-15	CC Perf., V_T = 400	3/14/91
	1411/1427										1433	0-15	CC Perf., V_T = 500	
74	1428/1442	0	0	0	0	0	.003	0	.003	OTH	0	0-15	Mass Flow Check (no nozzles)	3/14/91
75	1443/1447	0	0	0	0	0	.003	0	.003	OTH	0	0	Check Loads	3/26/91
76	1448/1466	0	0	0	0	0	.003	0	.003	CCSH	716	0-15	CC Perf., V_T = 250	3/26/91
	1467/1483										759	0-15	CC Perf., V_T = 265	
77	1484/1501	0	0	0	0	0	.003	0	.003	CCSH	1146	0-15	CC Perf., V_T = 400	3/26/91
	1502/1517										1433	0-15	CC Perf., V_T = 500	
	1518/1535										573	0-15	CC Perf., V_T = 200	
78	1536/1552	0	0	0	0	0	.003	0	.003	CCSH	1146	0-12	CC Perf., Outboard 1 in. taped	3/26/91
79	1553/1569	0	0	0	0	0	.003	0	.003	CCSH	1146	0-12	CC Perf., Outboard 2 in.	3/26/91
80	1570/1586	0	0	0	0	0	.003	0	.003	CCSH	1146	0-12	CC Perf., Outboard 3 in.	3/26/91
81	1587/1603	0	0	0	0	0	.003	0	.003	CCSH	1146	0-12	CC Perf., Inboard 3 in. taped	3/26/91
82	1604/1621	0	0	0	0	0	.003	0	.003	CCSH	1146	0-12	CC Perf., Inboard 6 in.	3/26/91
83	1622/1638	0	0	0	0	0	.003	0	.003	CCSH	1146	0-12	CC Perf., Inboard 12 in.	3/26/91
84	1639/1643	0	0	0	0	0	.003	0	.003	OTH	0	0	Check Loads	3/27/91
85	1644/1663	0	0	0	0	0	.003	0	.003	CCSH	716	0-15	CC Perf., V_T = 250 Coanda Trip - Mono RI.	3/27/91
	1664/1680										1146	0-15	CC Perf, V_T = 400	
86	1681/1700	0	0	0	0	0	.003	0	.003	CCSH	716	0-15	CC Perf., V_T = 250 Coanda Trip - Tape	3/27/91
	1701/1717												CC Perf., V_T = 400	
87	1718/1736	0	0	0	0	0	.003	0	.003	CCSH	1146	0-15	CC Perf., V_T = 400 Full span strips at 2 in. intervals	3/27/91
88	1737/1755	0	0	0	0	0	.003	0	.003	CCSH	1146	0-15	CC Perf., V_T = 400, strips on outer 1/2 of slot span	3/27/91
89	1756/1774	0	0	0	0	0	.003	0	.003	CCSH	1146	0-15	CC Perf., V_T = 400 strips on inner 1/2 of slot span	3/27/91
90	1775/1789	0	0	0	0	0	0	0	0	CCSH	0-1433	0	CC Perf., No Blowing/Slots Taped	3/27/91
91	1790/1794	0	0	0	0	0	.002	0	.002	OTH	0	0	Check Loads	3/29/91
92	1795/1817	0	0	0	0	0	.002	0	.002	CCSH	716	0-20	CC Perf., V_T = 250 fps	3/29/91
93	1818/1836	0	0	0	0	0	.002	0	.002	CCSH	1146	0-20	CC Perf., V_T = 400	3/29/91
94	1837/1855	0	0	0	0	0	.002	0	.002	CCSH	1433	0-18	CC Perf., V_T = 500	3/29/91

*CCSH-CC/SHAPT DRIVE; CCTJ-CC/TIPJET; NOZ-TIPJET NOZZLE PERF; OTH-OTHER

RUN NO.	POINT NOS. FIRST/LAST	NOZZLE POS. #1 LE	#1 TE	#2 LE	#2 TE	SLOT POS. #1 LE	#1 TE	#2 LE	#2 TE	MODE	RPM	BLADE PRESSURE RANGE (PSI)	COMMENTS	DATE
95	1856/1871	0	0	0	0	0	.002	0	.002	OTH	0	0-20	Mass Flow Check; H_{TE} = .002 Nozzles Closed	3/29/91
96	1872/1890	0	100	0	100	0	.002	0	.002	CCSH	1146	0-17.4	TJ Roptor Perf., V_T = 400 fps	3/29/91
97	1891/1909	0	100	0	100	0	.002	0	.002	CCSH	1433	0-18	TJ Rotor Perf., V_T = 500	3/29/91
98	1910/1924	0	100	0	100	0	.002	0	.002	CCTJ	VAR	0-19	TJ Rotor Perf., TJ Drive Only	3/29/91
99	1925/1929	0	100	0	100	0	.002/ .0015	0	.002/ .0015	OTH	0	0	Check Loads	4/1/91
100	1930/1944	0	100	0	100	0	.002/ .0015	0	.002/ .0015	CCTJ	VAR	0-14.7	TJ Rotor Perf., TJ Drive Only	4/1/91
101	1945/1963	0	100	0	100	0	.002/ .0015	0	.002 .0015	CCTJ	VAR	0-18.7	TJ Rotor Perf., TJ DRive Only	4/1/91
102	1963/1976	0	0	0	0	0	.002/ .0015	0	.002/ .0015	OTH	0	0-12	Mass Flow Check - Run 101 Slot Config.	4/1/91
103	1977/1981	0	0	0	0	.003	0	.003	0	OTH	0	0	Check Loads	4/2/91
104	1982/2000	0	0	0	0	.003	0	.003	0	OTH	0	15	Mass Flow Check	4/2/91
105	2001/2015	0	0	0	0	.003	0	.003	0	CCSH	0-1433	0	CC Rotor Perf. - No Blowing - CW	4/2/91
106	2016/2032	0	0	0	0	.003	0	.003	0	CCSH	716	0-12	CC Rotor Perf., V_T = 250 fps	4/2/91
107	2033/2050	0	0	0	0	.003	0	.003	0	CCSH	1146	0-13.6	CC Rotor Perf., V_T = 400	4/2/91
108	2051/2069	0	0	0	0	.003	0	.003	0	CCSH	1433	0-15	CC Rotor Perf., V_T = 500	4/2/91
109	2070/2087	0	0	0	0	.003	0	.003	0	CCSH	1146	0-13.5	CC Rotor Perf., V_T = 400, 1/2" tape strip outboard	4/2/91
110	2088/2092	100	0	100	0	.003	0	.003	0	OTH	0	0	Check Loads	4/4/91
111	2093/2107	100	0	100	0	.003	0	.003	0	OTH	0	0-13.7	Mass Flow Check	4/4/91
112	2108/2125	100	0	100	0	.003	0	.003	0	CCSH	716	0-12	TJ Rotor Perf., V_T = 250 - cw	4/4/91
113	2120/2143	100	0	100	0	.003	0	.003	0	CCSH	1146	0-14	TJ Rotor Perf., V_T = 400 - cw	4/4/91
114	2144/2162	100	0	100	0	.003	0	.003	0	CCSH	1433	0-15	TJ Rotor Perf., V_T = 500 - cw	4/4/91
115	2163/2177	100	0	100	0	.003	0	.003	0	CCTJ	VAR	0-15	TJ Rotor Perf, TJ Drive Only - cw	4/4/91
116	2178/2194	100	0	100	0	0	0	0	0	OTH	716/1146	0-6	TJ Retrotorque - CCW Rotation	4-4-91
117	2185/2199	JF	0	JF	0	.003	0	.003	0	OTH	0	0	Check Loads	4/5/91
118	2200/2215	JF	0	JF	0	.003	0	.003	0	OTH	0	0-15	Mass Flow Check	4/5/91
119	2216/2233	JF	0	JF	0	.003	0	.003	0	CCSH	716	0-15	CC Rotor Perf, V_T = 250 CW Rot.	4/5/91
120	2234/2251	JF	0	JF	0	.003	0	.003	0	CCSH	1146	0-15	CC Rotor Perf, V_T = 400 CW Rot.	4/5/91
121	2252/2269	JF	0	JF	0	.003	0	.003	0	CCSH	1433	0-14	CC Rotor Perf., V_T = 500 CW Rot.	4/5/91
122	2270/2286	0	0	0	0	.003	0	.003	0	CCSH	716	0-12	CC Rotor Perf., V_T = 250 CW Rot.	4/5/91
123	2287/2303	0	0	0	0	.003	0	.003	0	CCSH	1146	0-13.5	CC Rotor Perf., V_T = 400 CW Rot.	4/5/91
124	2304/2323	0	0	0	0	.003	0	.003	0	CCSH	1433	0-15	CC Rotor Perf., V_T = 500 CW Rot.	4/5/91

*CCSH-CC/SHAPT DRIVE; CCTJ-CC/TIPJET; NOZ-TIPJET NOZZLE PERF; OTH-OTHER

RUN NO.	POINT NOS. FIRST/LAST	NOZZLE POS. #1 LE	#1 TE	#2 LE	#2 TE	SLOT POS. #1 LE	#1 TE	#2 LE	#2 TE	MODE	RPM	BLADE PRESSURE RANGE (PSI)	COMMENTS	DATE
125	2324/2333	0	0	0	0	.003	0	.003	0	CCSH	573	0-3	CC Rotor Perf., V_T = 200 CW All except	4/5/91
	2334/2341										716	0-4	V_T = 250 CW outer 10"	
	2342/2353										1146	0-8	V_T = 400 CW of slots taped	
125	2354/2363	0	0	0	0	.003	0	.003	0	CCSH	1433	0-13.5	CC Rotor Perf., V_T = 500 CW All but outer 10" of slots taped	4/5/91
126	2364/2375	0	0	0	0	0	0	0	0	OTH	0	0-9	Transducer Check	4/5/91
127	2376/2380	JF	0	JF	0	.003	0	.003	0	OTH	0	0	Check Loads	5/20/91
128	2381/2396	JF	0	JF	0	.003	0	.003	0	OTH	0	0-13.5	Mass Flow Check	5/20/91
129	2397/2414	JF	0	JF	0	.003	0	.003	0	CCSH	716	0-15	CC Rotor Perf., V_T = 250; CW Rot.	5/20/91
130	2415/2431	JF	0	JF	0	.003	0	.003	0	CCSH	1146	0-13.5	V_T = 400	5/20/91
	2432/2447										1433	0-13.5	V_T = 500	
131	2448/2462	JF	0	JF	0	.003	0	.003	0	CCSH	1433	0-13.5	V_T = 500 (repeat)	5/20/91
132	2463/2471	0	0	0	0	.003	0	.003	0	OTH	0	0-13	Mass Flow Check	5/0/91
133	2472/2489	0	0	0	0	.003	0	.003	0	CCSH	1433	0-13.5	CC Rotor Perf., V_T = 500; CW Rot.	5/20/91
134	2490/2506	0	0	0	0	.003	0	.003	0	CCSH	716	0-13.4	V_T = 250	5/20/91
	2507/2521										1146	0-13.5	V_T = 400	
135	2522/2539	0	0	0	0	.003*	0	.003*	0	CCSH	1433	0-13.5	V_T = 500; Outboard 3" taped	5/20/91
136	2539/2557	0	0	0	0	.003*	0	.003*	0	CCSH	1433	0-13.5	V_T = 500; Outboard 3", inboard 4.5" taped	5/20/91
137	2558/2568	JF	0	JF	0	0	0	0	0	CCSH	1433	0-12	JF Perf. (Only), V_T = 500	5/20/91
138	2569/2580	0	0	0	0	.003*	0	.003*	0	CCSH	1433	0-12	Slots taped except LE outboard 1 3/4"	5/20/91
139	2581/2586	0	0	0	0	.003*	0	.003*	0	CCSH	0-750	0	Same config. as 138; 50 lb weight	5/20/91
140	2587/2591	0	0	0	0	.003	0	.003	0	OTH	0	0	Check Loads	5/21/91
141	2592/2606	0	0	0	0	.003	0	.003	0	CCSH	573	0-10.2	CC Perf., V_T = 200; Grit Strips	5/21/91
	2607/2619										716	0-10.4	V_T = 250	
142	2620/2633	0	0	0	0	.003	0	.003	0	CCSH	859	0-11.9	V_T = 300; Grit Strips	5/21/91
	2634/2646										1146	0-13.4	V_T = 400	
	2647/2659										1433	0-14.0	V_T = 500	
143	2660/2675	0	0	0	0	.003	0	.003	0	CCSH	716	0-13.4	CC Perf., V_T = 250	5/21/91
	2676/2691										1433	0-13.7	V_T = 500	
144	2692/2706	0	0	0	0	.003	0	.003	0	CCSH	1433	0-10	V_T = 500; Sample Rate x 2	5/21/91
	2707/2721										1433	0-10	Sample Rate x 1/2	
145	2722/2734	100	0	100	0	.003	0	.003	0	TJ	Variable	0-13.5	TJ Rotor Perf. (CW)	5/21/91
146	2753/2744	100	0	100	0	.003*	0	.003*	0	TJ	Variable	0-10	TJ Rotor Perf. (CW), Slot taped except outer 9"	5/21/91
147	2745/2749	100	0	100	0	.003	0	.003	0	OTH	0	0	Check Loads	5/22/91

*CCSH-CC/SHAPT DRIVE; CCTJ-CC/TIPJET; NOZ-TIPJET NOZZLE PERF; OTH-OTHER

RUN NO.	POINT NOS. FIRST/LAST	NOZZLE POS. #1 LE	#1 TE	#2 LE	#2 TE	SLOT POS. #1 LE	#1 TE	#2 LE	#2 TE	MODE	RPM	BLADE PRESSURE RANGE (PSI)	COMMENTS	DATE
148	2750/2763	100	0	100	0	.003"	0	.003"	0	TJ	Variable	0-14.5	TJ Rotor Perf. (CW) slot inboard 1/2 taped	5/22/91
149	2764/2770	100	0	100	0	0	0	0	0	TJ	Variable	0-5.9	TJ Rotor Perf. (CW) All slots taped	5/22/91
150	2771/2887	100	0	100	0	0	0	0	0	OTH	716	0-13.7	TJ Nozzle Rotating Perf., V_T = 250	5/22/91
	2888/2803									OTH	1433	0-13.5	TJ Nozzle Rotating, Perf., V_T = 500	
151	2804/2819	Def.	0	Def.	0	0	0	0	0	OTH	0	0-14.9	TJ Nozzle Static Perf.	5/22/91
152	2820/2835	Def.	0	Def.	0	0	0	0	0		716	0-13.6	TJ Noozle Rotating Perf., V_T = 250	5/22/91
	2836/2850										1433	0-13.5	V_T = 500	
153	2851/2865	Def.	0	Def.	0	.003	0	.003	0	CCTJ	Variable	0-13.6	TJ Rotor Perf. (CW) Defective Nozzles	5/22/91
154	2866/2880	Def.	0	Def.	0	.003	0	.003	0	CCTJ	600, 700 800, 900	0-8.3	Constant Lebow Torque = 0, ±1	5/22/91
155	2881/2885	0	0	0	0	.003"	0	.003"	0	OTH	0	0	Check Loads	5/23/91
156	2886/2900	0	0	0	0	.003"	0	.003"	0	CCSH	716	0-12	CC Rotor Perf., V_T = 250 *outboard slot tapered to 0	5/23/91
157	2901/2917	0	0	0	0	.003"	0	.003"	0	CCSH	1146	0-13.4	CC Rotor Perf., V_T = 400 *outboard slot tapered to 0	5/23/91
158	2918/2926	0	0	0	0	.003"	0	.003"	0	OTH	~0	0-9.4	"Static" Mass Flow Check	5/23/91
	2927/2935									CCSH	1433	0-10.5	CC Rotor Perf.,V_T = 500	5/23/91
159	2936/2952	0	0	0	0	.003"	0	.003"	0	CCSH	1433	0-10.4	CC Rotor Perf., Repeat of Run 158	5/23/91
160	2953/2961	0	0	0	0	.003	0	.003	0	OTH	~0	0-7.5	"Static" Mass Flow Check	5/23/91
	2962/2972									CCSH	716	0-10	CC Rotor Perf., V_T = 250 Outboard slot	
	2973/2984									CCSH	1146	0-10.4	CC Rotor Perf., V_T = 400 tapered to h = .006 in	
	2985/2995									CCSH	1433	0-9	CC Rotor Perf., V_T = 500 @ tip	
	2996/3003									CCSH	600-1300	8	CC Rotor Perf., RPM sweep @ 8 psi	

END OF TEST

*CCSH-CC/SHAPT DRIVE; CCTJ-CC/TIPJET; NOZ-TIPJET NOZZLE PERF; OTH-OTHER

Def. signifies the alternate set of nozzles which are defective but have same exit area as 100% nozzles.

Appendix C

DATA DISKS

Test data are available on floppy diskettes from the author upon request. The data are most readily available as formatted for Cricket Graph software for a Macintosh computer. If necessary, the data can be converted to tab-delimited data files for greater transportability.

(This page intentionally blank)

Fig. 1. Tipjet 80-in. model rotor installed on DTMB hover test stand.

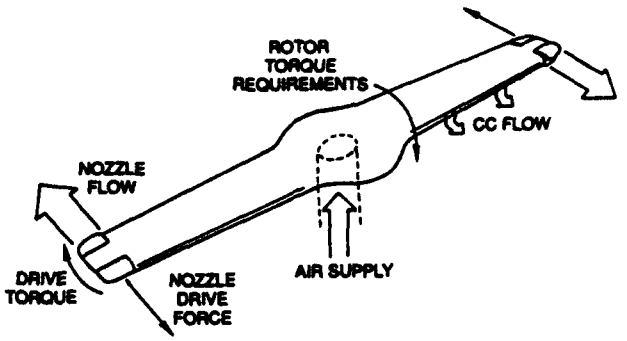

Fig. 2. Conceptual sketch of pneumatic rotor.

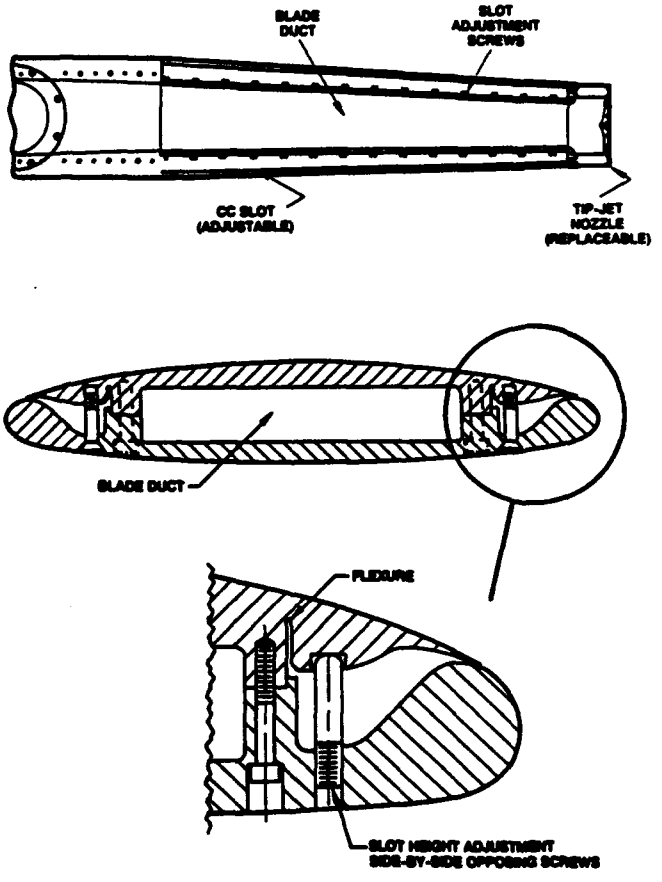

Fig. 3. Tipjet rotor model.

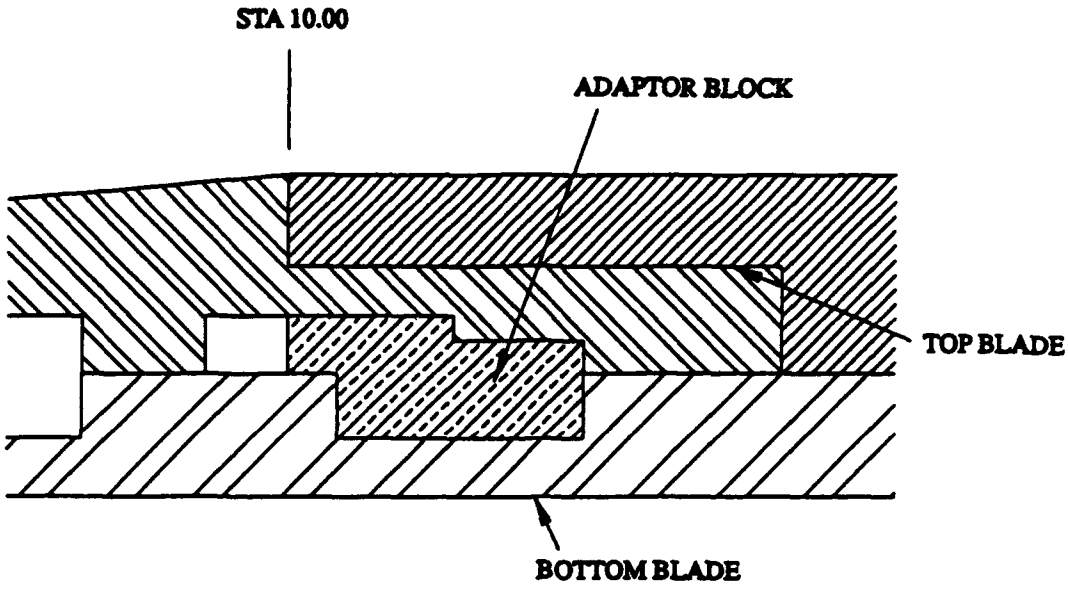

Fig. 4. Design modification to correct machining error.

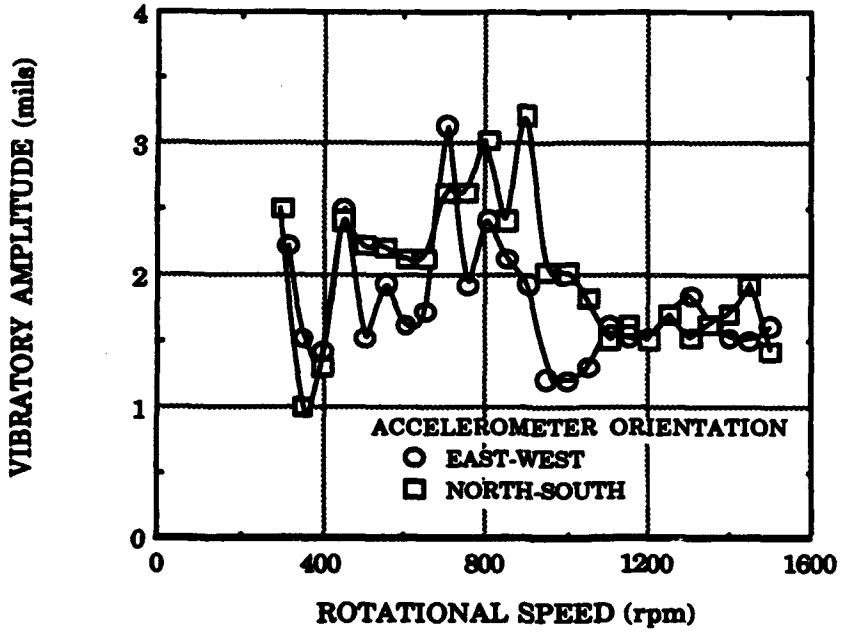

Fig. 5. Dynamic blance data.

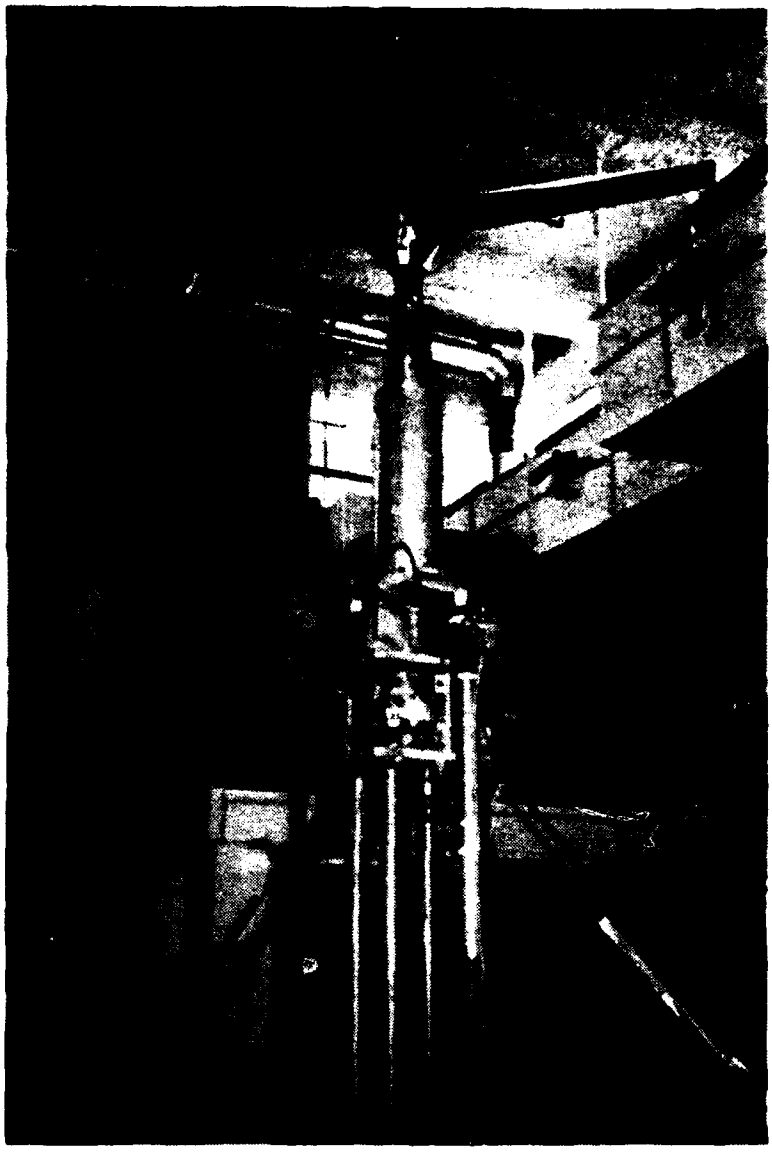

Fig. 6. DTMB hover test stand.

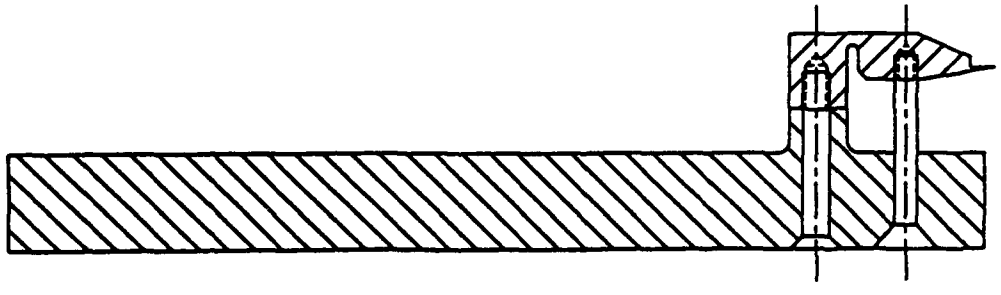

Fig. 7. CC slot flexure test specimen.

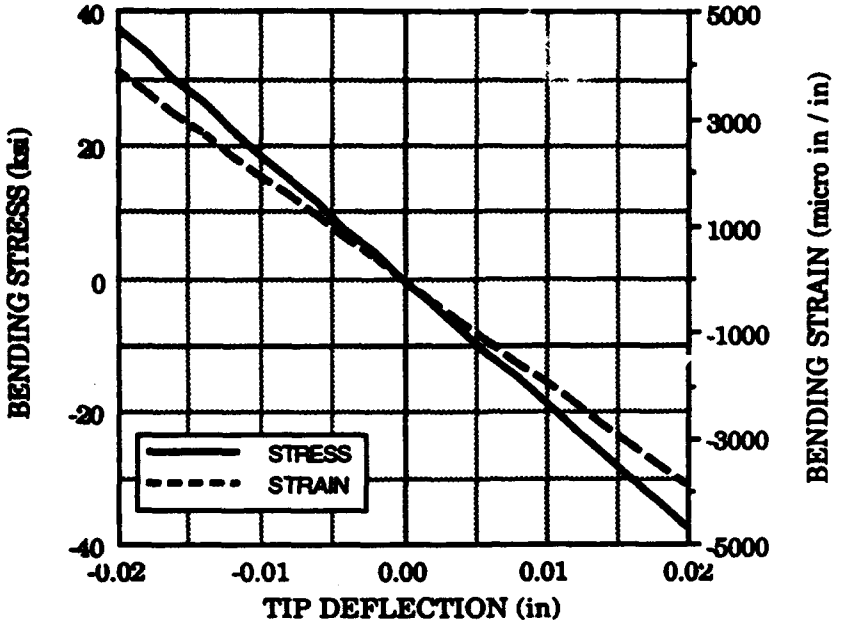

Fig. 8. Flexure specimen STA 10 flexure stress and strain versus tip deflection.

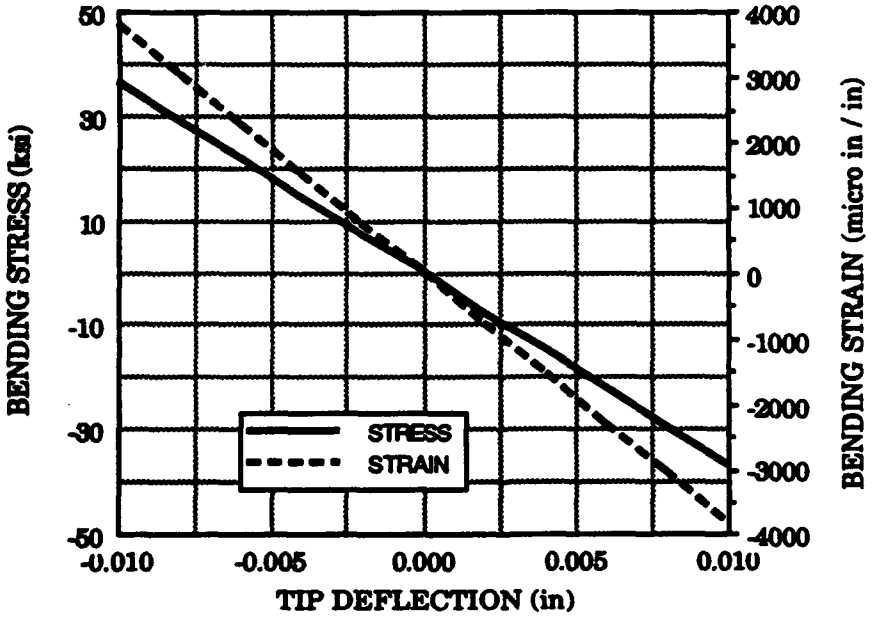

Fig. 9. Flexure specimen STA 37.275 flexure stress and strain versus tip deflection.

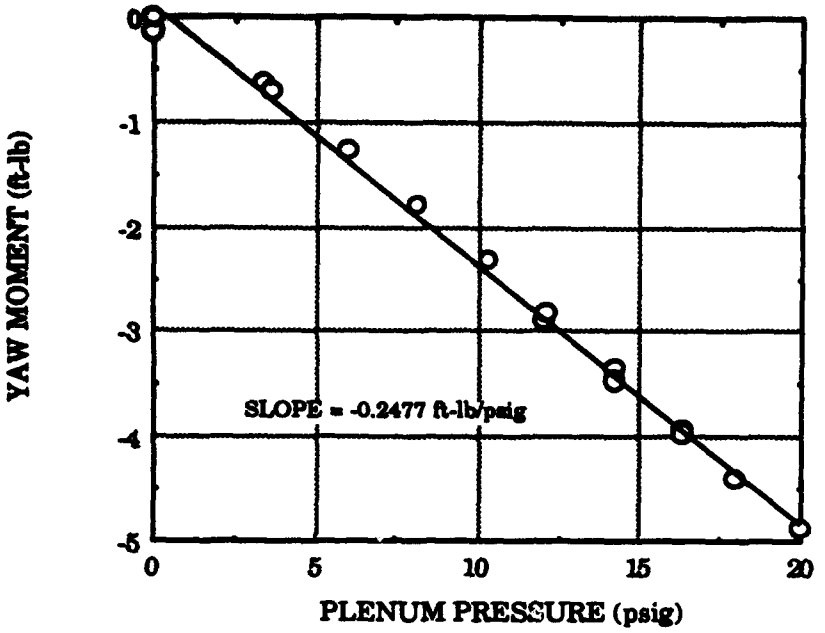

Fig. 10. Pressure tare results.

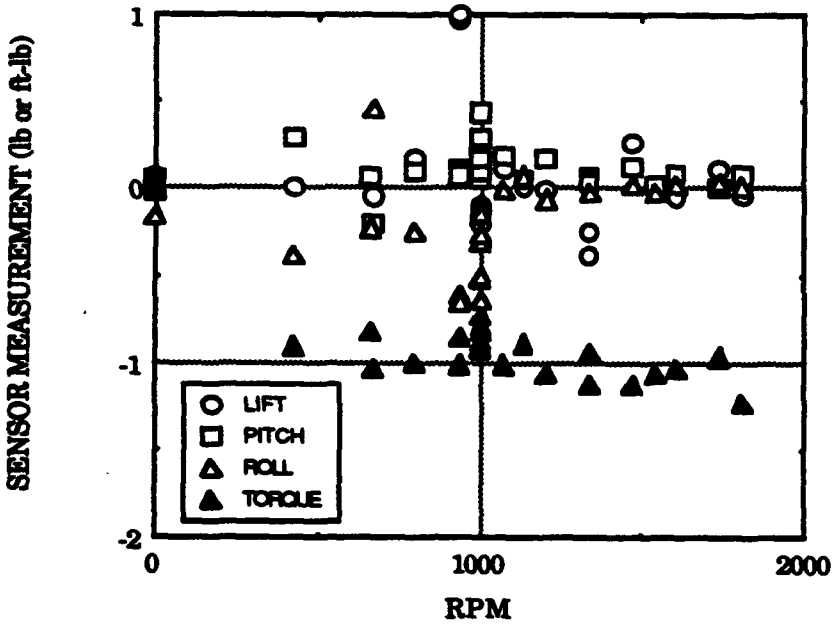

Fig. 11. Friction tare results.

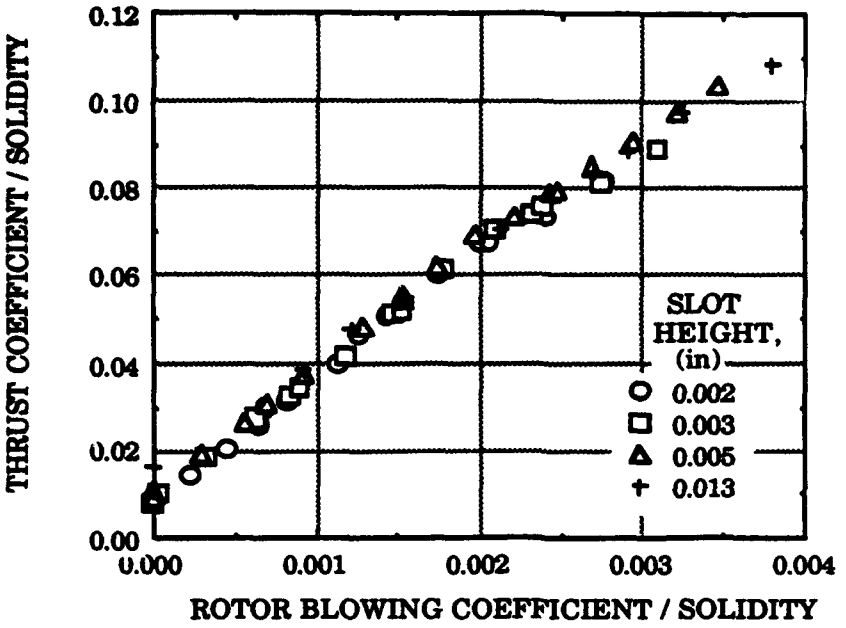

Fig. 12a. Thrust coefficient versus blowing coefficient for V_t = 500 ft/sec.

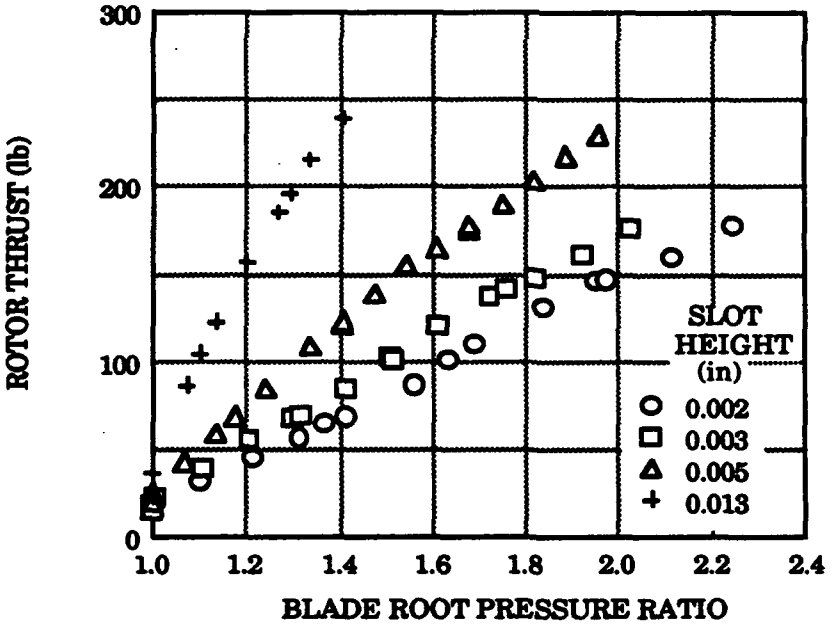

Fig. 12b. Thrust versus blade root pressure ratio for V_t = 500 ft/sec.

Fig. 12. Tipjet rotor performance in CC rotor mode - Slot height effect.

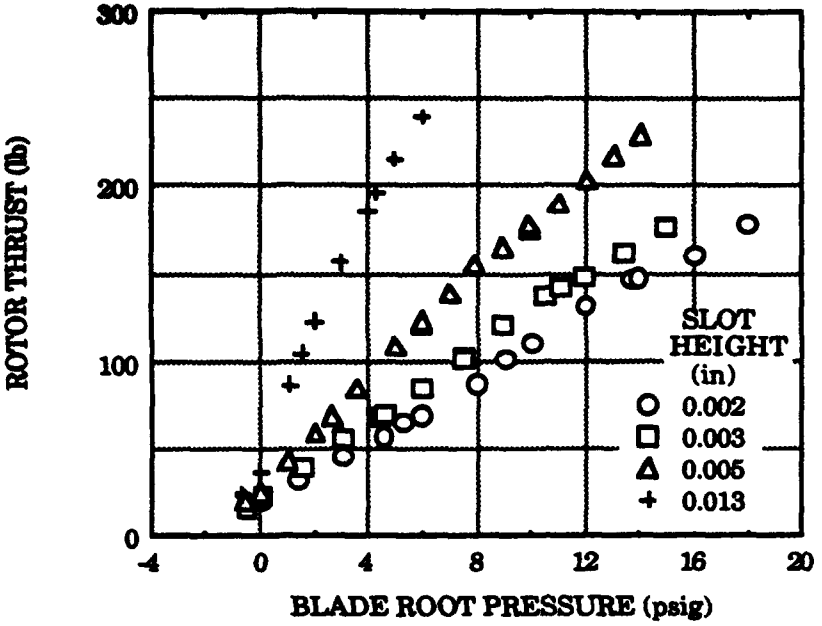

Fig. 12c. Thrust versus blade root pressure for V_t = 500 ft/sec.

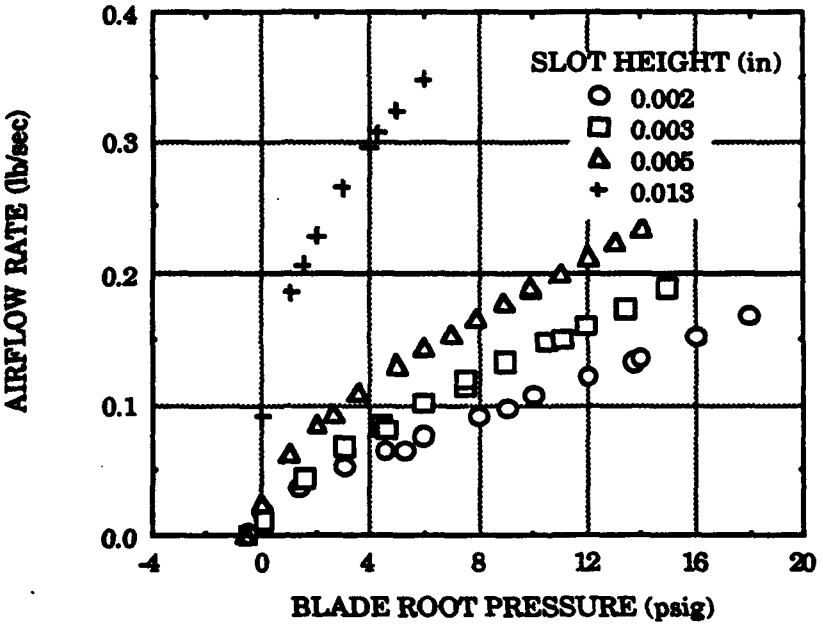

Fig. 12d. Airflow rate versus blade root pressure for V_t = 500 ft/sec.

Fig. 12. (Continued)

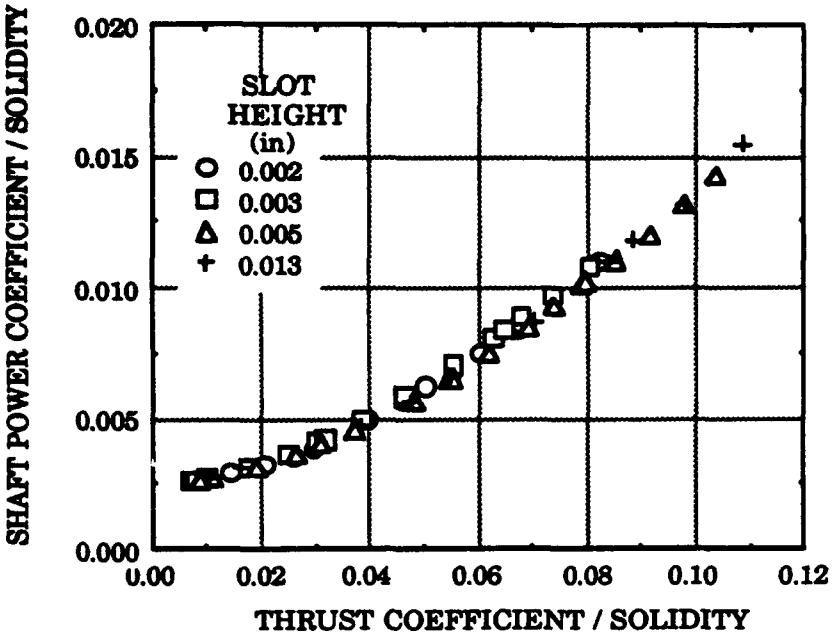

Fig. 12e. Shaft power coefficient / solidity versus thrust coefficient / solidity for V_t = 500 ft/sec.

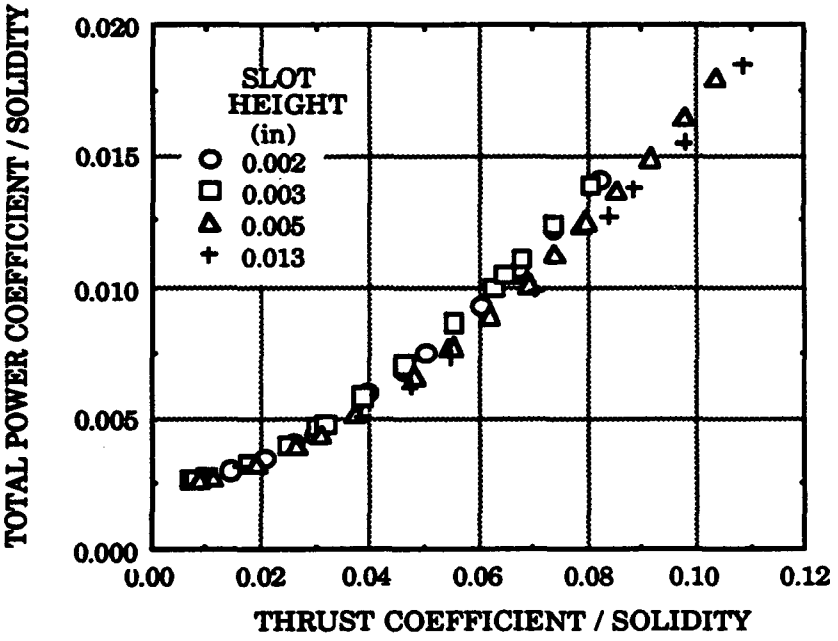

Fig. 12f. Total power coefficient / solidity versus thrust coefficient / solidity for V_t = 500 ft/sec.

Fig. 12. (Continued)

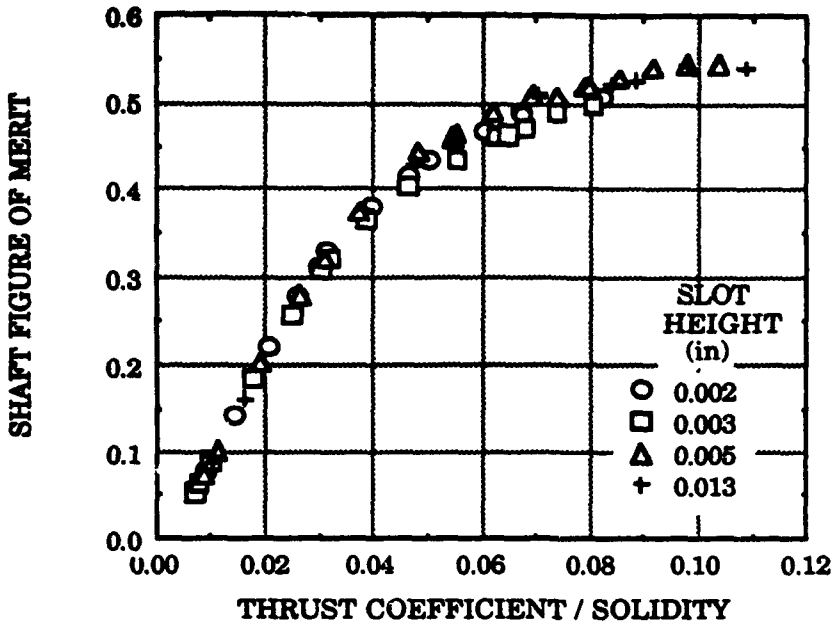

Fig. 12g. Shaft figure of merit versus thrust coefficient / solidity for V_t = 500 ft/sec.

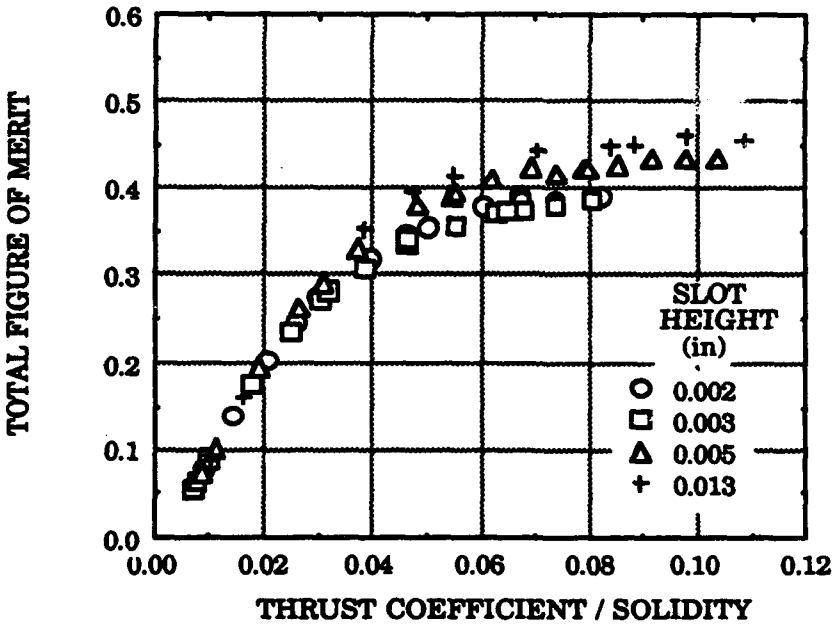

Fig. 12h. Total figure of merit versus thrust coefficient / solidity for V_t = 500 ft/sec.

Fig. 12. (Continued)

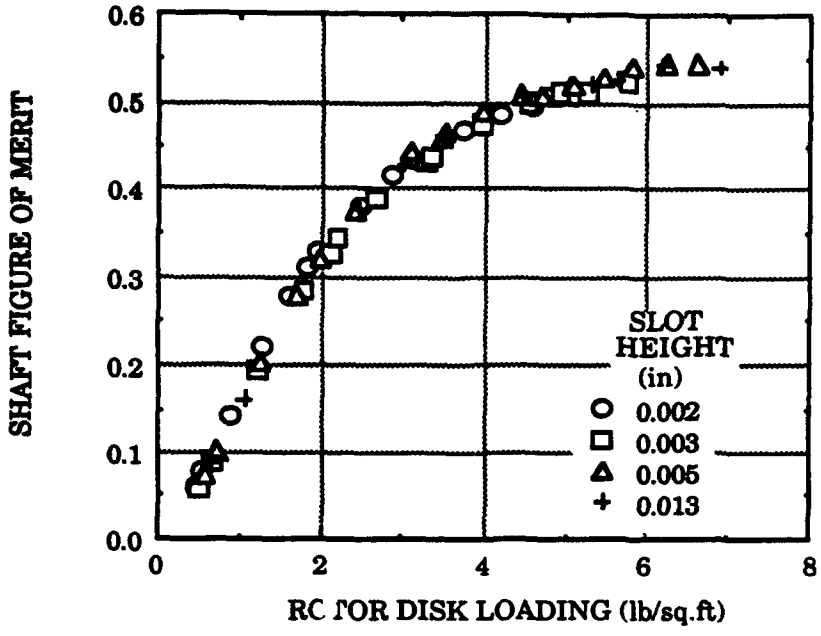

Fig. 12i. Shaft figure of merit versus disk loading for V_t = 500 ft/sec.

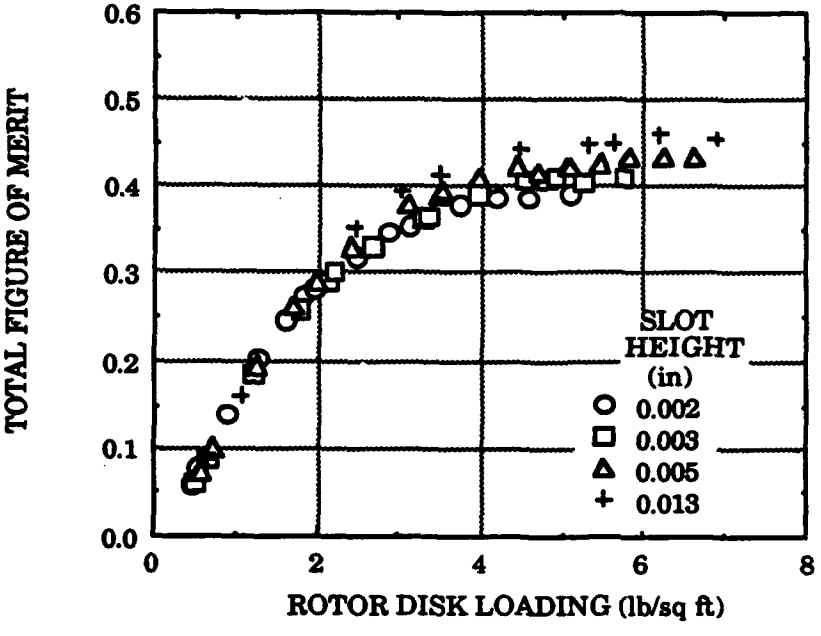

Fig. 12j. Total figure of merit versus disk loading for V_t = 500 ft/sec.

Fig. 12. (Continued)

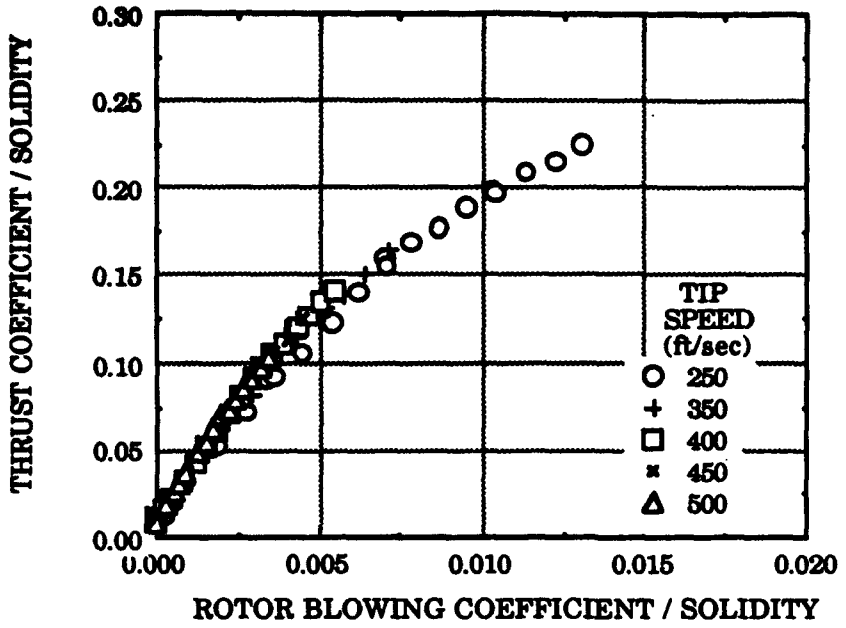

Fig. 13a. Thrust coefficient versus blowing coefficient for h = 0.005 in.

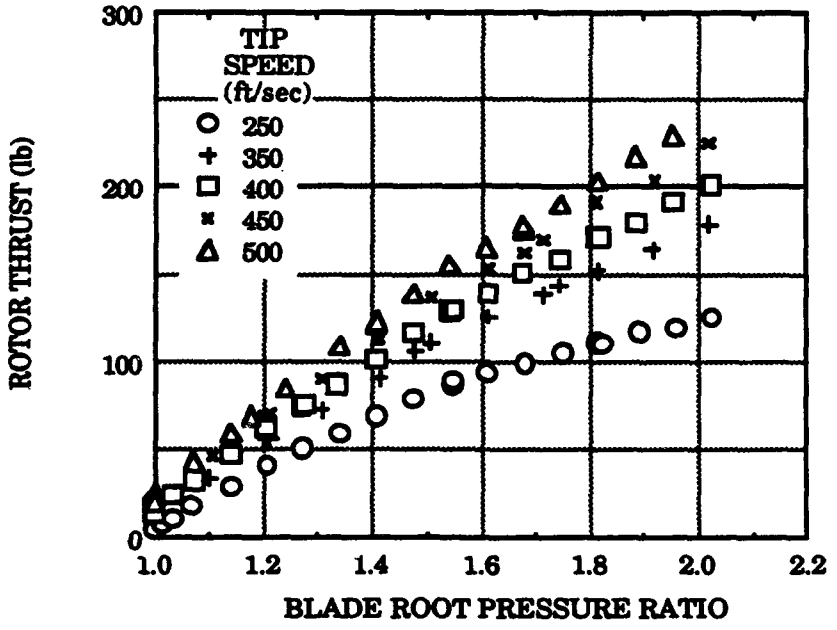

Fig. 13b. Thrust versus blade root pressure ratio for h = 0.005 in.

Fig. 13. Tipjet rotor performance in CC rotor mode - Tip speed effect.

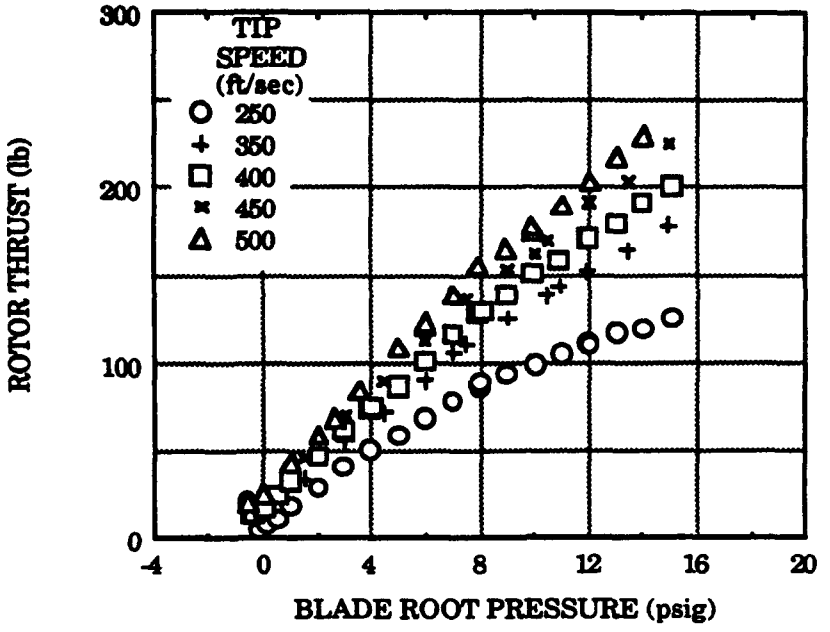

Fig. 13c. Thrust versus blade root pressure for h = 0.005 in.

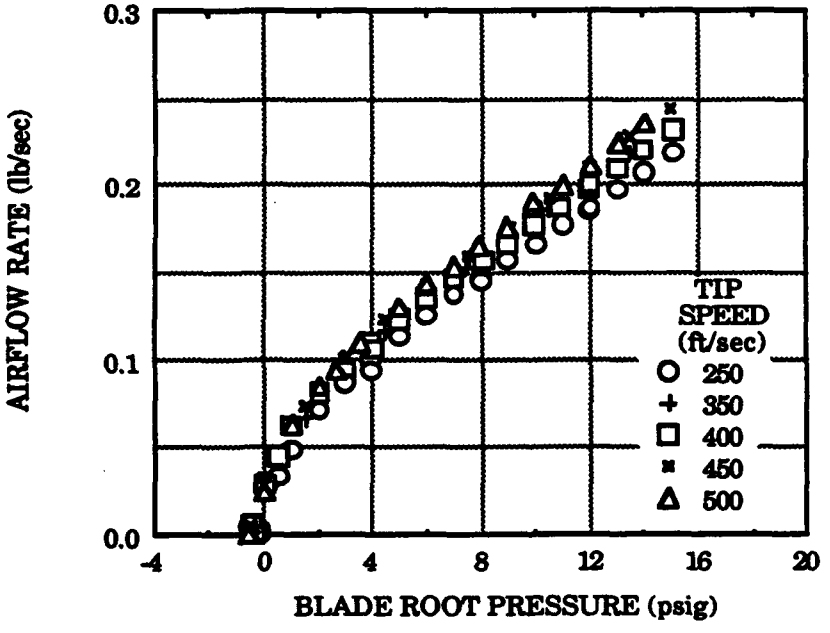

Fig. 13d. Airflow rate versus blade root pressure for h = 0.005 in.

Fig. 13. (Continued)

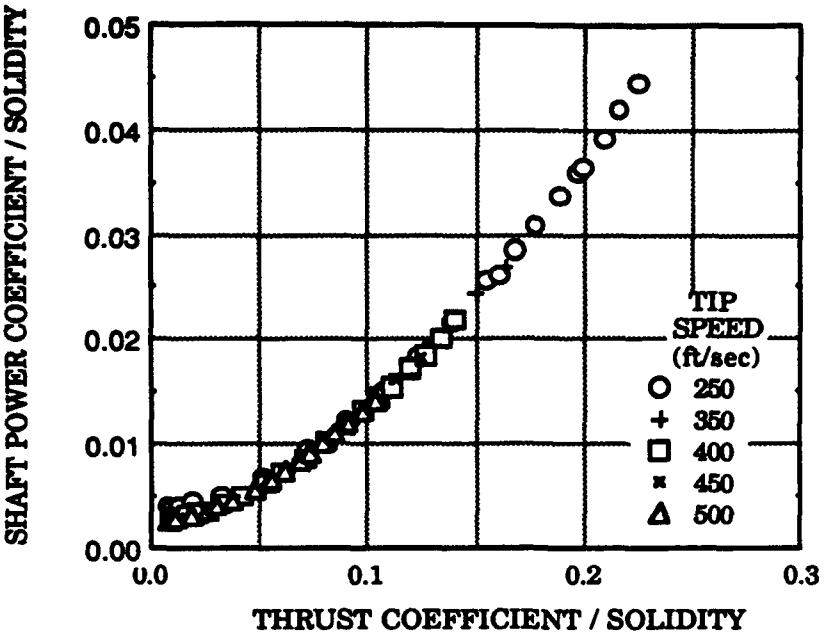

Fig. 13e. Shaft power coefficient / solidity versus thrust coefficient / solidity for h = 0.005 in.

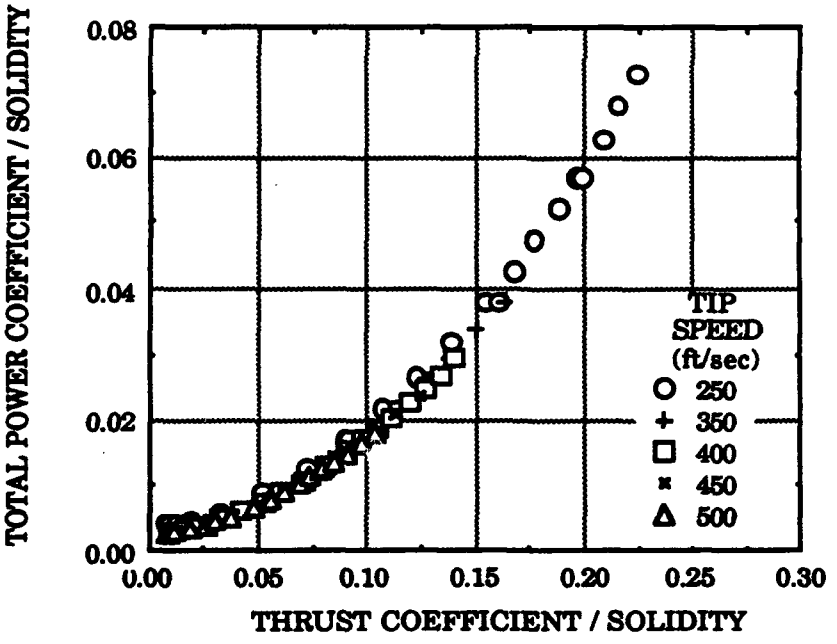

Fig. 13f. Total power coefficient / solidity versus thrust coefficient / solidity for h = 0.005 in.

Fig. 13. (Continued)

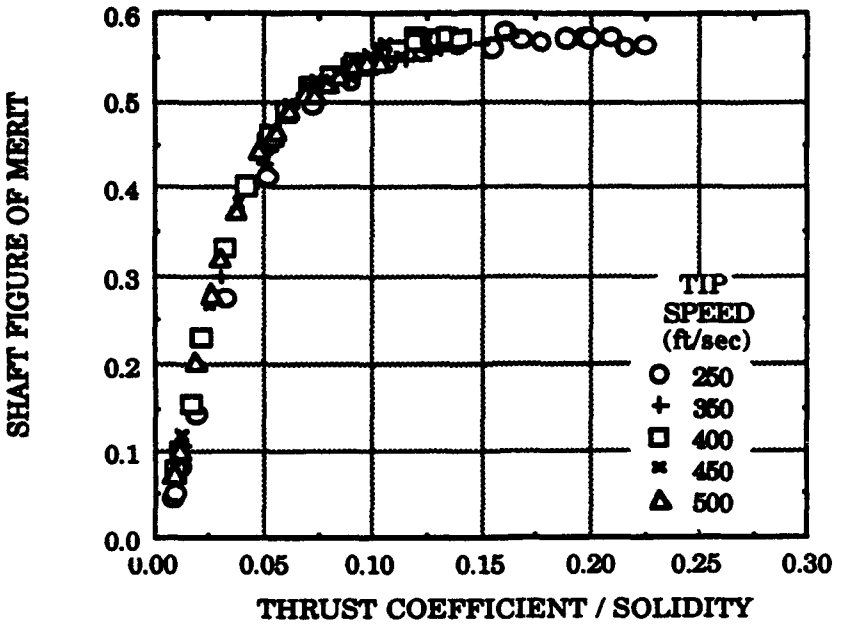

Fig. 13g. Shaft figure of merit versus thrust coefficient / solidity for h = 0.005 in.

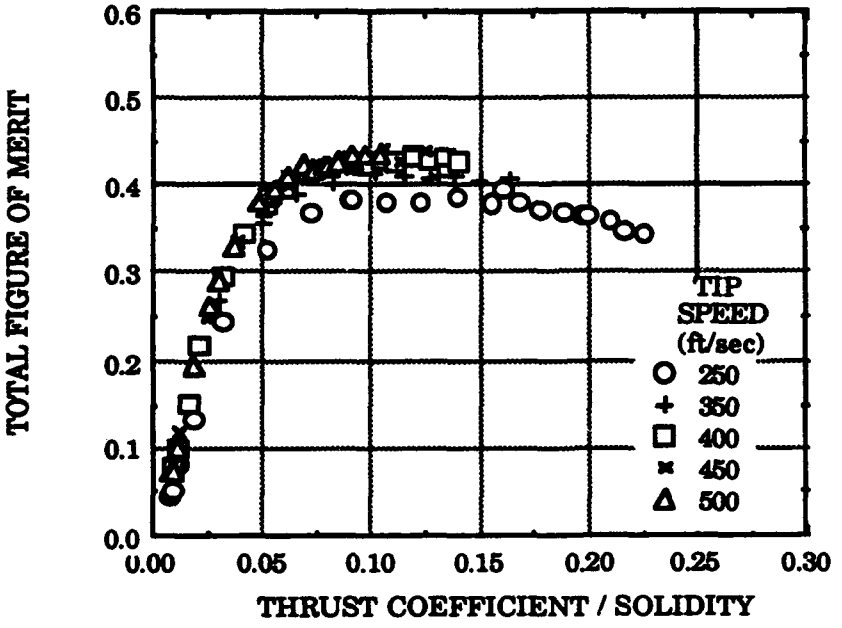

Fig. 13h. Total figure of merit versus thrust coefficient / solidity for h = 0.005 in.

Fig. 13. (Continued)

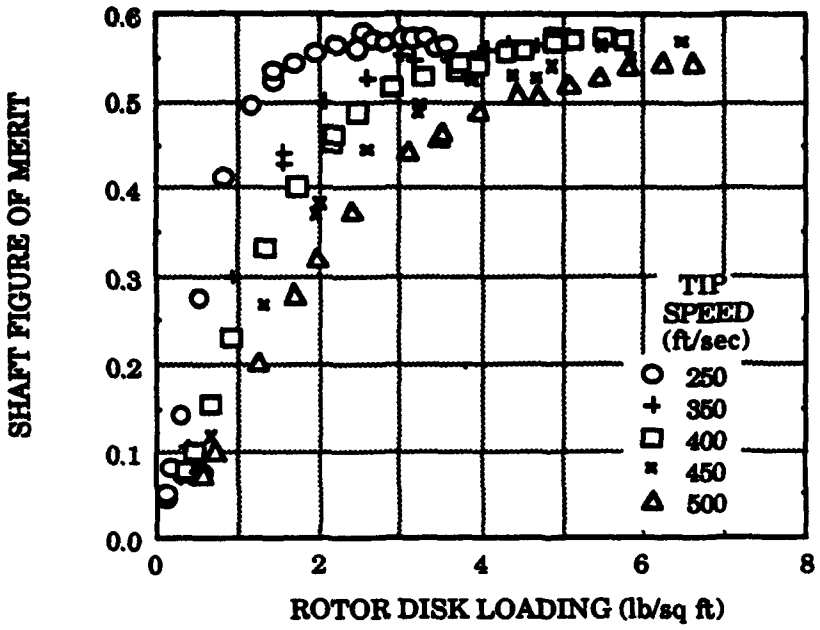

Fig. 13i. Shaft figure of merit versus disk loading for h = 0.005 in.

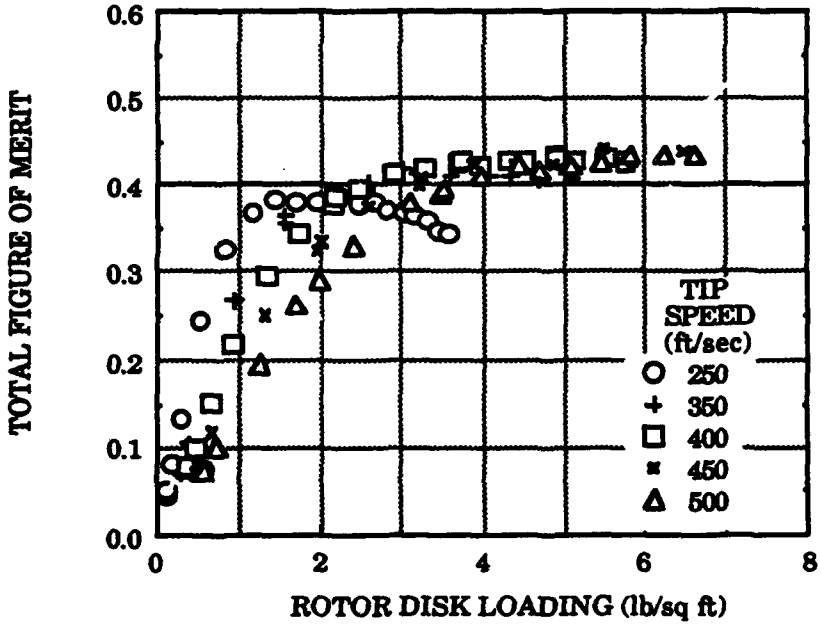

Fig. 13j. Total figure of merit versus disk loading for h = 0.005 in.

Fig. 13. (Continued)

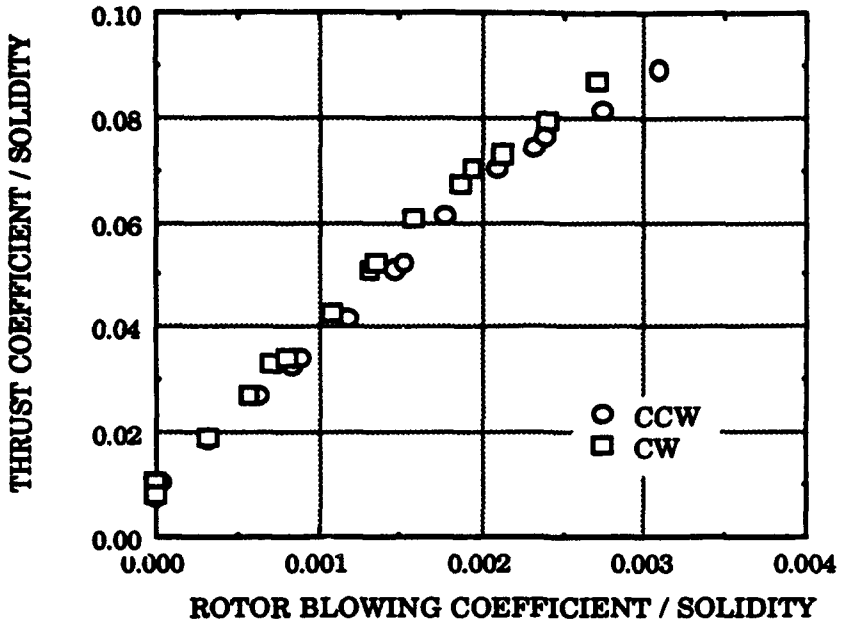

Fig. 14a. Thrust coefficient versus blowing coefficient for V_t = 500 ft/sec and h = 0.005 in.

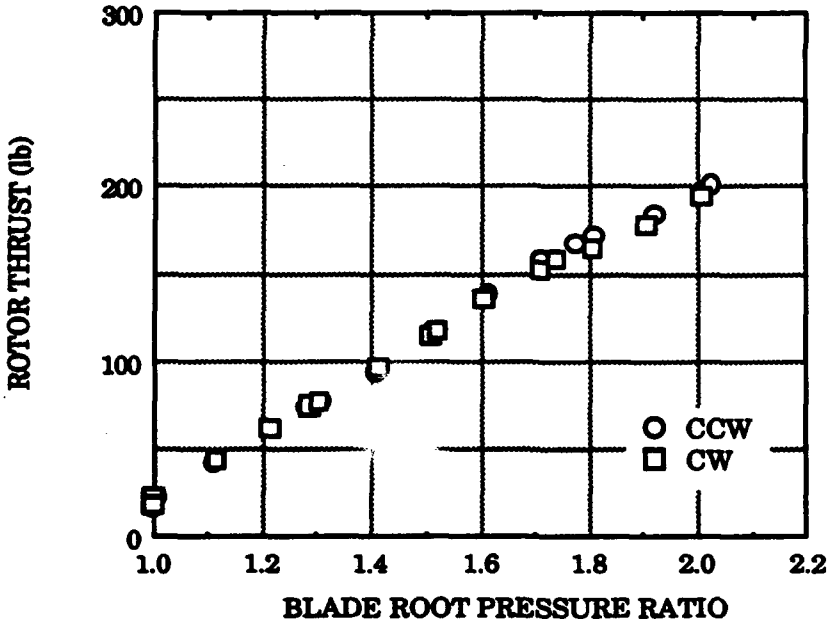

Fig. 14b. Thrust versus blade root pressure ratio for V_t = 500 ft/sec and h = 0.005 in.

Fig. 14. Tipjet rotor performance in CC rotor mode - Clockwise versus counterclockwise rotation.

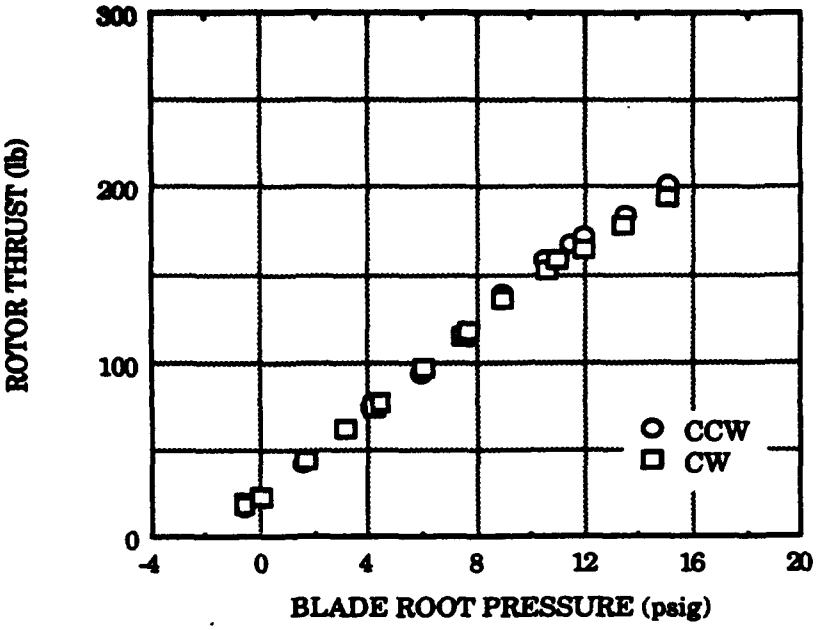

Fig. 14c. Thrust versus blade root pressure for V_t = 500 ft/sec and h = 0.005 in.

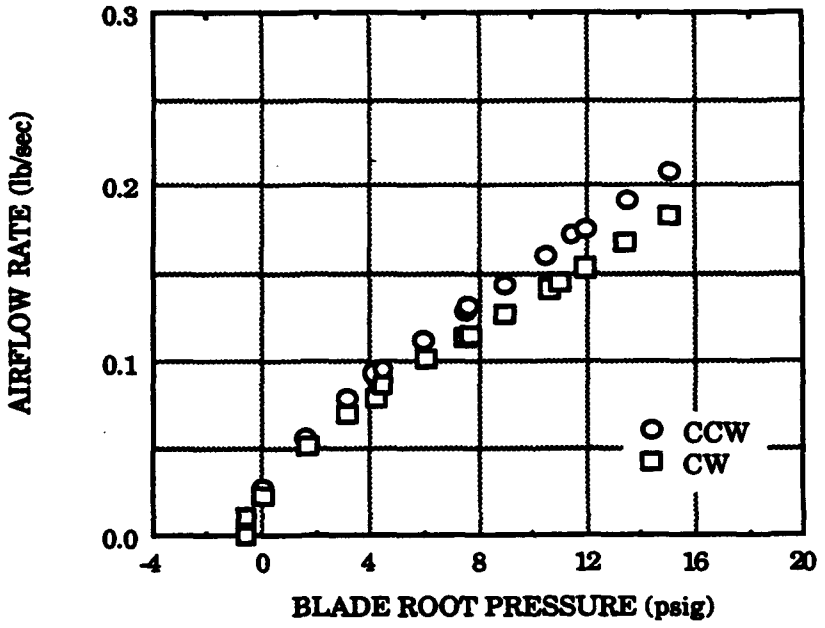

Fig. 14d. Airflow rate versus blade root pressure for V_t = 500 ft/sec and h = 0.005 in.

Fig. 14. (Continued)

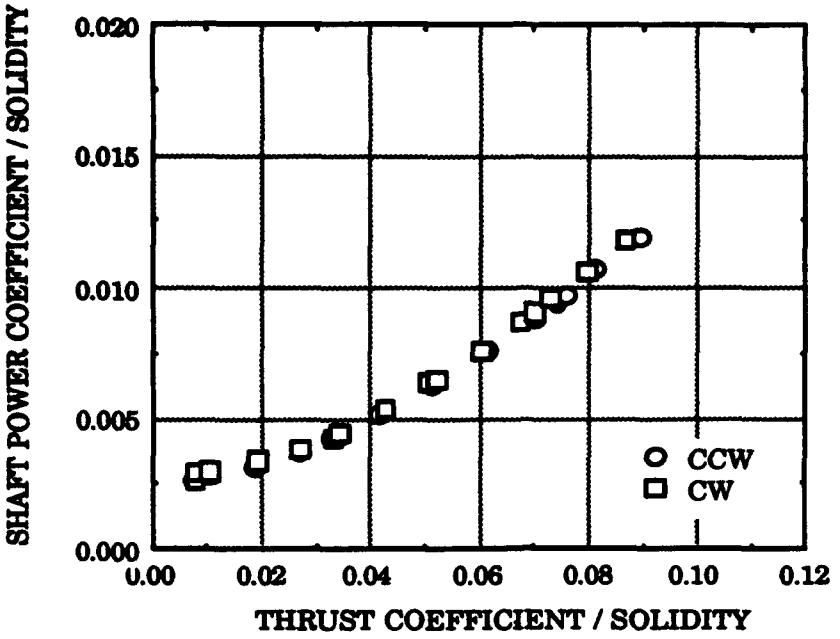

Fig. 14e. Shaft power coefficient / solidity versus thrust coefficient / solidity for V_t = 500 ft/sec and h = 0.005 in.

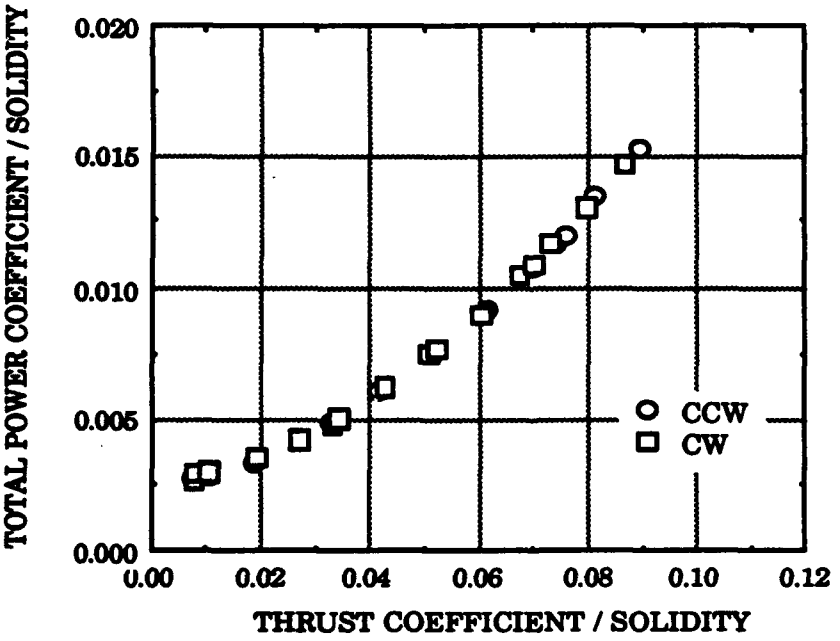

Fig. 14f. Total power coefficient / solidity versus thrust coefficient / solidity for V_t = 500 ft/sec and h = 0.005 in.

Fig. 14. (Continued)

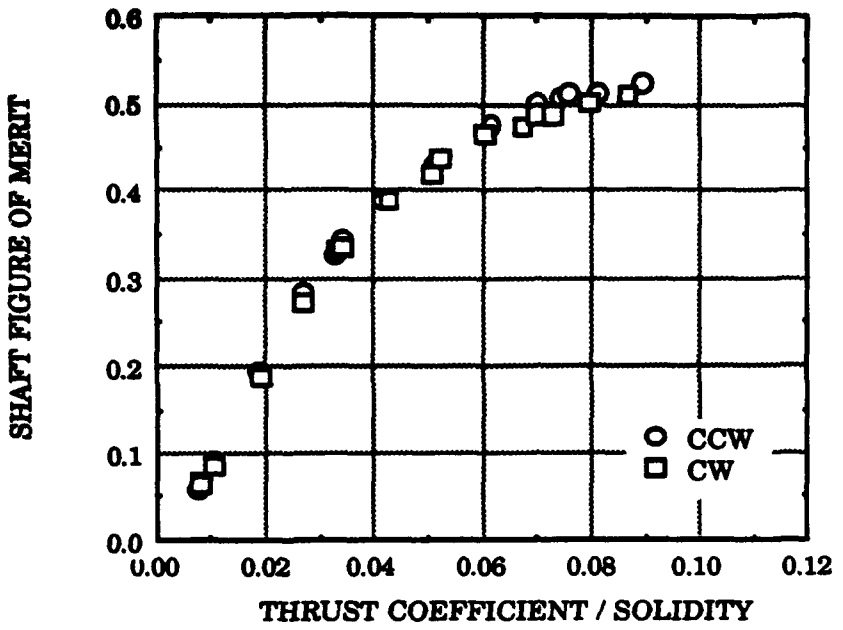

Fig. 14g. Shaft figure of merit versus thrust coefficient / solidity for V_t = 500 ft/sec and h = 0.005 in.

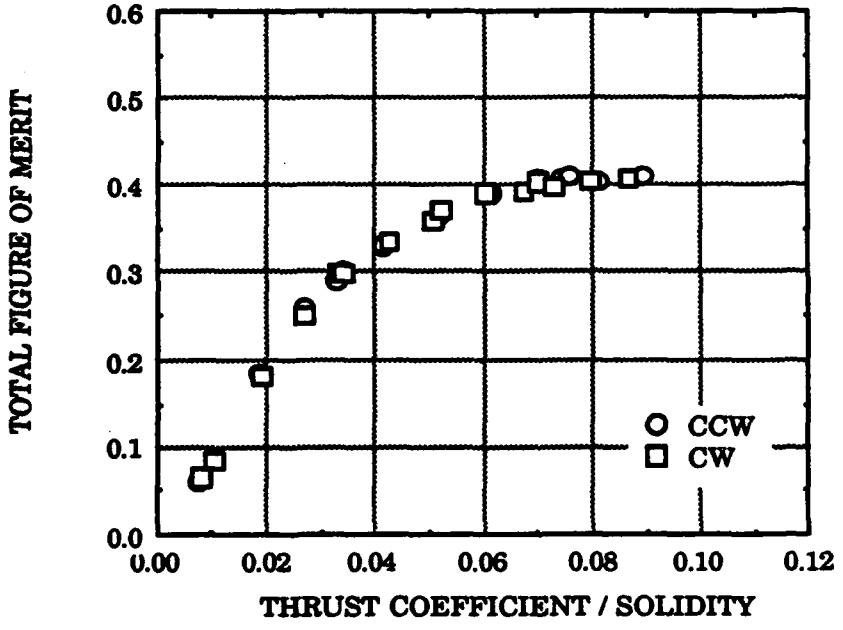

Fig. 14h. Total figure of merit versus thrust coefficient / solidity for V_t = 500 ft/sec and h = 0.005 in.

Fig. 14. (Continued)

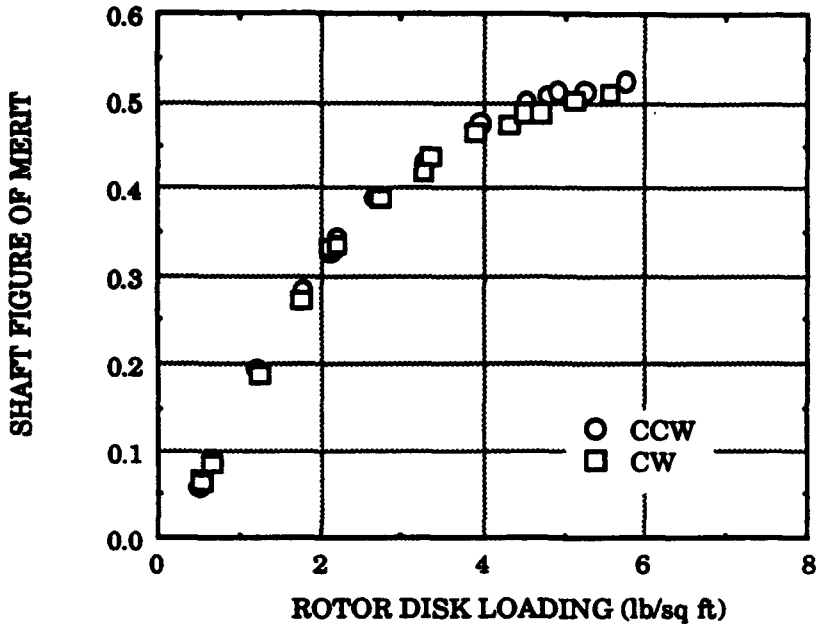

Fig. 14i. Shaft figure of merit versus disk loading for V_t = 500 ft/sec and h = 0.005 in.

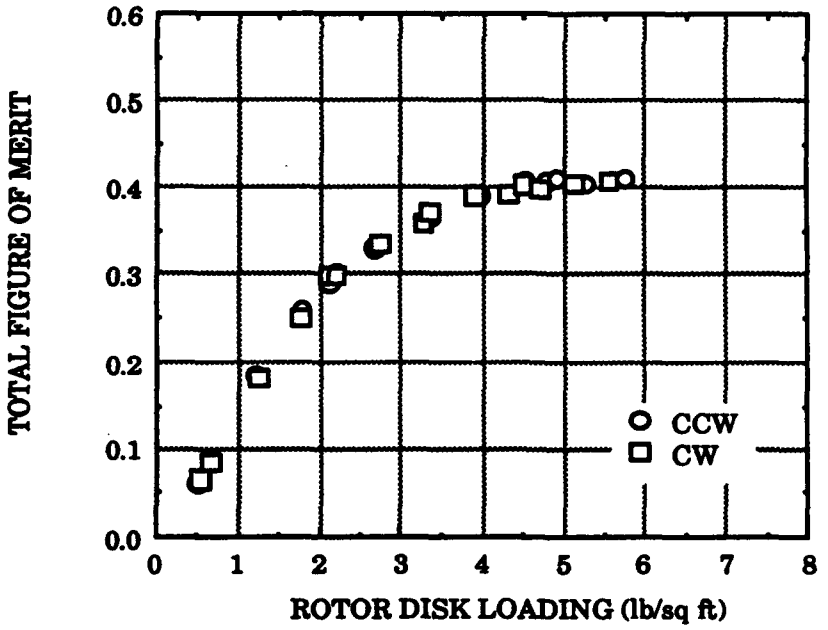

Fig. 14j. Total figure of merit versus disk loading for V_t = 500 ft/sec and h = 0.005 in.

Fig. 14. (Continued)

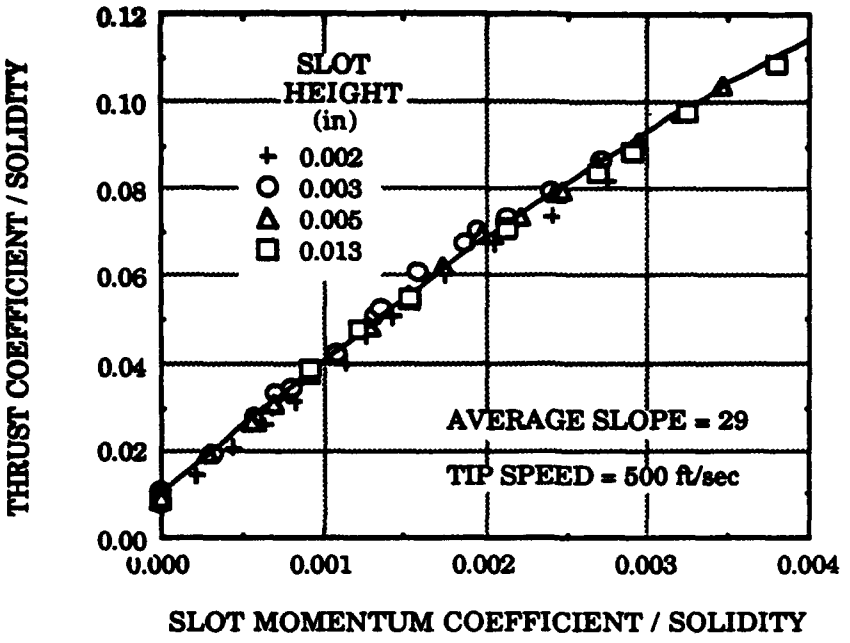

Fig. 15. Typical rotor lift augmentation performance.

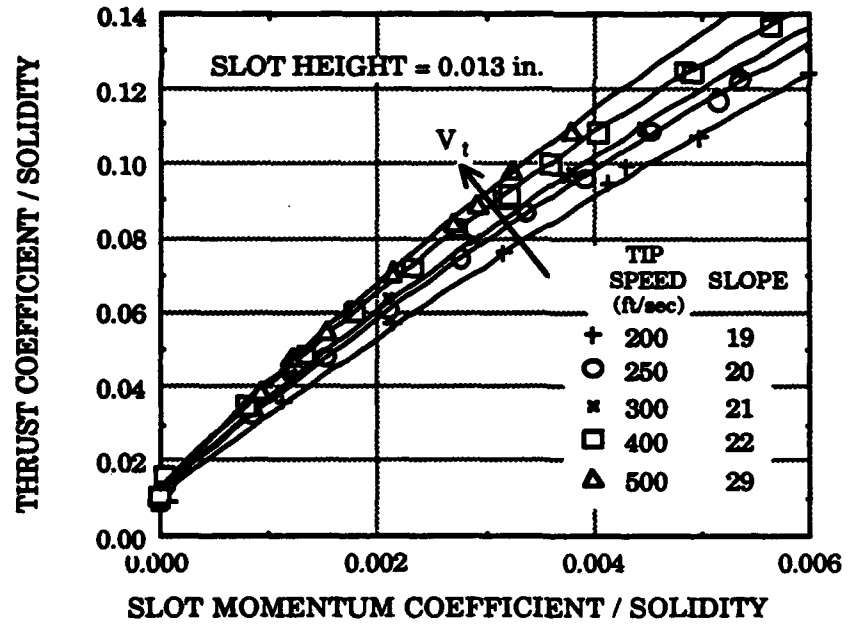

Fig. 16. Typical tip speed effect on lift augmentation.

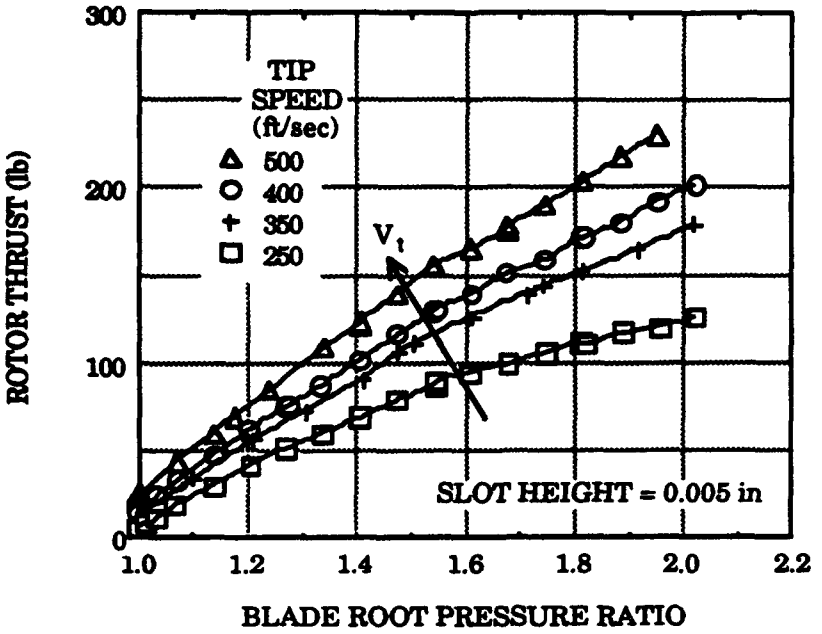

Fig. 17. Typical thrust response to pressure at various tip speeds.

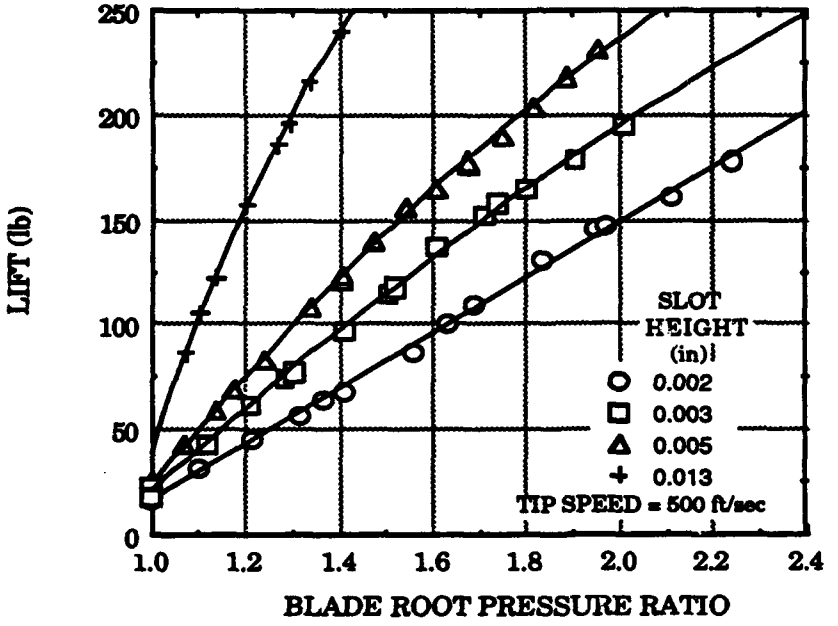

Fig. 18. Influence of slot gap on lift.

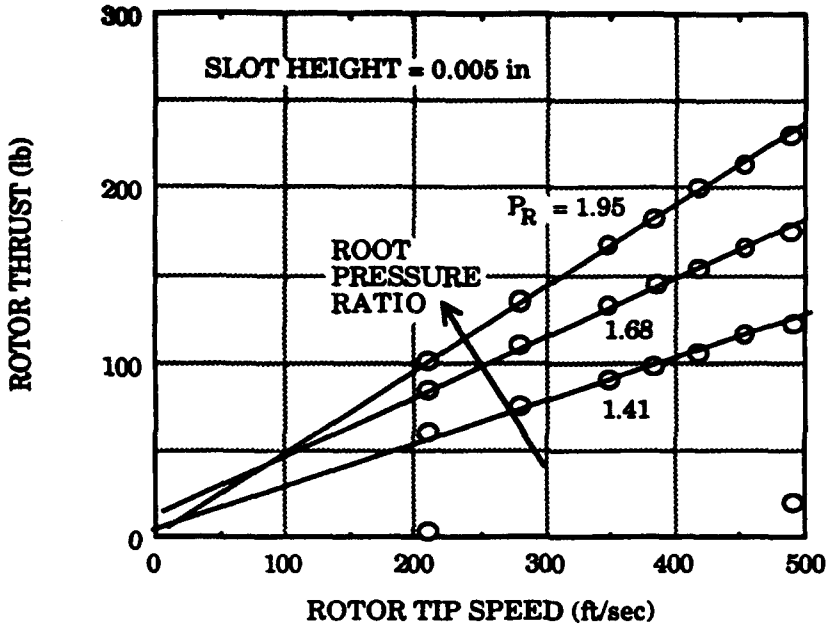

Fig. 19. Rotor thrust response to tip speed at constant pressure ratio.

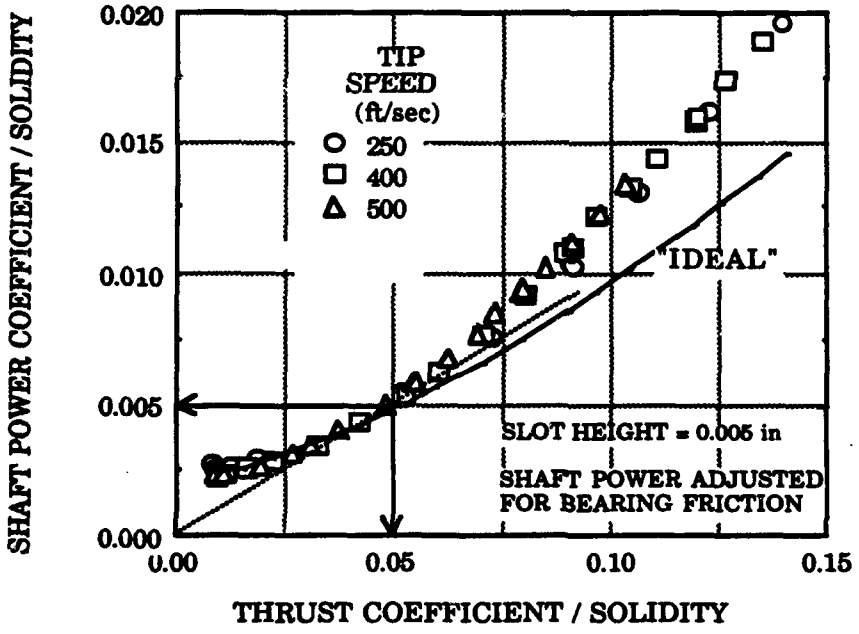

Fig. 20. Typical rotor shaft power-to-thrust relationship.

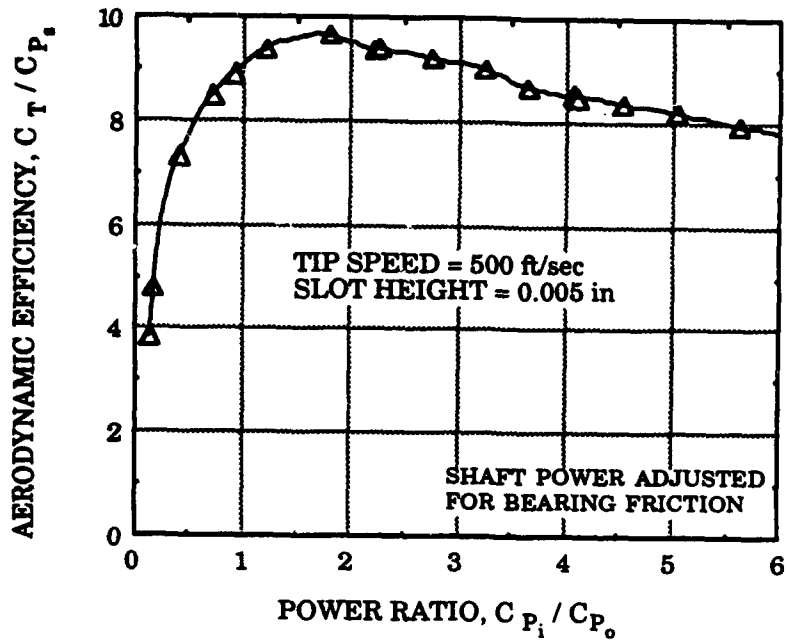

Fig. 21. Rotor shaft power efficiency versus induced power ratio.

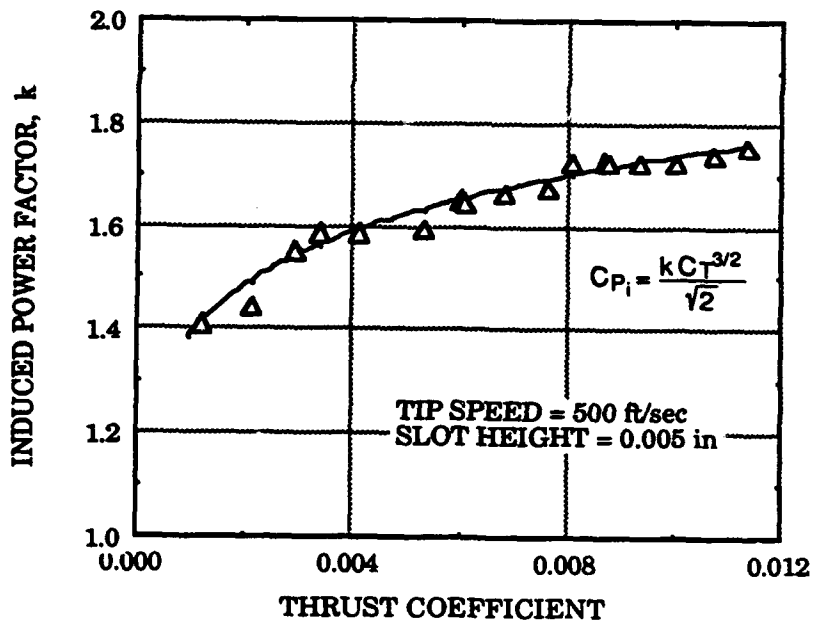

Fig. 22. Derived i. .uced power factor.

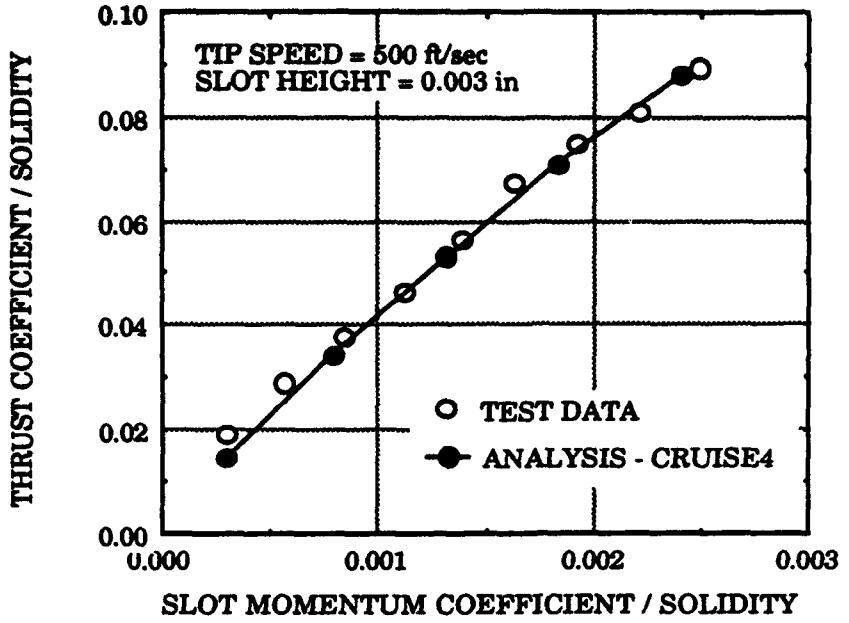

Fig. 23. Comparison of thrust test data with analysis.

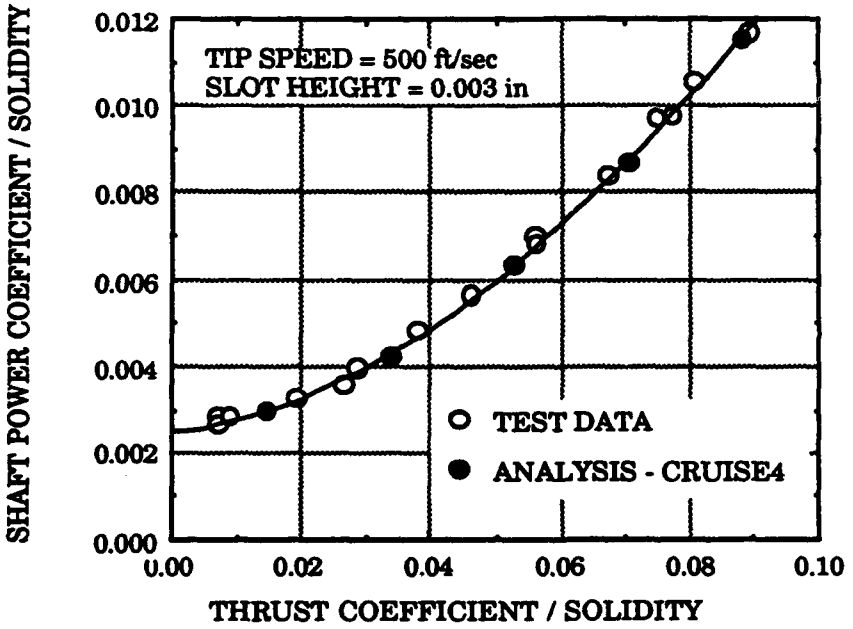

Fig. 24. Comparison of shaft power test data with analysis.

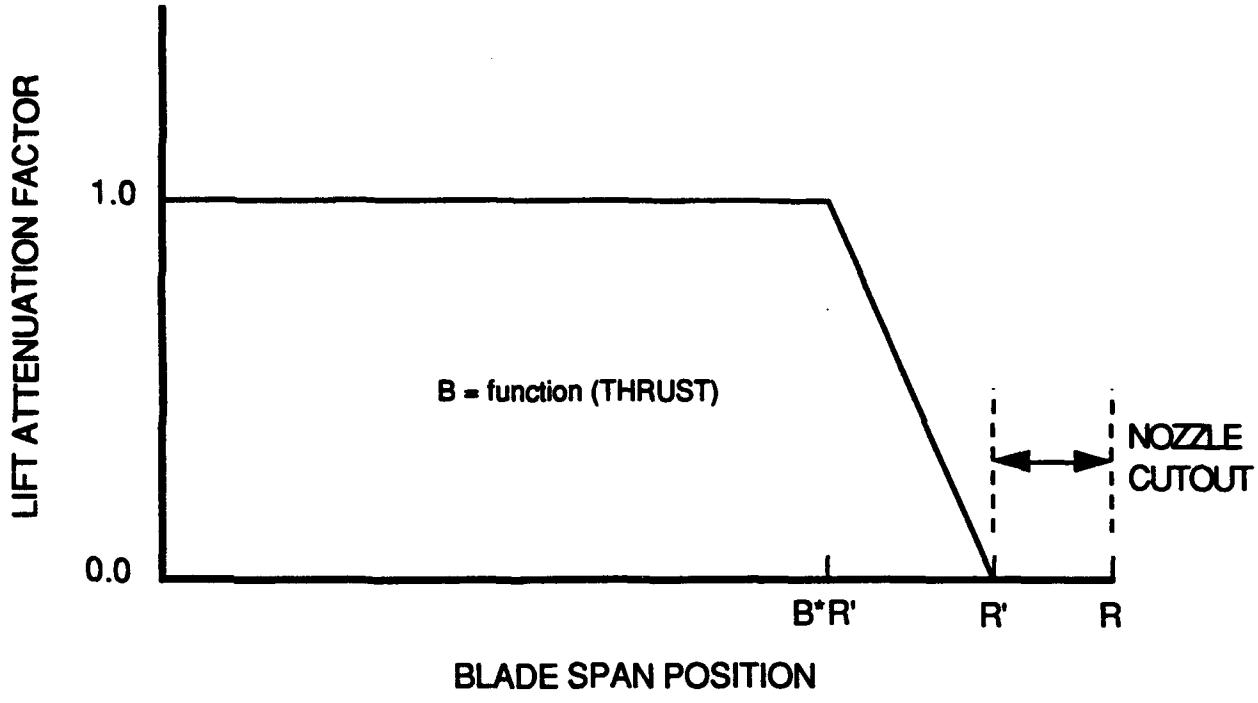

Fig. 25. Conceptual representation of blade effective lifting span modeling.

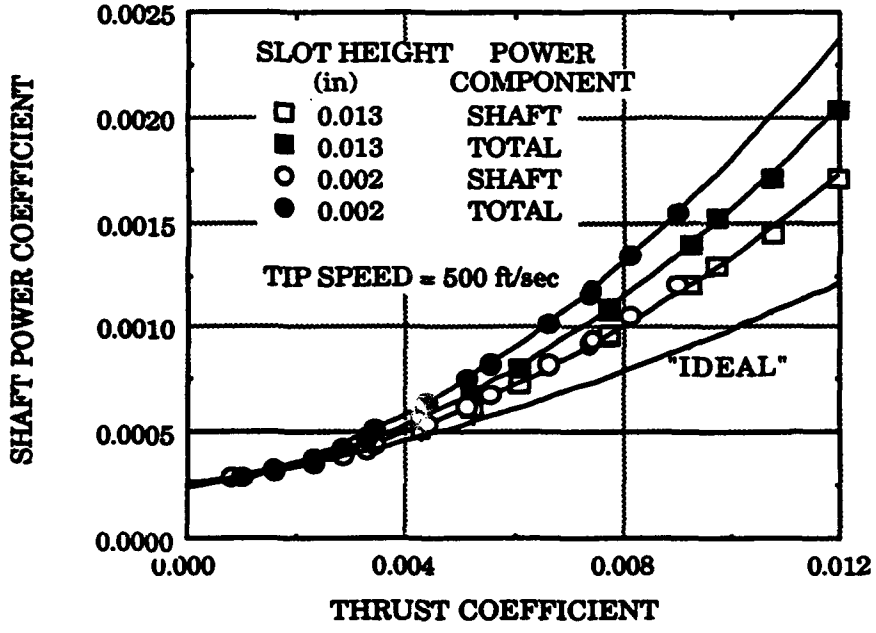

Fig. 26. Effect of slot height on total power (C_{P_s} + slot $C_{P_{pneumo}}$).

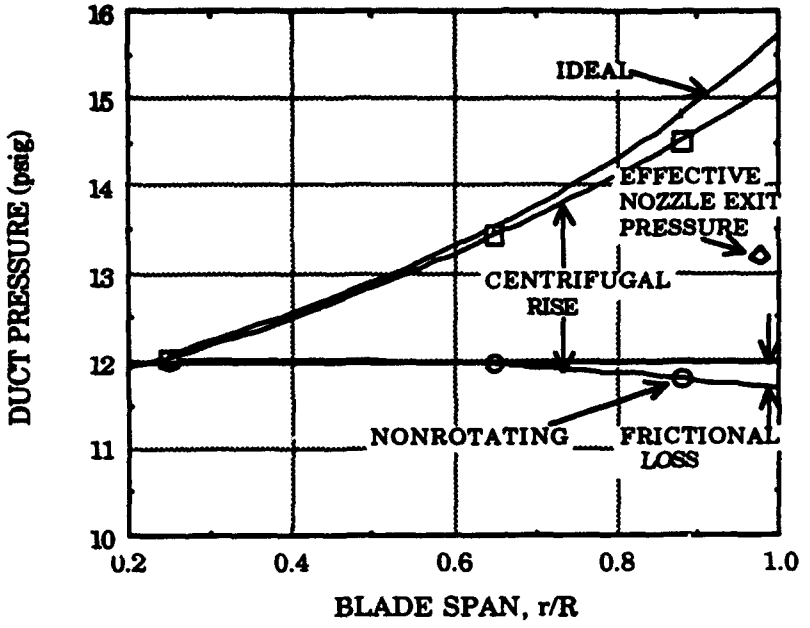

Fig. 27. Typical spanwise variations in duct centerline pressure.

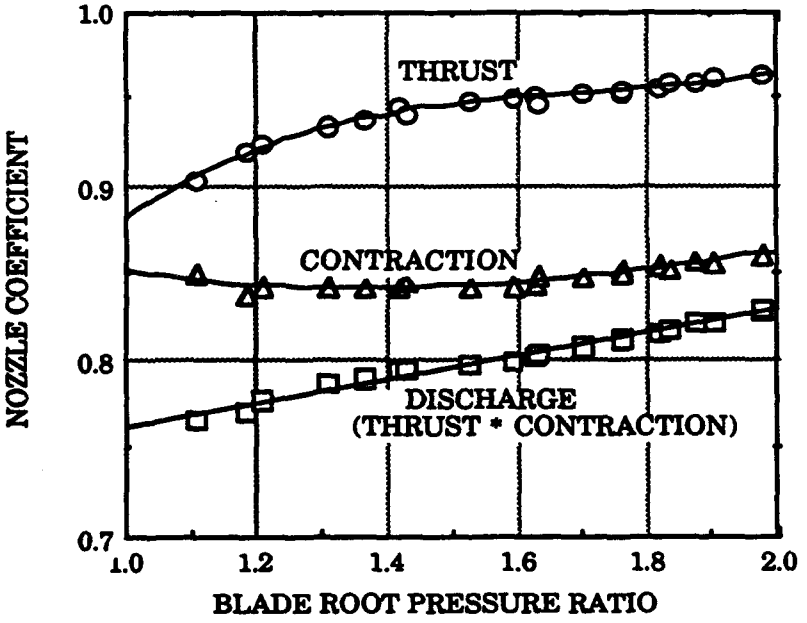

Fig. 28. Tip-jet nozzle static performance.

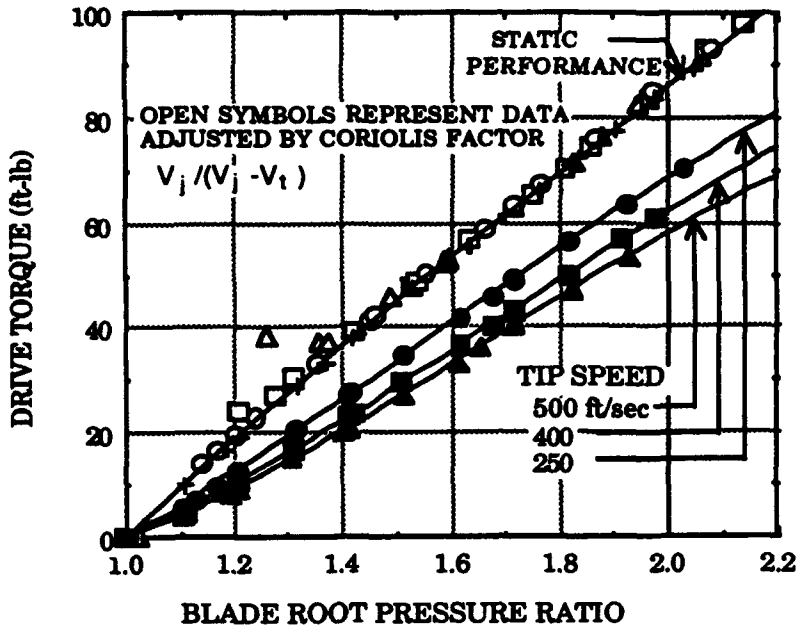

Fig. 29. Correlation of rotating-nozzle drive torque to nozzle static performance data.

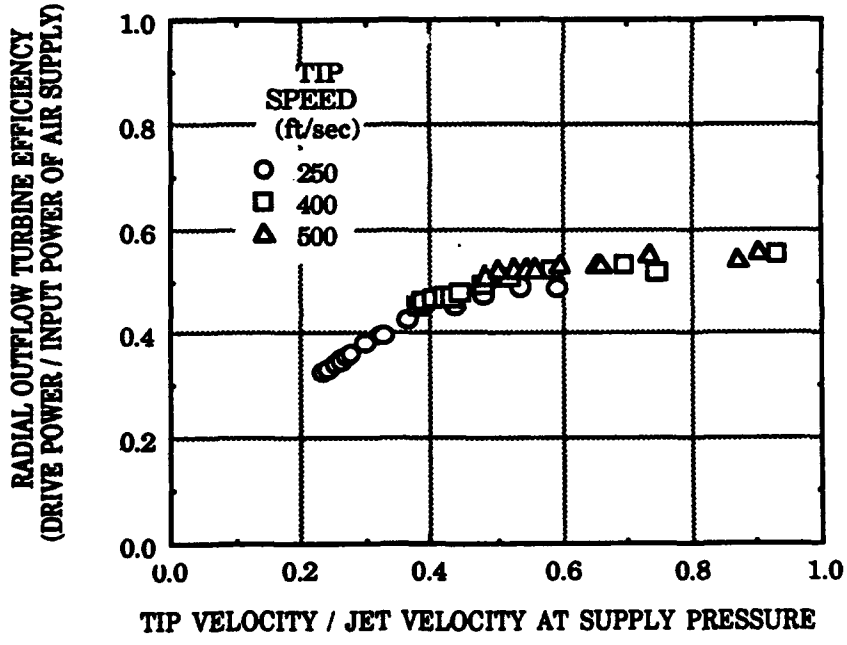

Fig. 30. Efficiency of pneumatic drive system.

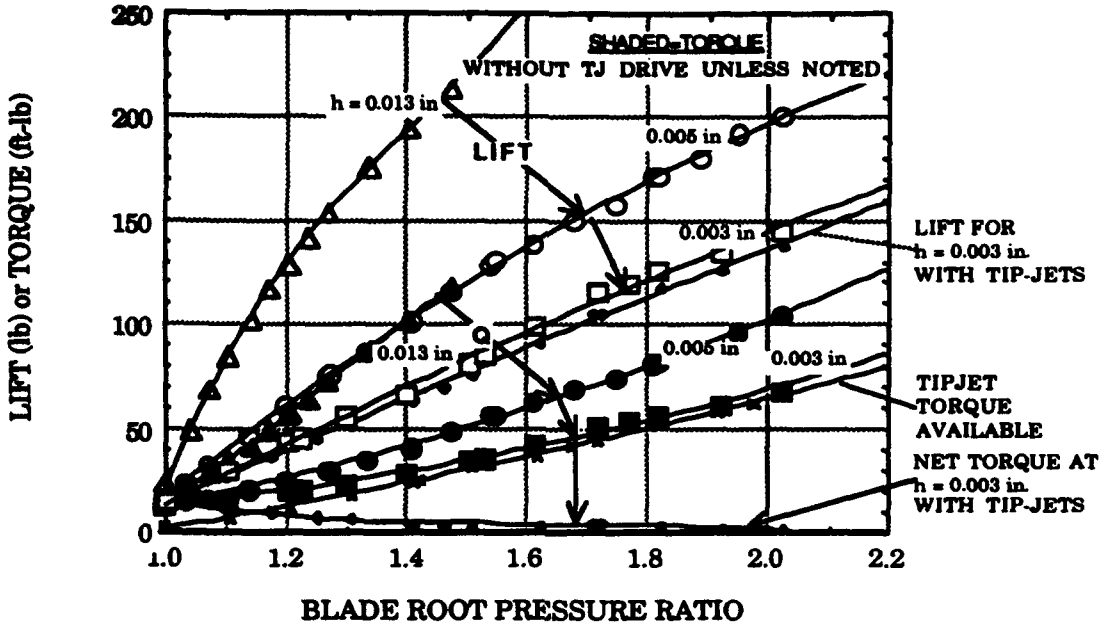

Fig. 31. Summary of operation at V_t = 400 ft/sec.

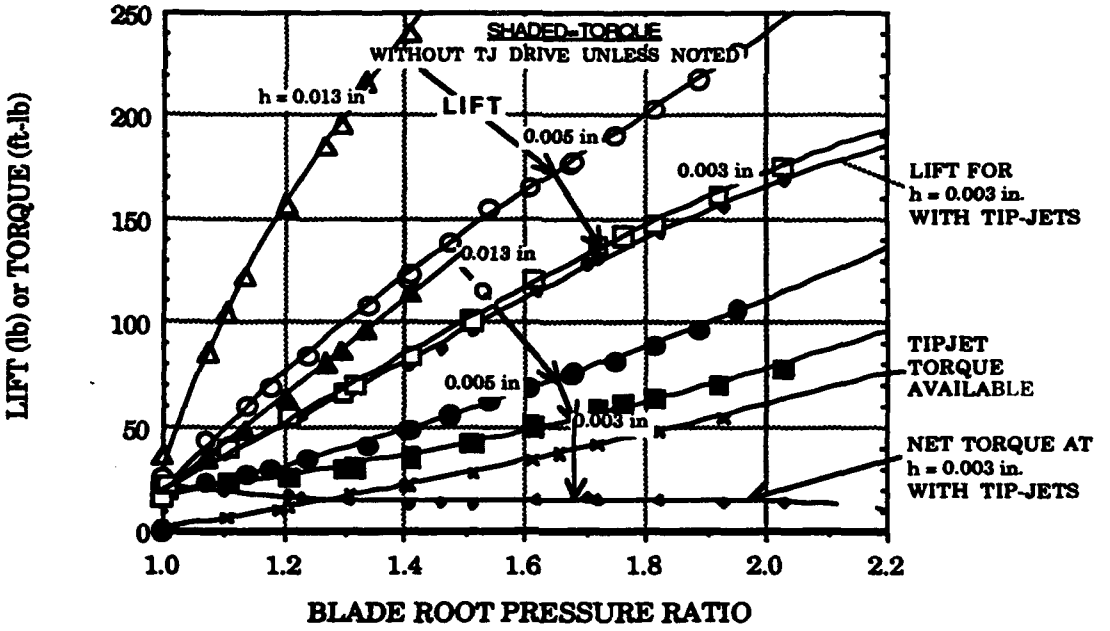

Fig. 32. Summary of operation at V_t = 500 ft/sec.

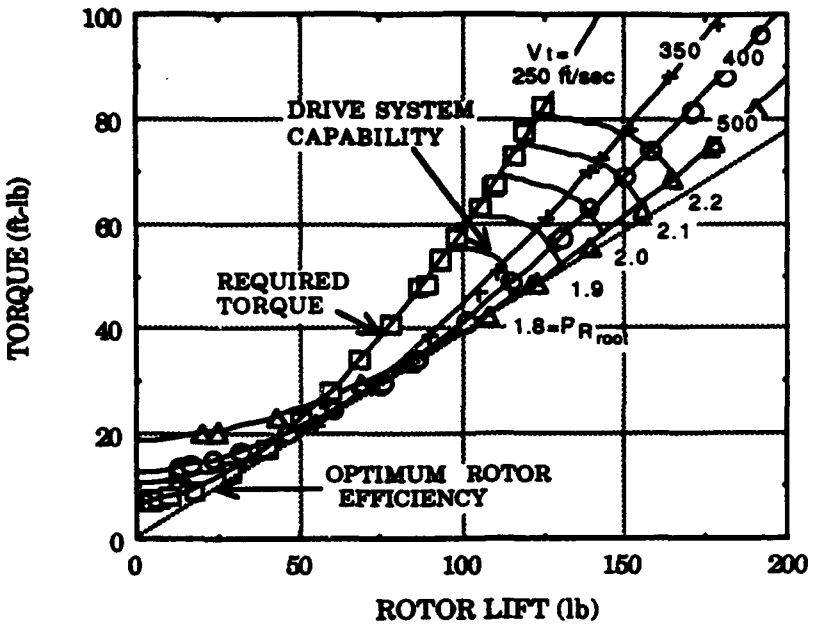

Fig. 33. Performance of isolated lift and drive systems.

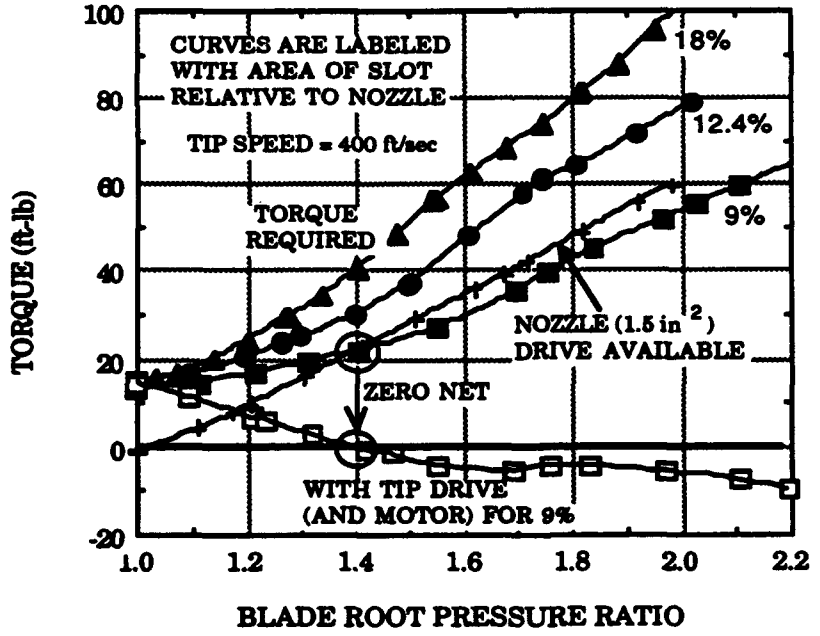

Fig. 34. Performance comparison of independent lift and drive systems to integrated system.

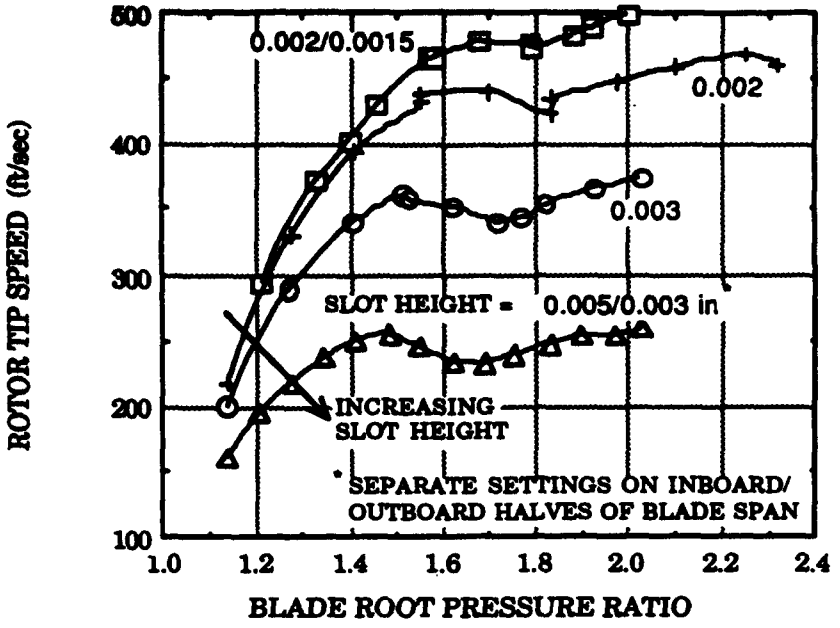

Fig. 35. Effect of slot height on tip speed limit in tip-jet drive mode.

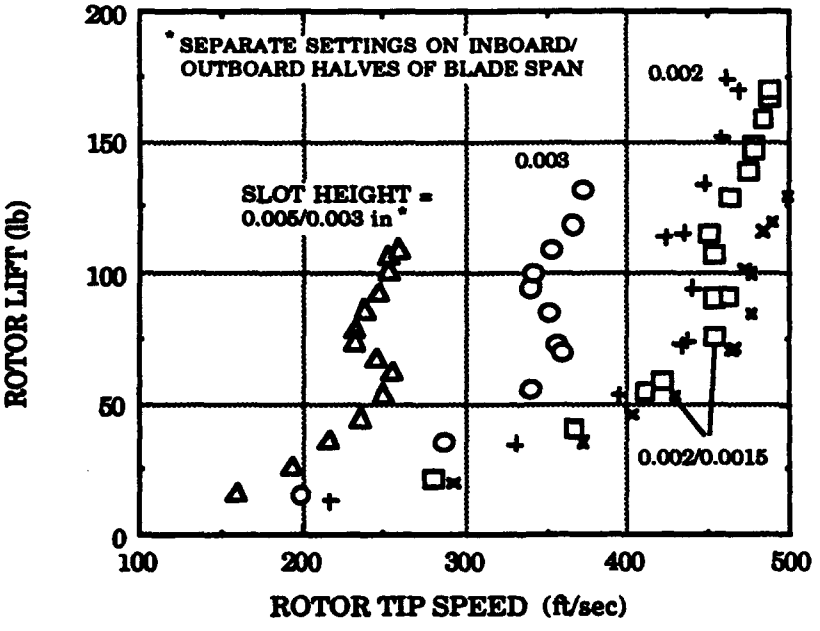

Fig. 36. Lift and tip speed relationship in tip-jet drive mode.

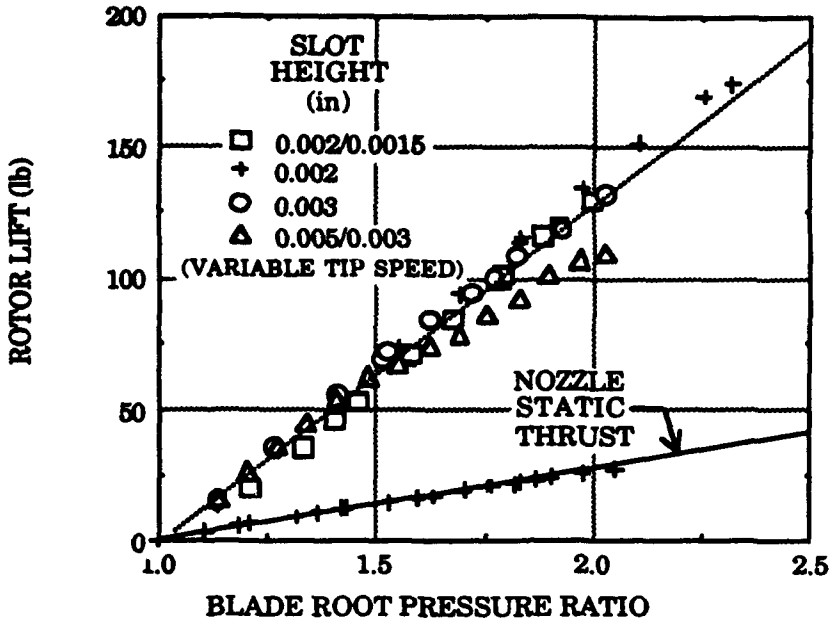

Fig. 37. Response of lift to blade pressure in tip-jet drive mode.

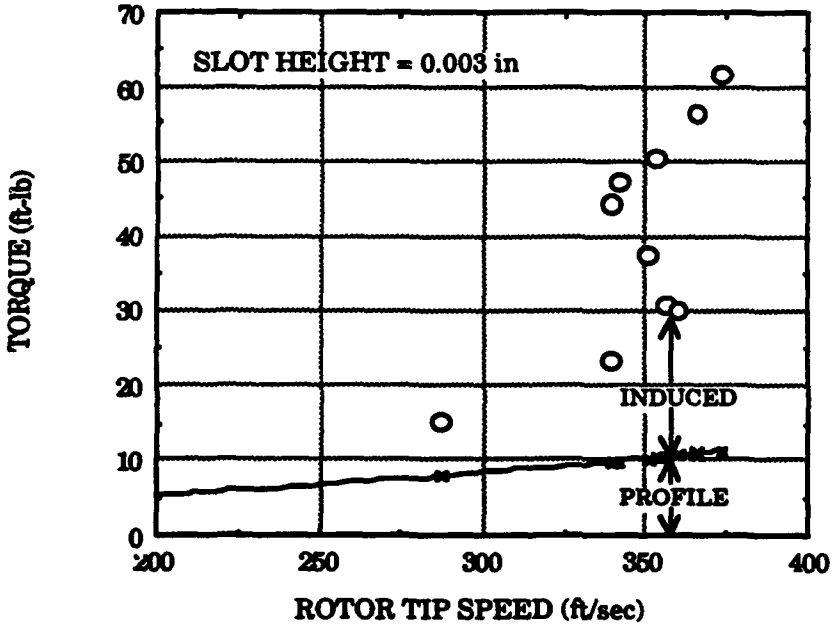

Fig. 38. Typical breakdown of rotor torque components.

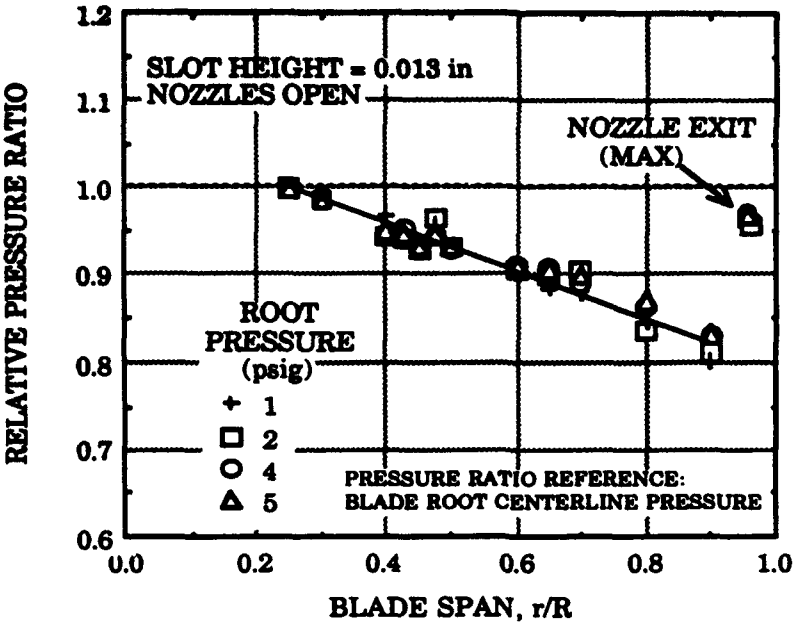

Fig. 39. Slot exit pressure measurements showing the "flowing plenum" effect.

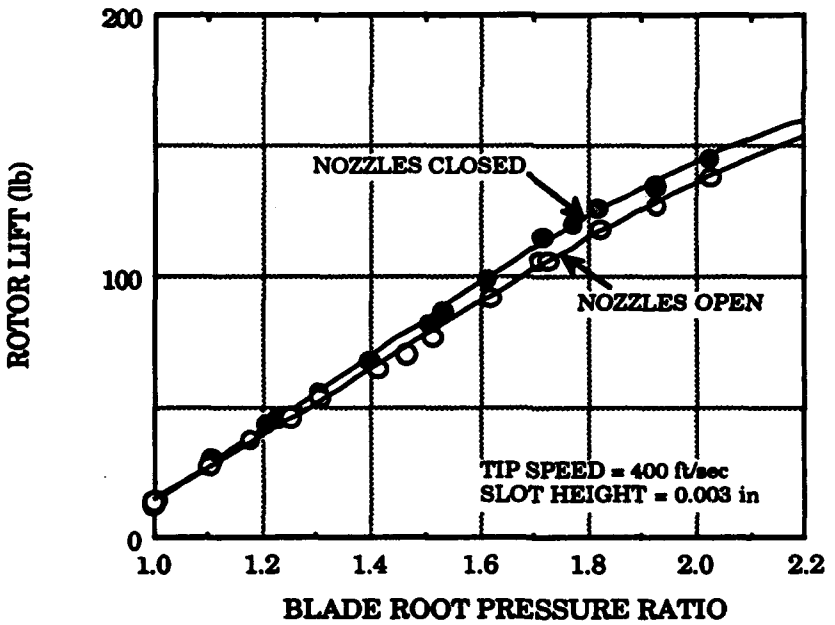

Fig. 40. Effect of "flowing plenum" due to nozzle flow to reduce thrust at a constant blade root pressure.

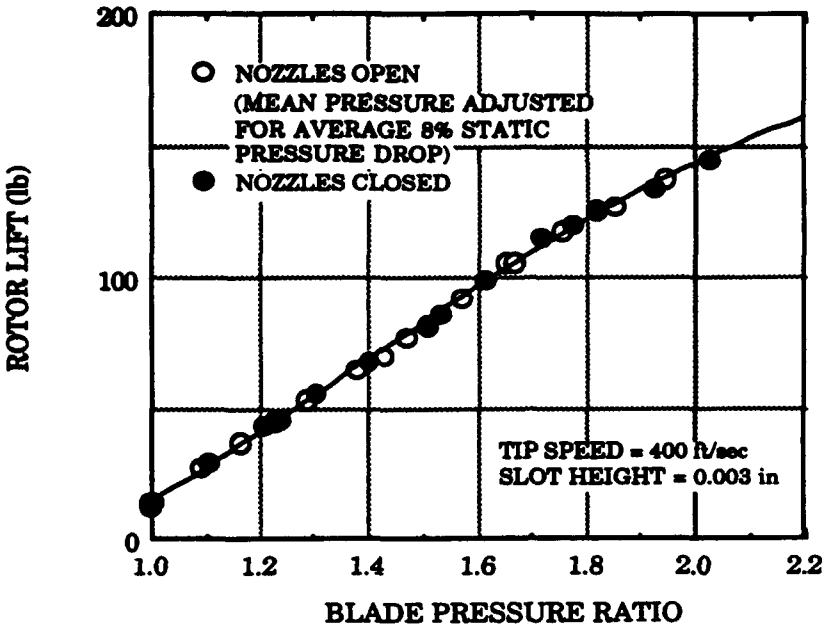

Fig. 41. Comparison of lift versus blade pressure ration with adjustment for static pressure drop.

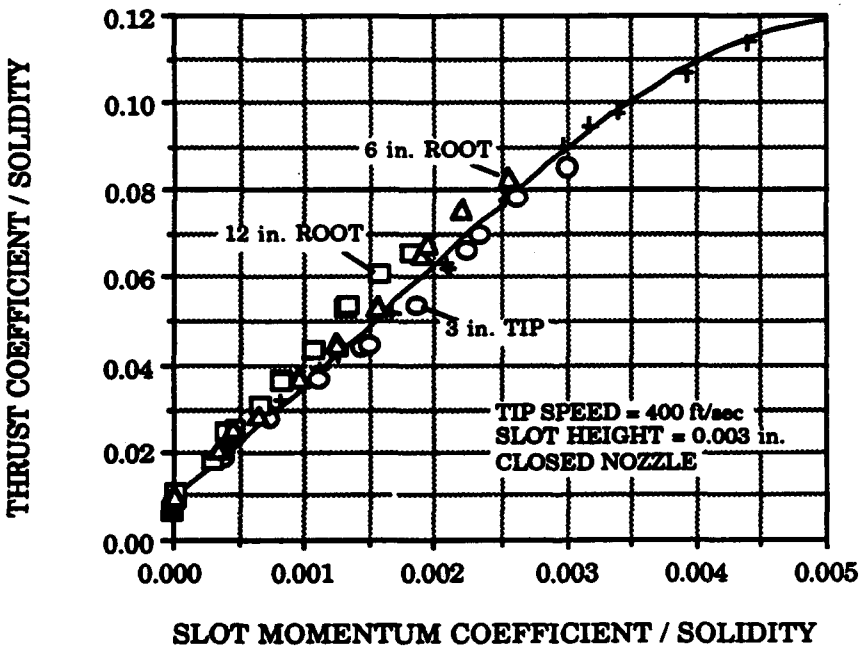

Fig. 42. Effect of taping blade root and tip slot sections.

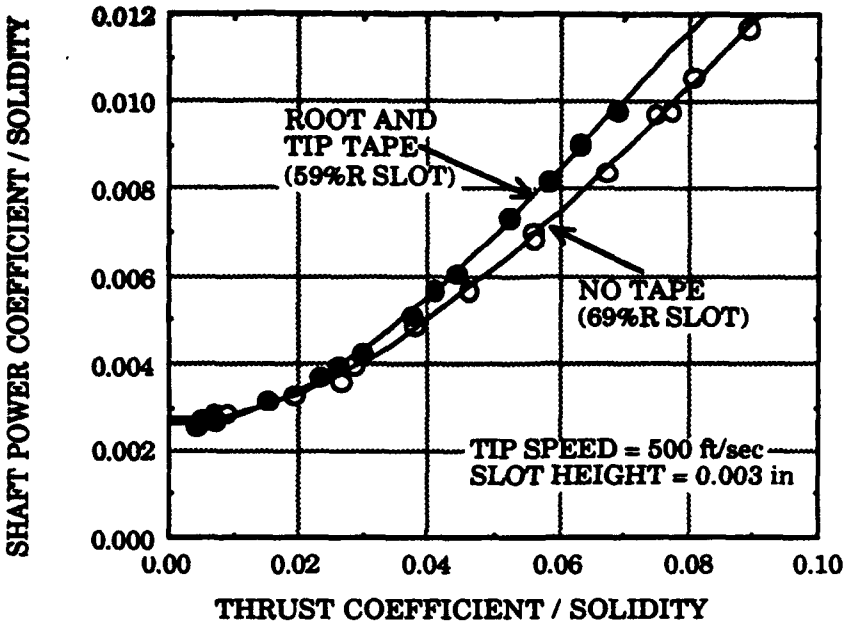

Fig. 43. Effect of slot length reduction (taping) on shaft power.

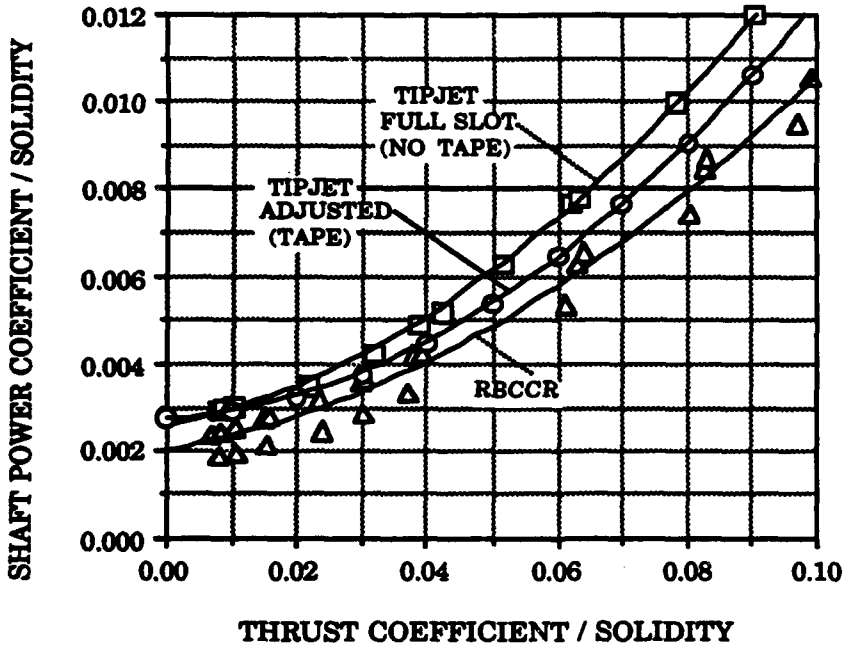

Fig. 44. Comparison of performance between Tipjet model and RBCCR model.

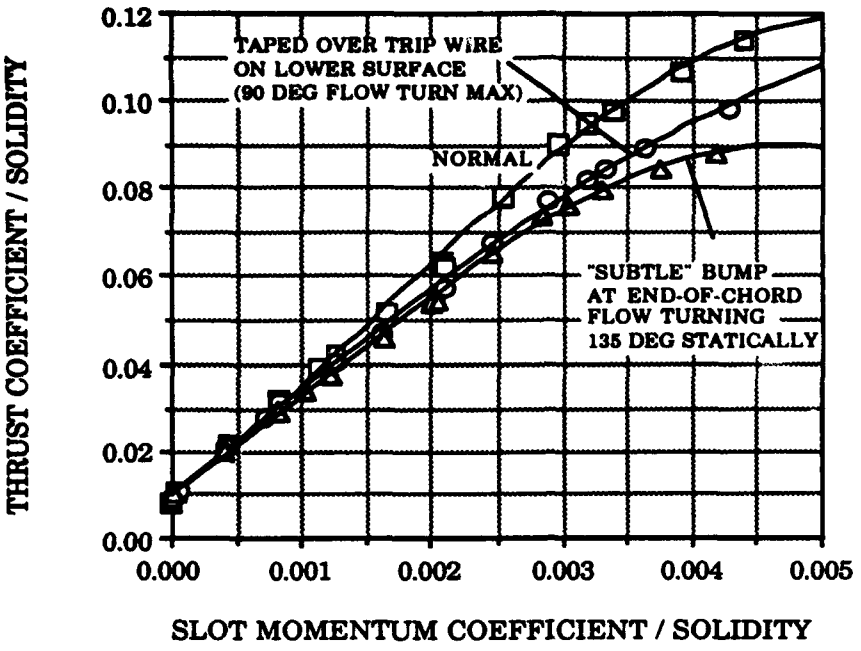

Fig. 45. Effect of Coanda surface flow trips on thrust augmentation.

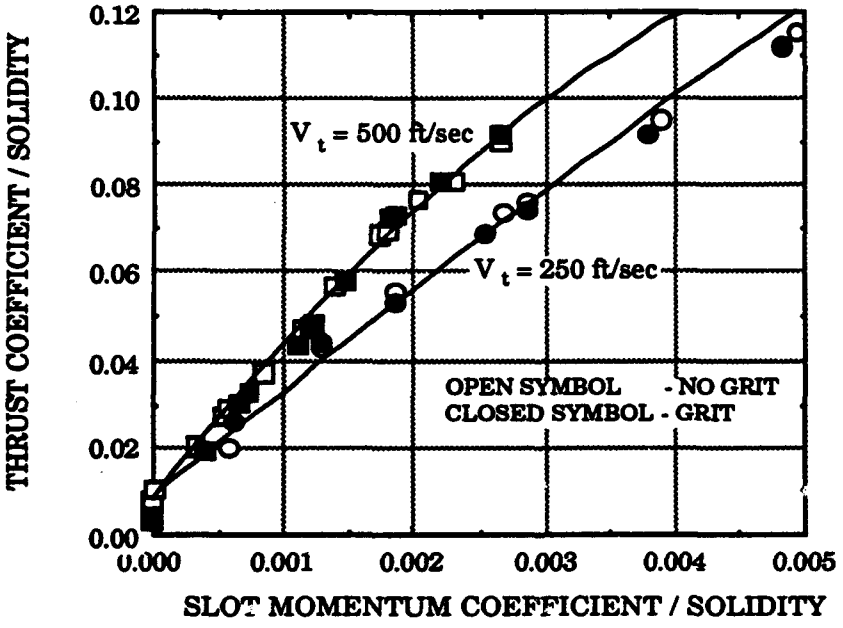

Fig. 46. Comparison of thrust augmentation with and without transition strips at V_t = 250 and 500 ft/sec.

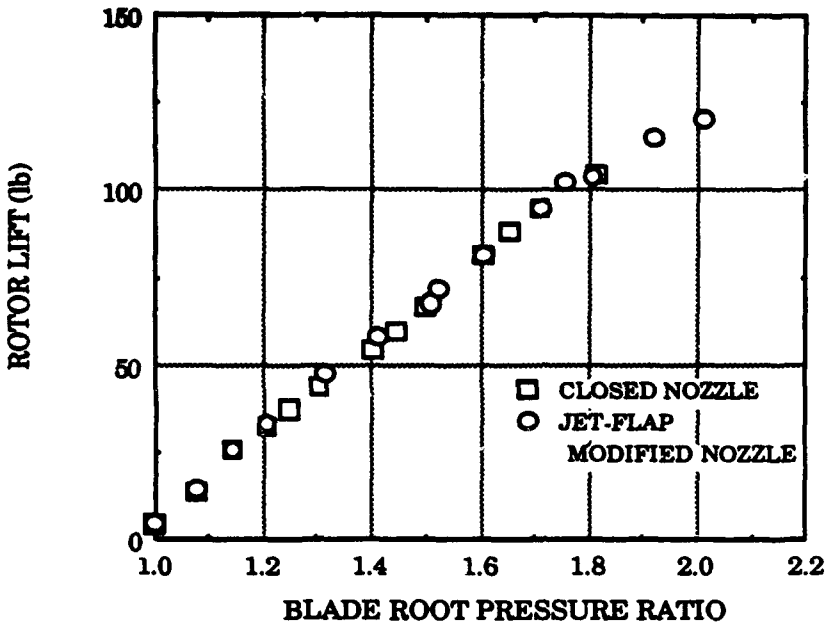

Fig. 47a. Comparison of rotor thrust augmentation.

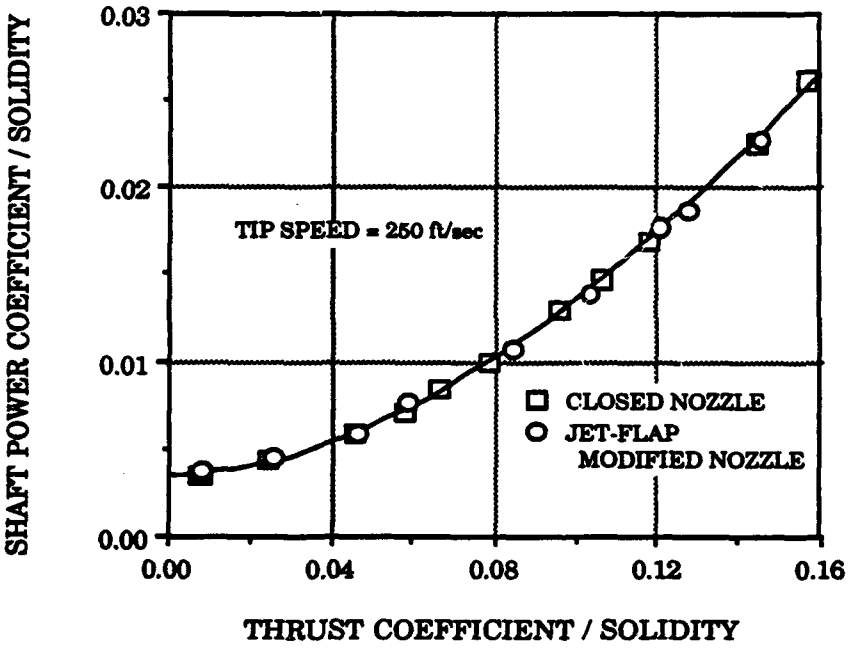

Fig. 47b. Comparison of power versus thrust.

Fig. 47 Rotor performance for configurations with and without jet-flap modified nozzles.

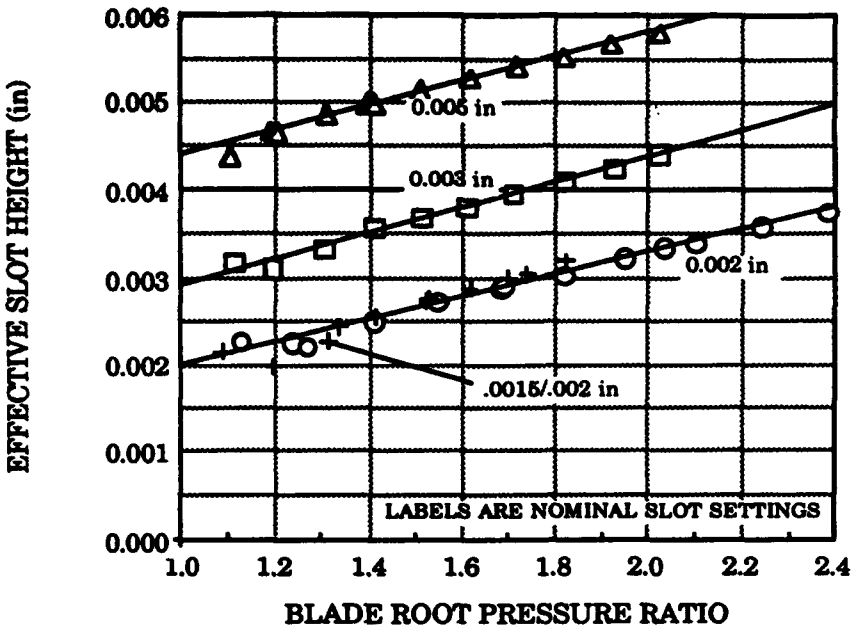

Fig. 48. Slot height expansion effect.

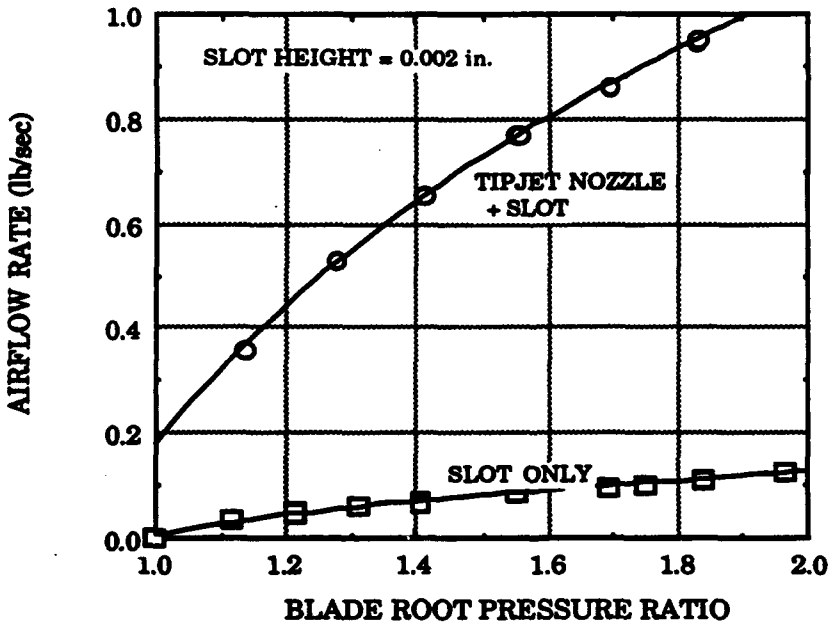

Fig. 49. Distribution of air between slots and nozzles.

Table 1. Test variables.

Parameter	Design Point	Test Range
V_t (fps)	500	0-500
h_{slot} (in.)	0.005	0.0-0.013
A_{nozzle} (in^2, each)	0.764	0.764
P_{blade} (psig)	13.2	0-20
Lift (lb)	165	0-230

Table 2. Model rotor geometric properties.

Blade			
Diameter, (ft)			6.67
Number of blades			2
Chord, c (in)	25% span		7.95
	93% span		5.40
Solidity ratio			0.110
Geometric twist, (deg)			0
Airfoils		25% Span	93% Span
Thickness ratio, t/c		0.213	0.170
Camber ratio, δ/c		0.053	0.011
Trailing edge radius, r_{te}/c		0.05	0.03
Slot height, h/c		variable	
Tip-jet nozzles (rectangular)			
Area/nozzle, (in^2)			0.764

Table 3. List of model drawings.

Drwg. No.	Description
E16-4121-1	Tipjet and Hub Assembly
E16-4121-2	Tipjet Sub-Assembly
E16-4121-3	Assembly Sections
E16-4121-4	Pressure Transducer Installation
E16-4121-5	Strain Gage Installation
E16-4121-6	Endcap and Flap Details
E16-4121-7	Lower Blade Machining Blank
E16-4121-8	Sections
E16-4121-9	Sections
E16-4121-10	Lower Blade Details
E16-4121-11	Lower Blade Details
E16-4121-12	Upper Blade Machining Blank
E16-4121-13	Machining Blank Upper Blade Sections
E16-4121-14	Upper Blade Details
E16-4121-15	Upper Blade Section Details
E16-4121-16	Tip & Hub Cover Details
E16-4121-20	Details

Table 4. Rotor balance calibration coefficients.

Loading	Run/Pt	dThrust/d	dPitch/d	dRoll/d	dTorque/d
+Pitch	2/22-30	-3.6167E-05	8.2208E-03	6.4519E-05	1.6880E-04
-Pitch	3/31-39	5.3437E-05	8.2767E-03	6.9206E-05	2.2415E-04
+Roll	6/83-91	-5.1070E-05	-1.6516E-05	7.8289E-03	-5.8564E-05
-Roll	7/92-100	-3.3514E-05	-1.1158E-05	7.8755E-03	-1.7078E-04
+Yaw	20/206-221	3.7780E-05	-3.0008E-05	2.7493E-04	2.3976E-02
-Yaw	19/190-205	1.8442E-05	3.2372E-05	2.1412E-04	2.3874E-02
-Thrust(1)	1/1-21	5.9588E-03	-1.5955E-05	-1.1320E-05	-5.1199E-05
-Thrust(2)	8/102-122	5.9593E-03	1.9333E-05	-1.9703E-05	-4.6678E-05
-Thrust(ave)		5.9590E-03	1.6889E-06	-1.5511E-05	-4.8939E-05

Table 5. CC rotor performance run summary.

Run	Direction	h (in.)	V_t (ft/sec)	P_{blade}(psig)	Notes
15	CCW	.013	350	0-7	Shakedown
16			400	0-6	
17			450	0-5	
20			450,500	0-6	
21			350,400	0-7	
22			250	0-12	
22			350-500	0,2,4	
27			0-500	0	Validation data set
27			250	0-8	
28			250,300	0-10	
29			350,400	0-10	
30			450,500	0-7	
32			210-490	0,1,2,3,4,5	
54		.005	0-500	0	
54			250	0-15	
55			400,500	0-15	
56			350,450	0-15	
57			210-490	6,10,14	
73		.003	400,500	0-15	
76			250,265	0-15	
77			200,400,500	0-15	
90		0	0-500	0	Slots taped
92		.002	250	0-20	
93			400	0-20	
94			500	0-18	
105	CW	.003	0-500	0	
106			250	0-12	
107			400	0-14	
108			500	0-15	
122			250	0-12	
123			400	0-13	
124			500	0-15	
133			500	0-13	
134			250,400	0-13	
143			250,500	0-14	
144			500	0-10	Varied sample rate
156		.003	250	0-12	Outbd slot to 0
157		.003	400	0-13	Outbd slot to 0
158		.003	500	0-10	Outbd slot to 0
159		.003	500	0-10	Repeat of Run 158
160		.003	250,400,500	0-10	Outbd slot to .006
160		.003	210-450	8	Outbd slot to .006

Table 6. Reaction-drive system performance run summary.

Run	Position	V_t (ft/sec)	P_{blade}	Notes
36	TE2	0	0-10	Preliminary check
37	TE1&2	0	0-11	
39	TE1&2	0	0-15	
40	TE2	0	0-15	
43	TE1	0	0-14	
45	TE1	0	0-15	Repeat of Run 43
46	LE1	0	0-15	
47	LE1&2	0	0-15	
48	LE1&2	0	0-15	Repeat
49	LE2	0	0-15	
51	LE2	0	0-15	Repeat of Run 49
52	TE2	0	0-15	No nozzle module
61	TE1&2	250	0-15	Dynamic performance
62	TE1&2	400,500	0-14	
67	TE1&2	0	0-15	
150	LE1&2	250,500	0-14	
151	LE1&2	0	0-15	Defective nozzle modules
152	LE1&2	250,500	0-14	Defective nozzle modules

Table 7. Integrated lift/drive system performance run summary.

Run	Direction	h (in.)	V_t (ft/sec)	P_{blade}(psig)	Notes
33	CCW	.013	210-490	0	
33			250	0-8	
34			400,500	0-7	
63		.005	400,500	0-10	
64			200,250	0-11	
65		.005/.003	250,400	0-15	
66			Variable	0-15	TJ Self-drive
70		.003	350,400	0-15	
71			500	0-15	
71			Variable	0-15	TJ Self-drive
96		.002	400	0-17	
97			500	0-18	
98			Variable	0-19	TJ Self-drive
100		.002/.0015	Variable	0-15	TJ Self-drive
101			Variable	0-19	TJ Self-drive
112	CW	.003	250	0-12	
113			400	0-14	
114			500	0-15	
115			Variable	0-15	TJ Self-drive
145			Variable	0-13	TJ Self-drive
153			Variable	0-14	TJ Self-drive; (defective nozzles)

Table 8. CC slot taping run summary.

Run	h (in.)	V_t (ft/sec)	P_{blade}(psig)	Notes
35	.013	500	0-7	Inboard 15.5 in. taped
58	.005	500	0-14	Outboard 1 in. taped
78	.003	400	0-12	Outboard 1 in. taped
79				2 in.
80				3 in.
81				Inboard 3 in. taped
82				6 in.
83				12 in.
87	.003	400	0-15	0.1 in. strips;full span
88				;outbd 1/2 span
89				;inbd 1/2 span
109			0-13	Outboard 1/2 in. taped
125		200,250,400	0-8	All except outboard 10 in.taped
135		500	0-13	Outboard 3 in. taped
136				Outboard 3 in. & inboard 4.5in.
138			0-12	All except outboard 1.75 in.
139				Repeat of Run 138
146		Variable	0-10	All except outboard 9 in. taped
148		Variable	0-14	Inboard 1/2 span taped
149		Variable	0-6	All slots taped

Table 9. Static mass flow / slot height checks run summary.

Run	LE/TE*	h (in.)	Nozzles
18	TE	0.013	Closed
19	TE	0.013	Closed
60	TE	0.005	Closed
72	TE	0.003	Open
74	TE	0.003	Closed
95	TE	0.002	Closed
102	TE	0.002/0.0015	Closed
104	LE	0.003	Closed
118	LE	0.003	Jet-Flap
132	LE	0.003	Closed

* Geometric slot (from top)